Self-assembly of perovskite nanocrystals

Atanu Jana[a], Abhishek Meena[a], Supriya A. Patil[b], Yongcheol Jo[a], Sangeun Cho[a], Youngsin Park[c], Vijaya Gopalan Sree[a], Hyungsang Kim[a], Hyunsik Im[a,*], Robert A. Taylor[d]

[a] Division of Physics and Semiconductor Science, Dongguk University, Seoul 04620, Republic of Korea. Email: *hyunsik7@dongguk.edu (H.I.)*

[b] Department of Nano Technology and Advanced Materials Engineering, Sejong University, Seoul, South Korea

[c] Department of Chemistry, School of Natural Science, Ulsan National Institute of Science and Technology (UNIST), Ulsan 44919, Korea

[d] Clarendon Laboratory, Department of Physics, University of Oxford, Parks Road, Oxford OX1 3PU, UK.

Keywords: Self-assembly, colloidal, perovskite NCs, superlattices, driving forces

Table of contents

ABSTRACT

The self-assembly phenomenon plays a significant role in atomic, molecular, and biological self-assemblies. This phenomenon has also been found in colloidal nanocrystals (NCs). Self-assembly of colloidal NCs into superlattices (SLs) is a promising approach for manipulating nanometre-sized particles and exploiting physical and chemical properties that are distinct from both individual NCs and bulk assemblies. The development of SLs of colloidal perovskite NCs through self-assembly has recently attracted remarkable attention; it is quickly developing as a new frontier in nanotechnology. This review presents the different driving forces, crucial factors for self-assembly of perovskite NCs, recent developments in the synthesis, and properties of self-assembled colloidal perovskite NCs. We also discuss the formation of various SLs from perovskite NCs with different morphologies. Finally, we shed light on multiple challenges in developing numerous perovskite SLs for optoelectronic devices.

1. Introduction

Self-assembly is a process by which individual units, such as colloidal nanoparticles and protein molecules, are arranged spontaneously into a highly ordered structure [1]. In 1959, Richard Feynman coined the concept of self-assembly in his famous talk titled, “There’s Plenty

of Room at the Bottom" [2]. He envisioned a world in which atoms can be arranged one by one, exactly as per our needs. It was found later that this process plays a significant role in biology and materials science. The higher-order structures of various nanoparticles have been developed through this self-assembly process. After the discovery of perovskite NCs, several groups have explored the self-assembly of such NCs [3,4]. Halide perovskite NCs are potentially applicable in diverse fields such as solar cells, photodetectors, light-emitting diodes, X-ray scintillator and direct detectors, lasers, and catalysis [5,6,15,7–14]. Their self-assembly at the nanoscale can create materials imparting excellent device performance [16,17]. All-inorganic perovskites have been reported to have various size units, such as nanocubes [18,19,28,20–27], nanoplates [18,23,29–33], nanosheets [34,35], nanorods [36–41], nanowires [36,42], quantum dots [43], and nanoribbons [36,42]. The smallest units are responsible for developing superlattices through the self-assembly phenomenon. The smallest units are passivated by different types of surfactants, such as long-alkyl chain amines [33,44–46], acids [47], and zwitterions [48]. $CsPbX_3$ perovskite NCs, unlike normal semiconductor NCs, have fragile ionic bonding with dynamic capping ligands, resulting in intriguing surface characteristics. Different types of cooperative interactions, such as dipole-dipole, hydrophobic, and van der Waals between these capping ligands play a critical role in creating SLs [49,50]. The interaction between these surfactants provides a great opportunity for developing various SLs. The extent of the self-assembly phenomenon largely depends on the shape and size of NCs and ligand interactions with solvents. The self-assembly of perovskite NCs can be achieved by several methods: (1) a template substrate with controlled solvent evaporation, (2) using air/liquid or liquid/liquid interfaces, and (3) the solvent-dependent interaction of surface passivating ligands. The electronic structure of individual $CsPbX_3$ NCs (X = Cl, Br, and I) allow for defect tolerance, rapid radiative decays, and extended exciton dephasing. These characteristics make them promising building blocks for NCs solids for investigating collective quantum phenomena that are difficult to obtain with conventional semiconductor NCs. The SLs of $CsPbBr_3$ NCs show various quantum phenomena, such as electronic coupling with the formation of minibands and superfluorescence [3].

Various synthetic methods have been reported for synthesizing halide perovskite NCs. The shape of the single unit has been changed by varying the precursors, temperature, ligands, and solvent medium. However, controlling the self-assembly of these single units has been rarely investigated. Mostly, all-inorganic perovskites are found to be SLs of nanocubes. Why does it form the SLs and not a single nanocube unit? There are also few reports on SLs of

nanoplatelets [51], nanodisks [52], and nanosheets [53] as building blocks. What are the driving forces for the growth of these intriguing SLs? How can we vary the structure of halide perovskite SLs? Why do all inorganic perovskites form long-order SLs? How can we control the size of SLs? How does facet chemistry control the self-assembly process? The questions mentioned above needs to be investigated properly concerning these emerging energy materials.

2. Driving forces for self-assembly

The self-assembly process drives the arrangement of identical or distinct types of randomly arranged particles into an ordered structure using different types of driving forces (**Scheme 1**) [54]. It is critical to have an analytical understanding of how diverse interparticle forces drive the self-assembly of building blocks into customised SL structures. Various key forces play an essential role in self-assembly, including the Brownian force, steric force, dipole-dipole interaction, van der Waals (vdW) force, capillary force, and hydrogen bonding interactions.

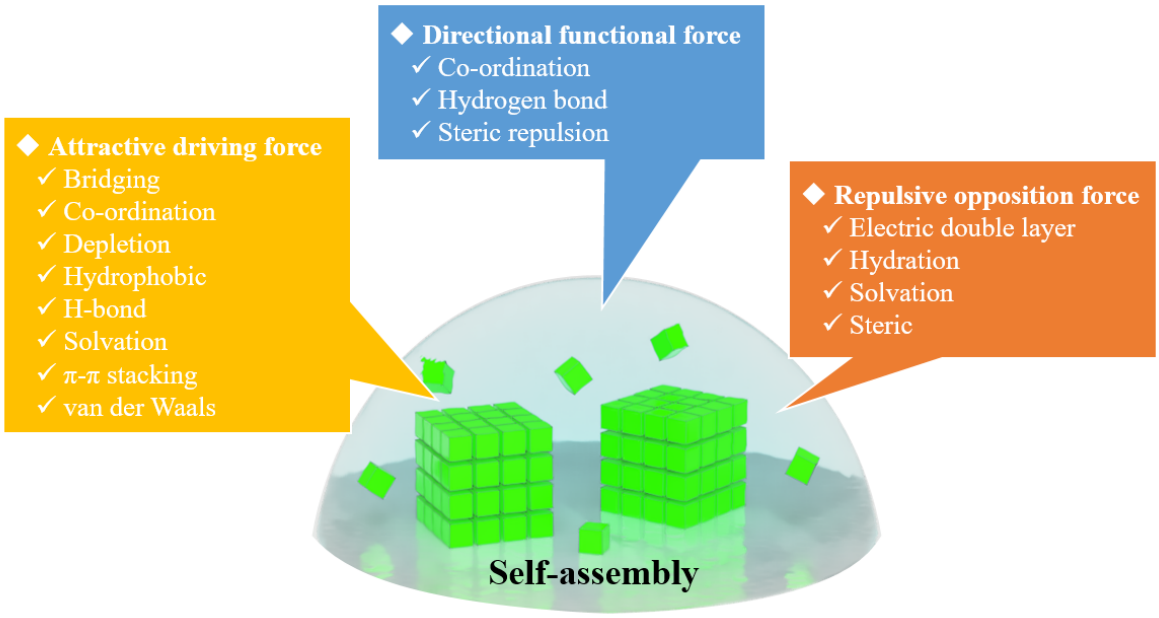

Scheme 1: Various attractive, directional, and repulsive forces for self-assembly.

2.1. van der Waals force

vdW forces are the attractive forces acting between molecules and atoms separated by some distance that are primarily electromagnetic in origin and have a long-range order. They are the result of fluctuations or dislocations of partial charges within the individual components

in the form of permanent-permanent dipole interactions (Keesom forces), instantaneous (fluctuating) dipole-induced dipole interactions (London dispersion forces), and permanent-induced dipole interactions (Debye forces) [49,55–58] (**Scheme 2)**. All of these forces and their corresponding equations are shown in **Table 1**.

Table 1: vdW forces and associated equations [59]

Serial No	van der Waals forces	Origin of interactions	Interaction energy
1	Keesom force	Permanent dipole-dipole	$V(r) = \frac{-2\mu_1^2\mu_2^2}{3(4\pi\varepsilon_0)^2 k_B T} \times \frac{1}{r^6}$
2	Debye force	Permanent dipole-induced dipole	$V(r) = \frac{-\mu_1^2\alpha_2'}{(4\pi\varepsilon_0)} \times \frac{1}{r^6}$
3	London dispersion force	Instantaneous dipole-induced dipole	$V(r) = -\frac{3}{2} \times \alpha_1'\alpha_2' \times \frac{I_1 I_2}{(I_1 + I_2)} \times \frac{1}{r^6}$
V(r) = Interaction energy, μ = permanent dipole moment, ε_0 = vacuum permittivity, T = temperature, α = polarizability, I = Ionization potential, r = the distance between the two molecules			

Permanent dipole-dipole interactions comprise either intermolecular attractions or repulsive interactions between two polarised molecules due to the inherent difference in their charge distributions (**Scheme 2a)**. They can play an important role in driving the self-assembly of nanoparticles [60–63]. Talapin et al. explored the role of dipole-dipole interactions between non-local dipoles of individual nanoparticles towards the formation of self-assembled SLs of monodisperse nanoparticles (PbS, PbSe, and Fe_2O_3) [61]. Dipole-dipole interactions between NCs have also been observed during the self-assembly of $CsPbBr_3$ NCs due to the inherent dipole moment of cubic $CsPbBr_3$ [64]. A dipole-induced dipole attraction (London dispersion forces) involves a charged or polar molecule that induces a charge redistribution in non-polar species (**Scheme 2b)**[49,57,65]. As a result of this redistribution, the non-polar species acquires partial positive and negative charges and therefore becoming polar. Hence, the two molecules attract. London dispersion forces are short-range forces between molecules; their strength

depends on geometry, shape, interparticle distances, and the chemical composition of interacting molecules. Induced dipole–induced dipole interaction is the weakest intermolecular interaction arising in molecules without permanent dipoles (**Scheme 2c)**. It is a temporary interaction resulting from transient dipoles related to the non-spherical instantaneous distribution of electrons in a molecule or atom inducing a dipole in an adjacent molecule or atom resulting in a weak attractive force.

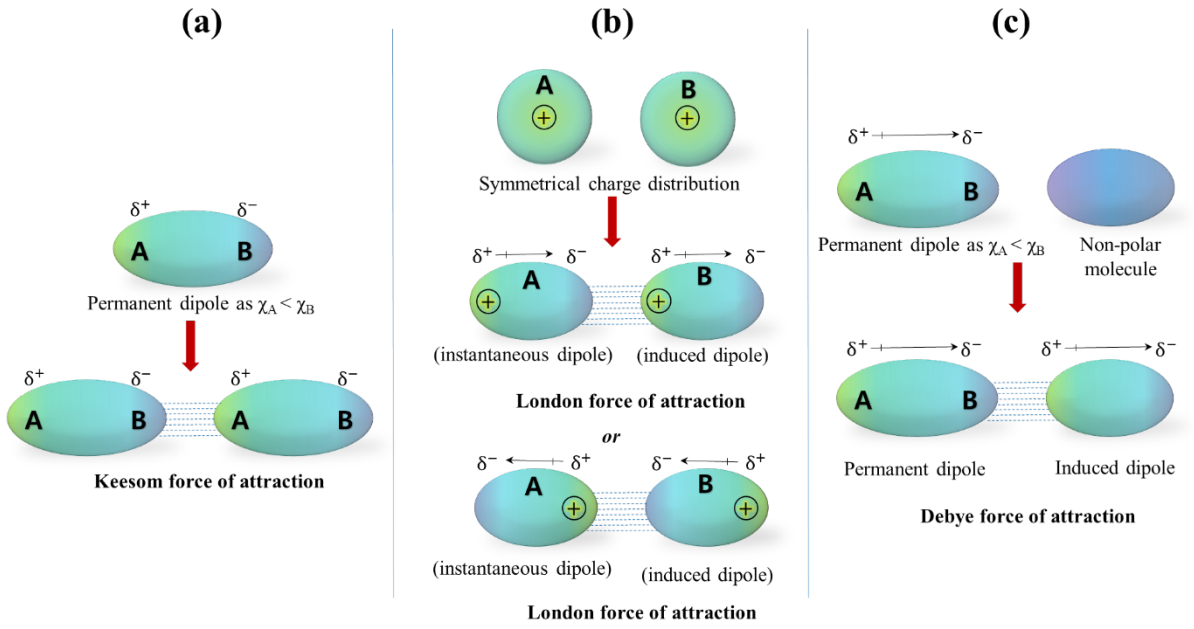

Scheme 2. A schematic diagram of the various vdW forces: (a) Keesom force, (b) London dispersion force. (c) Debye force.

Ohara et al. showed that vdW-type dispersion attractions between NCs result in ordered gold NCs [65]. In an organic solvent, polydisperse mixtures of alkylthiol-capped gold NCs crystallise into ordered, size-segregated opals on a TEM grid. They concluded that the resulting structures are formed due to the size dependence of the dispersion interactions. The biggest particles at the centre in this assembly process are surrounded by successively smaller ones because of the unique and intermediate-range of the interactions. Wu et al. demonstrated the transformation of copper nanoclusters (Cu NCs) into ultrathin ribbons by self-assembly process. The dipolar attraction between Cu NCs and the vdW attraction between 1-dodecanethiol (DDT) ligands play an important role in such kind of self-assembly process [60]. The vdW forces

between the hydrophobic ligands and the perovskite NCs core also regulate the self-assembly process that results in the formation of perovskite SLs [66,67].

2.2. Brownian force

In 1827, biologist Robert Brown discovered the phenomenon of random and continuous motion of colloidal particles suspended in a medium. This phenomenon is triggered by momentum transfer due to the thermal activities of the particles in the suspending medium. Brownian motion is the driving factor for the diffusion and collision of particles, and thus, it intrinsically influences the ordering process during particle self-assembly [68] (**Scheme 3**). The thermal motion provided by the thermal energy is an arbitrary process that can prevent self-assembly if the kinetics due to the thermal energy become equivalent to, or surpass, these assembly forces. The diffusion and collision of particles through Brownian motion are the driving factors that intrinsically affect the ordering process during molecular self-assembly [69,70].

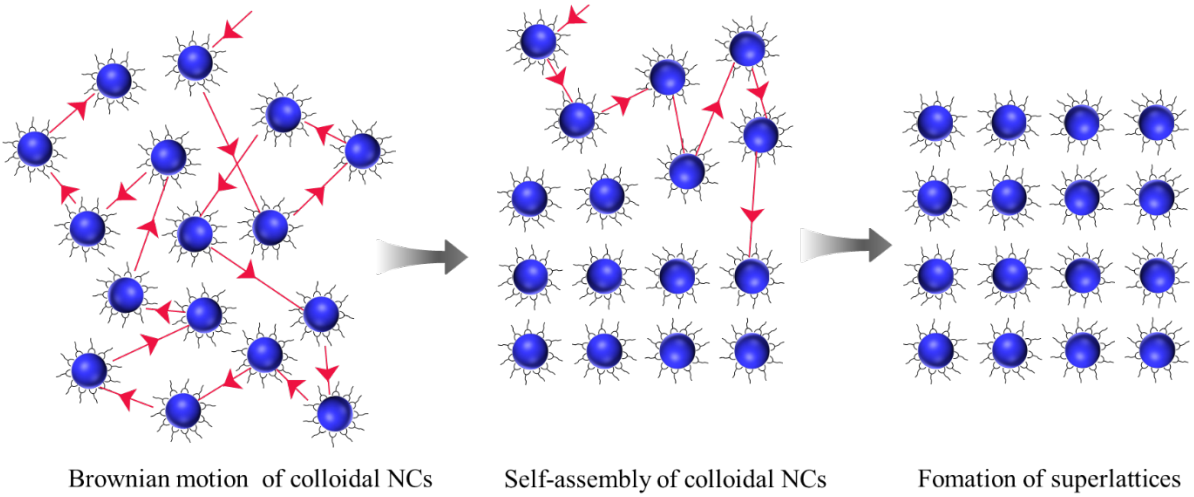

Scheme 3. A schematic diagram of the Brownian motion of colloidal NCs and formation of SLs via self-assembly colloidal NCs.

Many approaches for using spontaneous nanoscale self-assembly have been devised with great success thanks to the considerable influence of Brownian motion. When the size of the components in a system increases, gravity becomes more powerful and can override Brownian forces, resulting in partial self-assembly and the generation of non-organized materials [51]. Dang et al. reported the conversion of ordered $CsPbBr_3$ nanoplatelets into disordered nanotiles. Initially, they synthesized an ordered structure of self-assembled $CsPbBr_3$ nanoplatelets.

However, after few months, their size increased due to self-assembly, and then the free Brownian motion of the larger particles became restricted and eventually, disordered mosaic-like nanotiles appeared [71]. Since, larger non-Brownian particles are less likely to form crystalline arrays on their own, an external driver should be used as a "thermalizing force", thereby, inducing particle motion and crystallization.

2.3. Steric force

Steric effects occur because each atom in a molecule inhabits a specific amount of space. Overlapping of electrons clouds occur when atoms are brought significantly close, affecting the preferred assembly and reactivity of the molecule. When atoms in a molecule get too close together due to molecular vibration or rotation, electric repulsion between their electrons can hinder certain conformations and favour others. This phenomenon is known as the steric effect. This effect can lead to conformations in which repelling forces are minimized, and thus, the molecule becomes stable by reducing its potential energy. Attractive interactions in particles may accumulate strongly, preventing ordered self-assembled structure. Therefore, resisting attractive interactions with softer repulsive forces can empower controlled self-assembly [72,73]. One common approach to control the self-assembly of particles using electrostatic repulsions between like-charged elements can be modified by changing the ionic strength of the solvent molecule. Miszta et al. showed how monodisperse colloidal octapod-shaped self-assembly of NCs (CdSe core and CdS arms) occurs in an appropriate solution environment [74]. They demonstrated that octapod-shaped colloids have steric hindrance that limits the assembly of particles into intercalated chains that self-assemble into three-dimensional superstructures. Furthermore, Grzelczak et al. showed that the combination of attraction and steric hindrance transform gold nanodumbbell building unit into cross-like dimers, with appropriate relative orientation and interparticle distance [75]. The directional interactions between particles can be improved by steric hindrance leading to well-defined self-assemblies [75,76].

2.4. Capillary force

Capillary force is an interaction phenomenon occurring at the interfaces of solid, liquid, and air phases (**Scheme 4)**; it depends on the interaction between liquids and particle surfaces. The capillary bridge between two particles is formed by the liquid phase. It results in capillary forces, which can be repulsive or attractive, depending on the property of the capillary bridge:

convex or concave. This attractive force causes the three-dimensional self-assembly of particles. Attractive force may arise from the overlap of perturbations (menisci) formed around the two separate particles, resulting in a lateral capillary force between them. The lateral capillary forces can be attractive or repulsive, depending on the similarity or dissimilarity of the overlapping menisci formed around the two particles. The attractive lateral capillary forces are significant driving force of two-dimensional self-assembly (aggregation) and ordering of particles on a relatively broad length scale [77,78]. Self-assembly driven capillary forces have emerged as an efficient approach for large-scale manufacturing of various advanced materials with novel electrical, mechanical, optical, adhesion, and wetting properties. Capillary force is often negligible on macroscopic structures. However, surface capillary forces are the prevalent force that induces deformation in structures at small scales [79]. Gracias et al. developed a new self-assembling process of self-folding based on surface tension to fabricate patterned 3D components from 2D precursors [80]. Furthermore, Zhou et al. showed the capillary force-based single-crystalline colloidal gold nanoprisms and concave nanocubes through templated self-assembly process [81]. Ciszek et al. suggested that the combination of templating and capillary forces is virtually scale-independent and is effective for inter-rod spacing [37]. They demonstrated that the two-segment gold-polypyrrole nanorods are assembled into kinetically controlled superstructures.

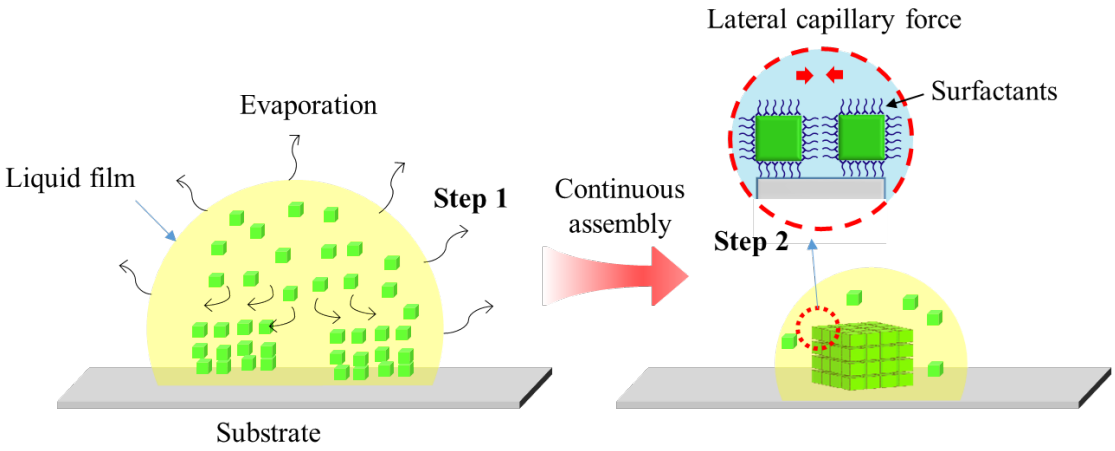

Scheme 4. A schematic diagram of the self-assembly of NCs through capillary forces. Transfer of the NCs from solution to the surface of the substrate via convection (step 1) and then self-assembly of the NCs in an ordered arrangement under the influence of lateral capillary forces (step 2).

2.5. Hydrogen bonding interactions

Hydrogen bonding interactions commonly arise when a hydrogen atom is located between a pair of other atoms with high electron affinity. Such interactions are weaker than an ionic or covalent bond but slightly more effective than vdW forces. Average hydrogen bonds have energies in the range of – 0.2 to – 40 kcal mol^{-1} based on the solvent nature [82]. The density of surface anchoring groups (–OH, –COOH, or $–NH_2$) determines the strength of hydrogen bonding interactions between nanoparticles. The best example of hydrogen bonding interactions is the self-assembly of DNA, where hydrogen-bonded base pairs of DNA double helix combine to provide excellent stability to the structure [83,84]. Brown et al. showed robust self-assembly of $CsPbBr_3$ NCs using extensive inter-ligand hydrogen bonding forces of octylphosphonates (OPA) (**Scheme 5**)[85]. OPA binds with unsaturated Pb^{2+} ions through P-O^- whereas P=O and P-OH groups remain free to form inter-ligand H-bonding which can help in building a robust hydrogen-bonded octylphosphonate network through self-assembly process.

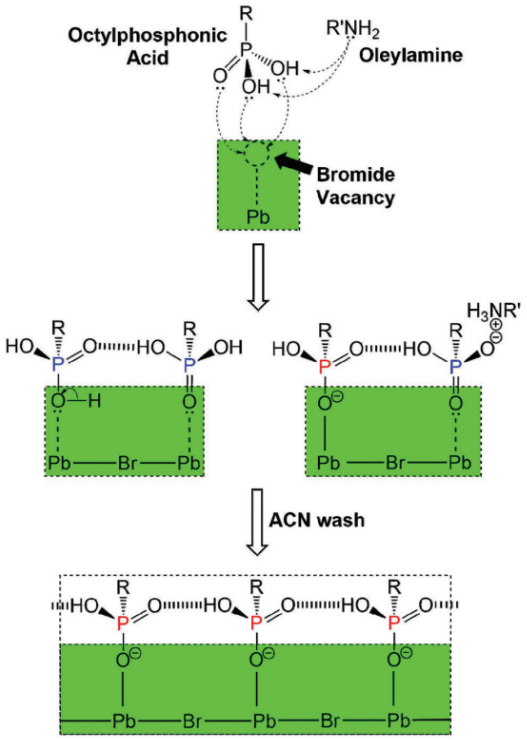

Scheme 5. Schematic diagram of octylphosphonic acid ligands bonding to $CsPbBr_3$ NCs (R = octyl, R' = oleyl). The Pb–Br–Pb linkages are corner sharing $[PbBr_6]^{4-}$ octahedra of the perovskite lattice. Reprinted with permission from Ref [85].

The polymer with a large number of hydroxyl group, such as poly(vinyl alcohol) (PVA), can form directional hydrogen-bonds through the polar hydrogen and electronegative ion groups. Xiangyue et al. fabricated a highly stable and efficient $FASnI_3$-based solar cells by adding PVA to the $FASnI_3$ precursor solution [86]. PVA introduces hydrogen bonding with $FASnI_3$, affecting the crystalline rate, reducing the trap states, and suppressing the migration of iodide ions. Li et al. improved the performance and stability of $CH_3NH_3PbI_3$ perovskite by modifying the surface by spin-coating its precursor solution in the presence of butylphosphonic acid 4-ammonium chloride [87]. The additive acts as a crosslink between neighbouring grains in the $CH_3NH_3PbI_3$ perovskite structure through robust hydrogen bonding between $–PO(OH)_2$ and $–NH_3^+$ terminal groups of the perovskite surface. Additionally, Li et al. showed strong hydrogen bonding interaction of fluoride ions with triple-cation perovskite $(Cs_{0.05}FA_{0.54}MA_{0.41})Pb(I_{0.98}Br_{0.02})_3$ for stable solar cells [88]. They reported a certified power conversion efficiency of 21.3% in a device based on triple-cation perovskites. Molecular proton donors such as chloroform and dichloromethane also play an important role in tuning the optical properties of self-assembled perovskite microcrystals. Rogach *et al.* reported the 2D Dion–Jacobson (DJ) phase of $ODASnBr_4$ (ODA = 1,8-octanediammonium) perovskite microcrystals that showed improved crystallinity and photoluminescence quantum yield (PL QY) in chloroform ($CHCl_3$) and dichloromethane (CH_2Cl_2). This is attributed to the formation of hydrogen bonds between the perovskite lattice and the C-H protons of $CHCl_3$ and CH_2Cl_2 [89].

2.6 Hydrophobic interaction

Hydrophobic interaction plays an important role in biological systems, especially in the formation of lipid bilayers. It has also been observed in colloidal NCs. Mixing surfactant-capped hydrophobic NCs and oil droplets can lead to the formation of self-assembled 3D colloidal crystals during the emulsification process, which is attributed to the hydrophobic effect of surfactant. Polystyrene coated-Au nanorods can also undergo solvent-mediated self-assembly phenomenon due to the hydrophobic effect of the polymer. Recently, León et al. explored the breath figure (BF) approach, involving self-assembling $CsPbBr_3$ NCs distributed evenly within a hydrophobic polymer matrix but preferably enclosed within pore spaces (**Fig. 1**). BF is a well-known technique for producing well-ordered honeycomb-patterned surfaces with regulated topography and composition in a single step [90]. The majority of surfaces patterned by using BF approach comprise polymers, copolymers, or blends. However,

nanoparticles or metal ions can be embedded in high molecular weight polymers to produce hybrid materials [74,91]. León et al. used amino-terminated polystyrene (PS-NH_2) to create well-ordered pores. The surface of the $CsPbBr_3$ NCs was passivated by using oleylamine (OAm), which has a hydrophobic moiety comparable to PS-NH_2, but also a hydrophobic chain that prevents the formation of well-ordered porous structures. During the formation of thin films, PS-NH_2 is driven towards the interface of pores created by its large hydrophobic block (PS), and the hydrophobic interactions allow the creation of honeycomb-like porous structures through BF.

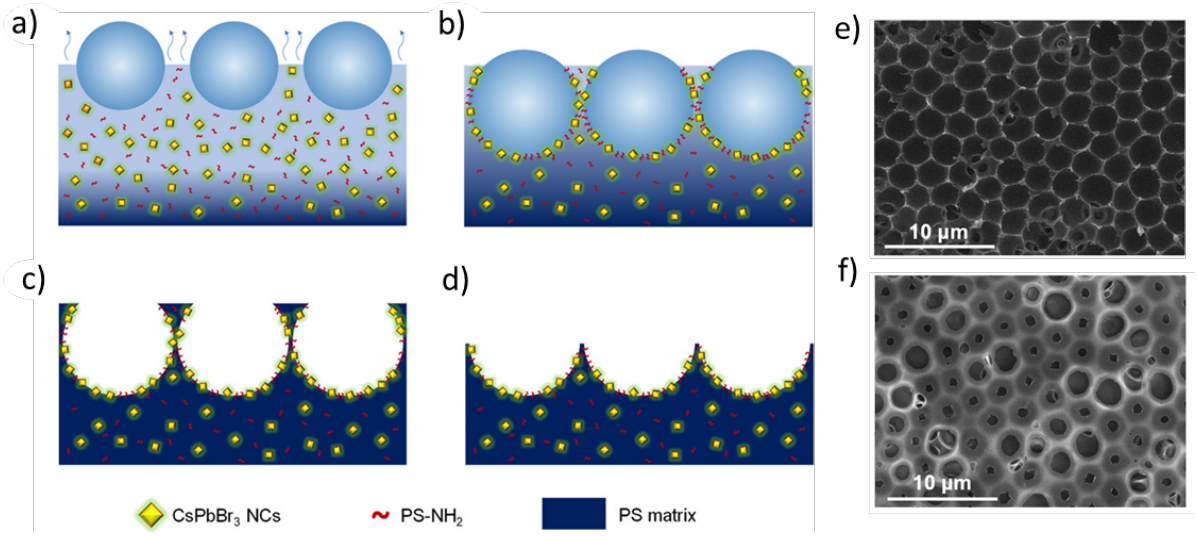

Fig. 1. The self-assembly of $CsPbBr_3$ NCs in a micro-patterned polymeric surface via hydrophobic interactions. (a) Formation of micron-sized water at the air-liquid surface due to the fast evaporation of $CHCl_3$. (b) Migration of PS-NH_2 and $CsPbBr_3$ NCs towards the $CHCl_3$–water interface, thereby stabilizing the condensing water droplets in a well-ordered honeycomb pattern. (c) Formation of a porous surface after completely evaporating off of $CHCl_3$ and water. (d) A pincushion-like surface after peeling with Scotch tape. SEM images (e) before and (f) after peeling. Reprinted with permission from [92].

There have also been several reports concerning the formation of well-ordered $CsPbBr_3$ NCs passivated by a large amount of long-chain alkyl ligands such as oleylamine (OAm) and oleic acid (OA). Hydrophobic interactions between the tail parts of the alkyl ligands play a critical role in the self-assembly of the NCs by keeping the NCs at a specific distance. Interestingly, the interparticle spacing among these NCs was revealed to be 2 nm, which matches the lengths of both OAm and OA [92,93].

3. Self-assembly on different scales

A natural mechanism, either thermodynamic or kinetic, can expand self-assembly further. Atomic, molecular, and interfacial self-assemblies are included in the first category, whereas colloidal and certain interfacial self-assemblies are included in the second one. Molecular, colloidal, and interfacial self-assemblies are examples of random self-assembly processes. Others, such as atomic and biological self-assemblies, have some degree of directionality [54,94–96]. Colloidal self-assembly process can be modulated by external stimuli such as electric field, magnetic field, gravity, flow, and so on. The spontaneous self-assembly occurs in a wide range of length scales, from angstrom to millimetre (**Scheme 6**). Repulsive forces have been seen in the interactions of different colloidal particles. The interaction of molecules or colloids with different charges, or with the same charge but separated by a small distance, or between zwitterionic molecules and colloids can cause an attractive attraction. The coordination bond is a strong chemical connection in comparison to the other forces, yet it can act as an attractive force in supramolecular self-assembly.

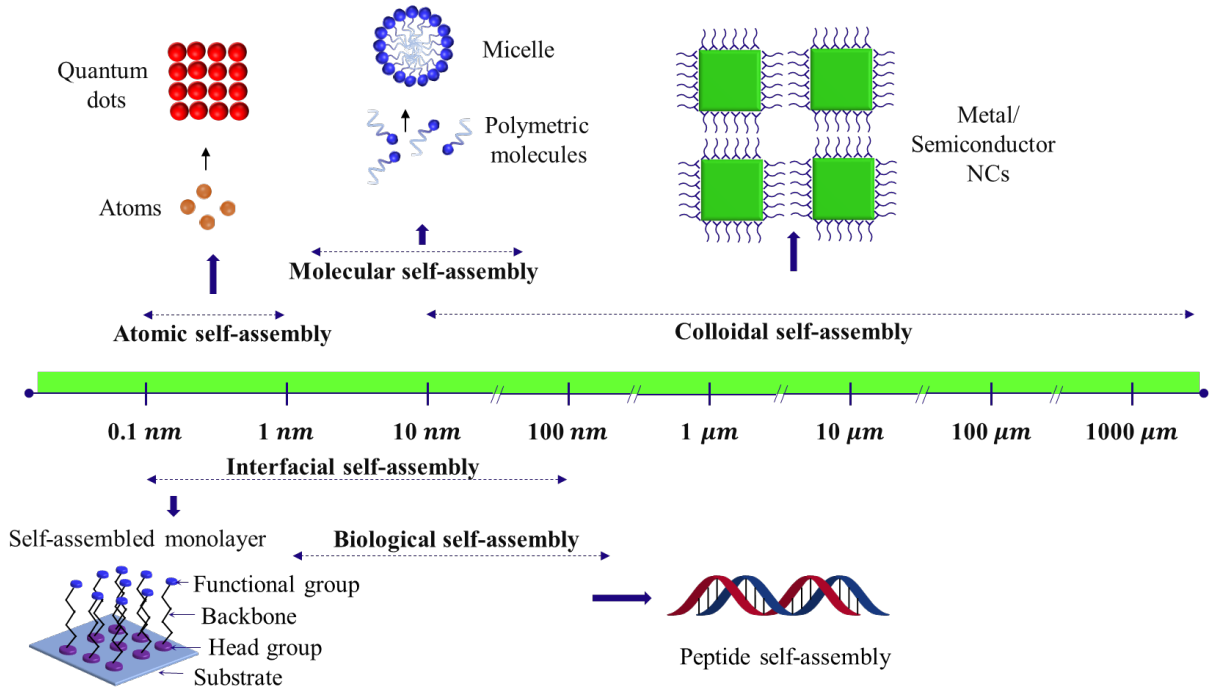

Scheme 6. A schematic diagram of atomic, molecular, colloidal, biological, and interfacial self-assemblies at different scales. The scale also applies to the building units.

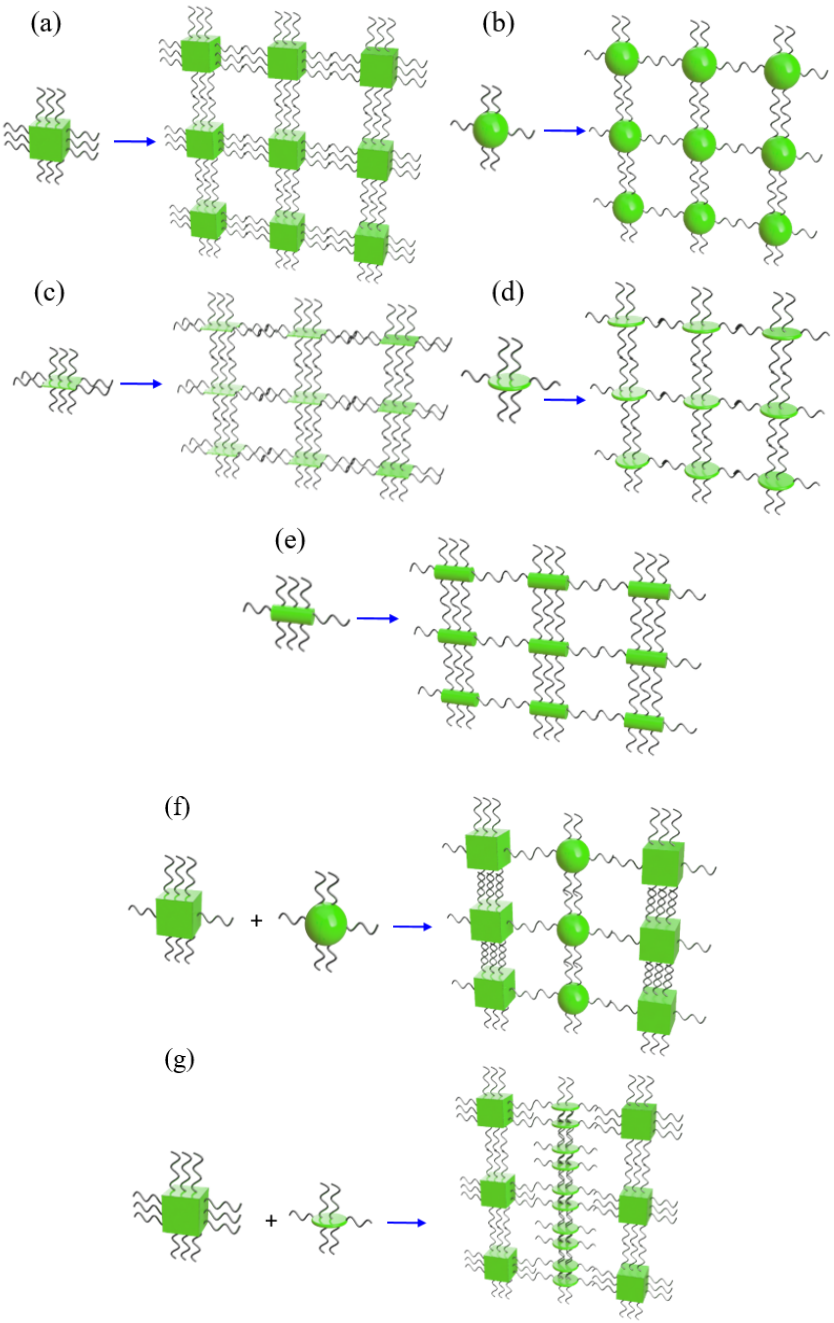

Scheme 7. Schematic representation of different units for perovskite self-assembly. Monocomponent self-assembly of (a) nanocubes, (b) quantum dots, (c) nanoplates, (d) nanodisks, (e) nanorods. Multicomponent self-assembly of (f) nanocubes and quantum dots, (g) nanocubes and nanodisks.

4. Different units for perovskite self-assembly

Self-assembly of NCs has been observed for various morphologies e.g., nanocubes, quantum dots, nanoplates, nanodisks, nanorods, and so on. Based on the self-assembly of NCs, we can

classify the self-assembly as (a) monocomponent (one type of NCs) self-assembly, and (b) multicomponent (various types of NCs) self-assembly (**Scheme 7**). Most of the self-assemblies of perovskite NCs are reported with monocomponent perovskite NCs. For generating multicomponent self-assembly, Kovalenko et al. applied a variety of multi-nanocrystals ABO_3, NaCl, and AlB_2-type SLs, including spherical Fe_2O_3, spherical $NaGdF_4$ NCs, and truncated-cuboid PbS NCs, and cubic $CsPbBr_3$ NCs. Cubic NCs, unlike spherical NCs, adopt many orientations within the unit cell, making the production of multicomponent SLs difficult [97]. Cherniukh et al. recently reported the formation of binary SLs from steric-stabilized $CsPbBr_3$ nanocubes and disk-shaped LaF_3 NCs via self-assembly, yielding six columnar SLs [98].

5. Different parameters and approaches for self-assembly of perovskite nanocrystals

The formation of well-ordered self-assembled perovskite nanostructure crystal from colloidal nanoparticles has attracted a good deal of attention. However, different essential parameters, such as solvent, temperature, pressure, light, and template, need to be considered whilst fabricating various ordered architectures of perovskites; they are summarised in the following section (**Scheme 8**).

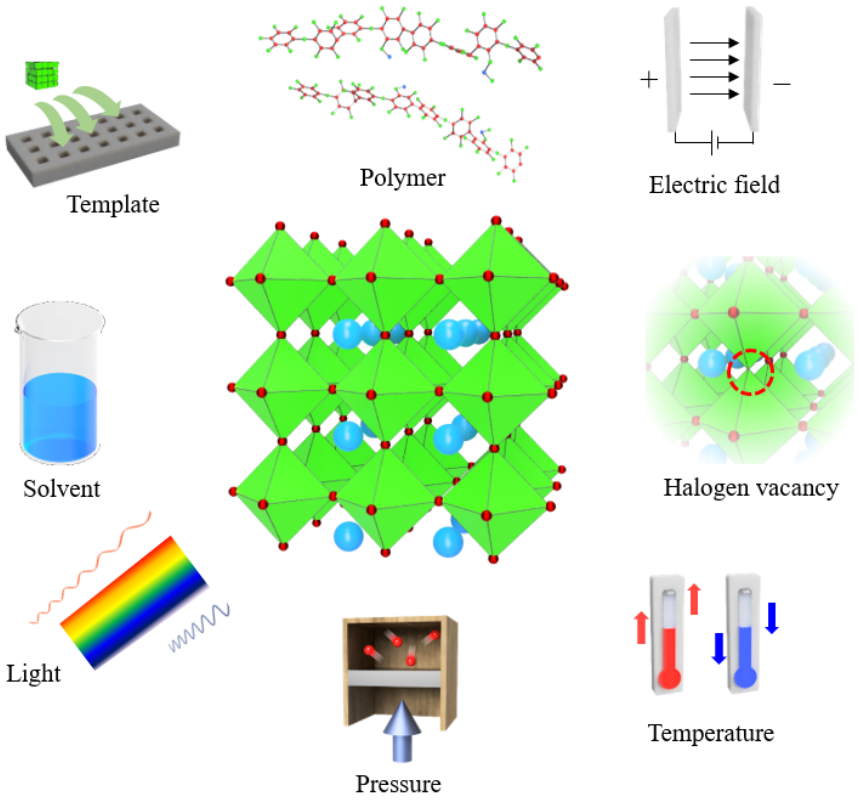

Scheme 8. Different parameters and approaches for self-assembly of perovskite NCs.

5.1. Solvent-assisted self-assembly

The solvent and its polarity play a crucial role in forming a well-organised crystalline nanostructure due to its ligand-solvent and ligand-ligand interactions. The monodispersity of NCs also plays an important role in organising the three dimensional (3D) superlattices (SLs). Kovalenko et al. synthesised 3D SLs of cubic-shaped $CsPbX_3$ (X = Cl, Br) NCs by solvent evaporation technique [3] (**Fig. 2**). Monodispersed cubic-shaped 9.5 nm-sized $CsPbBr_3$ NCs in toluene were spread onto the silicon substrate kept in a Teflon well.

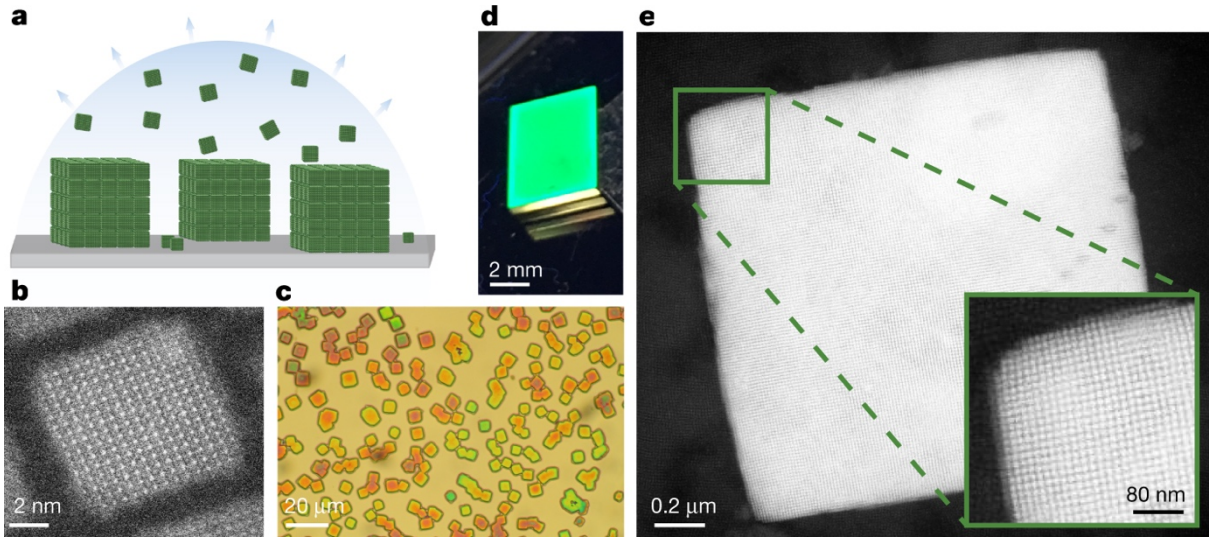

Fig. 2. (a) Solvent drying-mediated self-assembly phenomenon of $CsPbBr_3$ NCs. (b) High-angle annular dark-field scanning transmission electron microscopy (HAADF–STEM) image of a single $CsPbBr_3$ NC. (c) Optical microscopy image and (d) Green fluorescence image of 3D SL ((illuminated UV light). (e) HAADF–STEM image of a SL of $CsPbBr_3$ NCs. Inset: enlarged view of the marked area, exhibiting the individual NCs. Reprinted with permission from Ref. [3].

A glass slide was placed over the well, and the toluene was to gently evaporated. Micrometre-sized 3D SLs of $CsPbBr_3$ NCs formed after the toluene had completely evaporated. Individual cuboidal SL domains contain up to a million NCs. Soetan et al. reported the formation of 1D $CsPbBr_3$ NCs using non-polar solvent (hexane), in which solvent-ligand interactions play an important role [66]. However, the formation of 2D assemblies of NCs was observed when they were purified using low-polar solvents, such as toluene and ethyl acetate. The synthesised 1D $CsPbBr_3$ NCs get redshifted in absorbance and photoluminescence. This indicates that some

additional aliphatic ligands are leftover during purification of the NCs due to the hydrophobic effect, and other alkyl ligands are interconnected through the vdW force. The depreciation of repulsive forces between the solvent and ligands take place in short-range 2D assemblies in low-polar solvents, such as toluene and ethyl acetate, compared to non-polar solvent [99]. Previously, Pt nanocubes also show a solvent-assisted self-assembly (SA) phenomenon. Quan et al. reported Pt nanocubes that self-assemble into a simple cubic superstructure in toluene and a body-centred tetragonal superstructure in hexane [100]. These solvent-ligand interactions present innovative information to further understand the systematic fabrication and characterisation of the mechanisms involved the self-assembly of various nanoparticles [100]. Theoretically, the coupling energy between cubic NCs is three times larger than that between spherical ones [101]. The investigation of colloidal NCs SLs does not only reveal the role of organic ligands in directing self-assembly processes, but it may also lead to the discovery of novel, controllable collective features from nanocube ensembles. Pradhan et al. reported the formation of long ~12 μm and 1.2 nm thinnest self-assembly of $CsPbBr_3$ plates using Cs precursor reacting with oleic acid at room temperature [102]. Moreover, they studied the influence of oleic acid-amine on the fabrication of $CsPbBr_3$ plates. Successive formation of long-range self-assembly by tunning the oleic acid concentration with reaction time and the live ongoing reaction was monitored using optical microscopy and electron microscopy. Additionally, the uniqueness of this self-assembly was preserved in solution. This provided a new avenue for room temperature nanostructure formation, leading to the self-assembly of nanoplatelets. Recently, all-inorganic halide perovskite NCs film has been used directly in optoelectronics applications due to their inexpensiveness, direct band gaps, photoluminescence yield, and colour emission. However, unavoidable solvent-surfactant interactions during the fabrication of the films damage their properties, making device fabrication challenging. Hence, the first priority is to find a suitable solvent to fabricate self-assembled perovskite NCs for optoelectronic applications. Various solvents with different polarities were used to fabricate $CsPbBr_3$ NCs film for light-emitting diode (LED) applications. The influence of solvent-assisted surface engineering techniques on morphology and their optoelectronic properties were examined. The thin film fabricated with processed solvent is uniform, smooth, and favourable for charge transport. Moreover, photostability, external quantum efficiency (EQE), luminance, and power efficiency of the fabricated film were improved compared to unassembled $CsPbBr_3$ nanoparticles [103]. Babu et al. proposed a new method for tuning the self-assembly of $CsPbBr_3$ from nano to micro size using various simple antisolvents at room

temperature and normal atmosphere [104]. They explored the influence of antisolvents on the reprecipitation of $CsPbBr_3$ perovskite nanocubes to microcubes. They used approximately ten anti-solvents to reprecipitate the $CsPbBr_3$ NCs; Perfect cubic-dimensional microcrystals could be produced from tetrahydrofuran (THF) solution. Additionally, the physical properties and size of these microcubes are superior to others reported previously in the literature. Moreover, unusual self-assembly of $CsPbBr_3$ nanocubes morphology was observed in DCM solvent. Additionally, various cubes and self-assembled cube morphologies show excellent stability at room temperature. This simple method provides an innovative platform to fabricate various shapes and sizes of nanocrystal and is highly useful for different applications, such as LEDs, photodetectors, and biosensing [104].

In a similar manner to Pt NCs, gold nanoparticles (Au) functionalised with hexalkoxy-substituted triphenylene (TP) as a discotic molecule (Au-TP) also exhibit solvent-mediated self-assembly phenomena. The structure of Au-TP can easily be controlled using solvent polarity (methanol-toluene). The gold nanoparticles surrounded by organic ligands experience increasing π–π interactions between the neighbouring TP ligands on a particle surface when solvent polarity is increased by adding methanol quantity. This leads to the formation of self-assembled, 1D, or hexagonal closed packed (hcp) structures of Au-TP [105]. Nie et al. investigated self-assembly of inorganic nanoparticles using hydrophobic polymer chains and amphiphilic ABA triblock copolymers [106]. Solvent-based side-by-side self-assembly can also modify the hydrogen bonding interactions between Au-tipped CdSe nanorods [107]. The samples were dispersed in DCM to observe the influence of the interaction between the thymine group on the carbon nanotubes. The non-competitive solvent cannot generate H-bonding interactions. However, H-bonding interactions were observed when similar experiments were performed in dipolar aprotic solvent dimethylformamide (DMF) [108]. The shape property can also be utilised in combination with solvent. Gold nanorods have been self-assembled in DMF/THF water mixtures via hydrophobic interaction initiated by modifying water volume portion, leading to the formation of a dimer, chainlike structures or spherical aggregates formed from gold nano dumbbells by adding water to the THF/DMF mixture [109].

5.2. Light-induced self-assembly

Light can alter the physical and optical properties of materials. Even, it can initiate physical and chemical reactions [110]. Similarly, halide perovskites are sensitive to light that can change their structure and properties. The photo-induced structural variation of halide perovskites

represents an important issue from both fundamental and practical perspectives. However, the fabrication of perovskite NCs using light remains largely unexplored due to their poor stability under UV-light illumination [111].

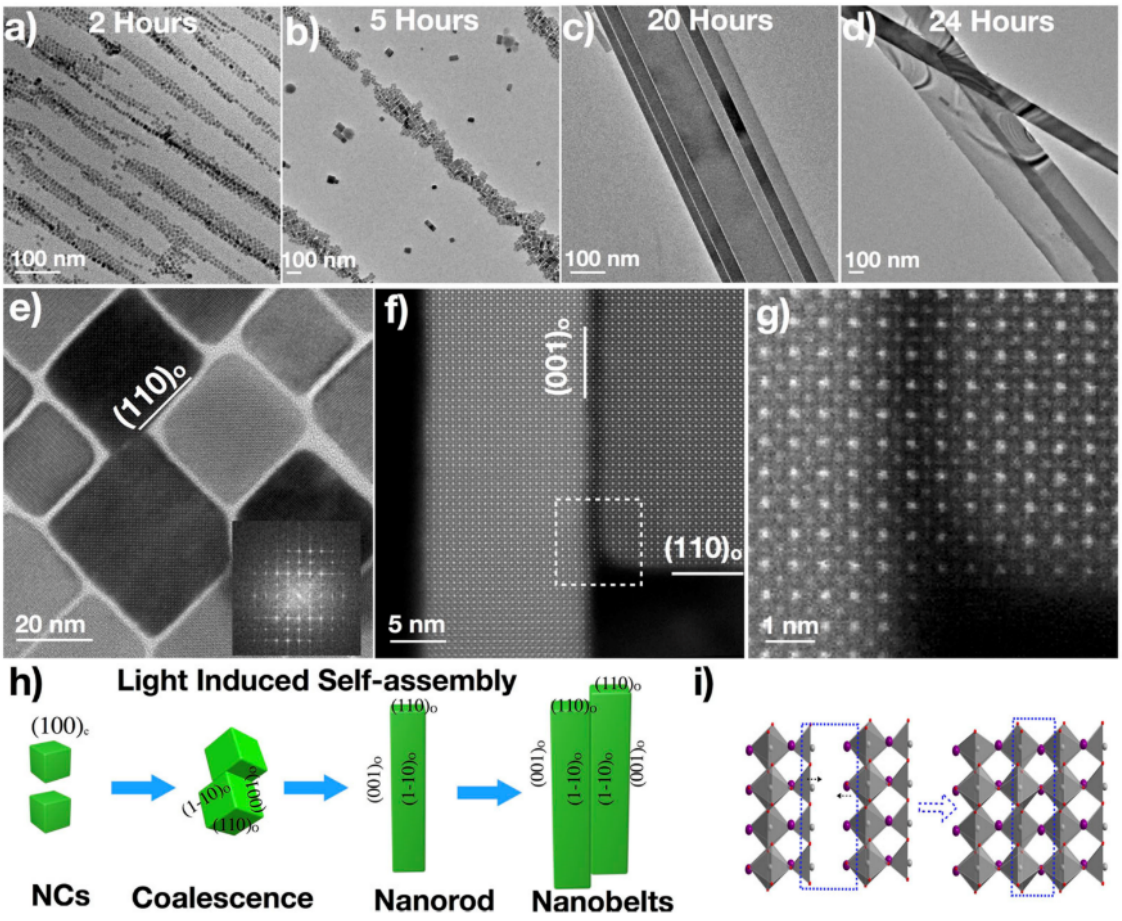

Fig. 3. (a–d) Formation of 1D $CsPbBr_3$ NWs under visible light. Time: (a) NCs (2 h), nanorods (5 h), (c) NWs (20 h), and (d) NWs (24 h). (e) HRTEM images of intermediate $CsPbBr_3$ NCs (after 5 h of illumination) merging along the $[110]_o$ plane. Inset: FFT patterns. (f) HAADF-STEM image of nanorods along the $[1\bar{1}0]_o$ plane, (g) enlarged selected area of (f). (h) Schematic diagram of transformation of $CsPbBr_3$ NCs to nanorods to NWs. (i) Diagram for fusion of CsBr- and $PbBr_2$-terminated $(001)_o$ planes. Reprinted with permission from Ref [112].

Recently, Liu et al. investigated the growth of $CsPbBr_3$ NWs from cubic NCs in the presence of visible light [112]. A solar simulator with an intensity of 1.7 suns (170 mW/cm^2) was employed for driving the self-assembly of $CsPbBr_3$ NCs. Defect-free NWs were spontaneously produced by assembling and fusing individual cubic $CsPbBr_3$ NCs under visible light (**Fig. 3**). They systematically investigated the shape evolution of $CsPbBr_3$ NCs with illumination time.

The self-assembly of $CsPbBr_3$ NCs was occurred via the light-induced removal of surface ligands, i.e., oleic acid (OA) and oleylamine (OAm). The removal of surface ligands releases steric repulsion between adjacent NCs. An anisotropic environment resulting from the carboxylate-rich ligand shell aids in the development of NWs. These NWs showed higher lifetime (~125 ns) than the initial precursor NCs (~2 ns). Surprisingly, the initial cubic NCs do not grow via isotropic coalescence. An anisotropic linear growth mechanism through direct attachment was followed and the cubic phase transformed to orthorhombic phase during the conversion. The NWs grow along the $[110]_0$ plane. Wang et al. reported photon-driven conversion (PDC) of $CsPbBr_3$ nanoplatelets to bulk analogue. A few-monolayer $CsPbBr_3$ nanoplatelets were transformed into bulk analogue under laser irradiation within few minutes [113]. The lamellar self-assembly can be done using low laser intensity of 20 mW cm^{-2}. Krahne et al. reported a heat-up and large-scale synthesis method of blue-emitting $CsPbBr_3$ nanoplatelets (NPLs) that converted into stacked lamellar structures through self-assembly process [114]. The morphology and the optoelectronic properties of such films can be tuned by UV-light, transforming the self-assembled stacks of NPLs into SLs, such as square-shaped disks and nanobelts. Perovskite NCs with weaker interparticle interactions assembled by visible light can provide insights into the growth kinetics, assembly mechanisms, and surface ligand chemistry of highly ionic perovskite NCs.

5.3. Templated self-assembly

Liarte et al. reported the colloidal $CsPbBr_3$ nanocubes prepared by ligand-assisted ultrasonication. These nanocubes were used for the fabrication of 2D photonic crystals (**Fig. 4)** [115]. A pre-patterned polydimethylsiloxane(PDMS) template was used for growing $CsPbBr_3$ NCs (10 nm) into 2D photonic crystals of large area (1 cm^2) following template-induced self-assembly. The dimension of the PDMS template controls the lattice parameters of these crystals. Crystals with lattice parameters ranging from 1700-400 nm have been successfully fabricated. In addition to template dimension, concentration and viscosity of the $CsPbBr_3$ NCs play a vital role for developing 2D photonic crystals. Pan et al. reported a templated self-assembly process for achieving 1D SLs of $CsPbX_3$ NCs arrays inside a pod-shaped lead sulphate scaffold, in which NCs are uniformly distributed with interparticle spacing of 2.2 nm (**Scheme 9)**. This is attributed to the host-guest like supramolecular interactions between lead sulphate and $CsPbX_3$ NCs. The stability of these SLs are strongly solvent-dependent. When dispersed in highly polar

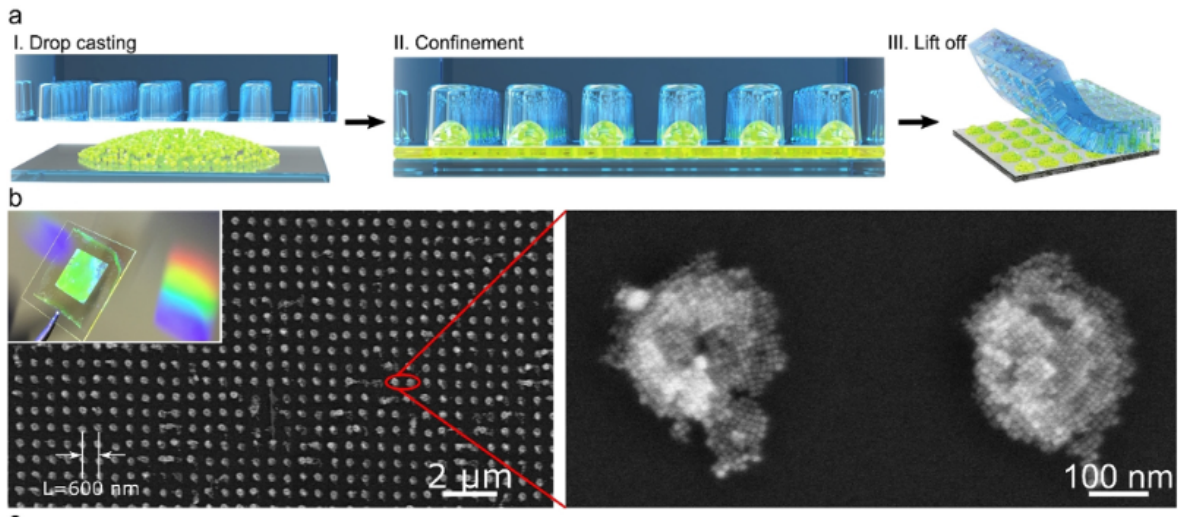

Fig. 4. a) Schematic diagram of PDMS template-assisted growth of 2D photonic perovskite supercrystals. b) SEM images of supercrystals made of $CsPbBr_3$ arrays. The inset in (b) $CsPbBr_3$ SC arrays on glass substrates (under white light). Reprinted with permission from [115].

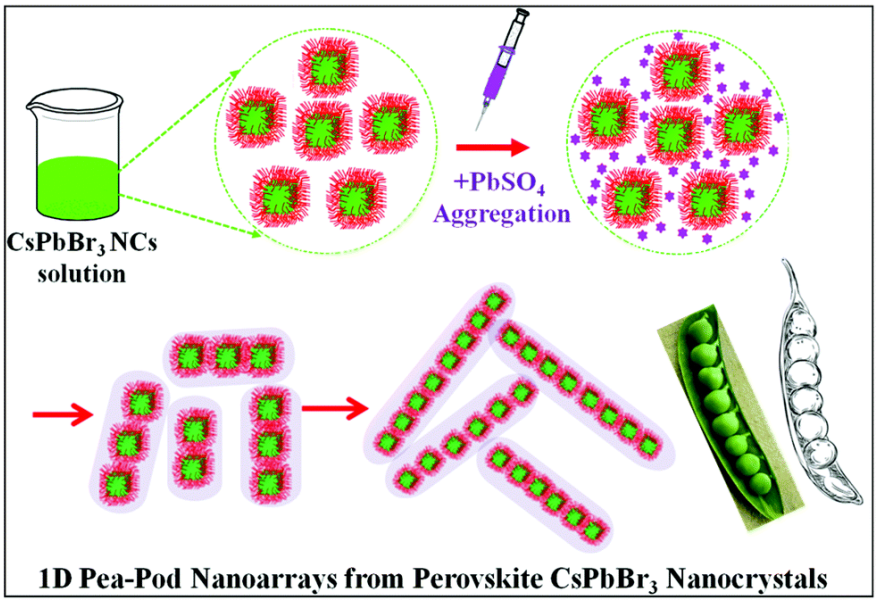

Scheme 9. a) Schematic diagram of 1D pea-pod like arrays of $CsPbBr_3$ NCs embedded in $PbSO_4$ shell. Reprinted with permission from [116].

solvents like $CHCl_3$ and THF, the 1D superlattices dissociate into random combinations of perovskite NCs and $PbSO_4$ clusters due to higher solubility of perovskite precursors, whereas the reverse phenomenon was observed by adding hexane due to poor solubility of those precursors. Adjusting the size and shape of the NCs using a variety of halide compositions can

further alter the geometric configurations of these SLs. The wide utility of this innovative self-assembly technique would allow 1D self-assembled SLs to be used as a platform for both basic and applied research. In order to analyse the self-assembly of $CsPbX_3$ NCs, a halide-free solvent must be used [116].

5.4. Pressure-driven self-assembly

Pressure provides a powerful way to study the structural, physical, and electronic behaviour of metal halide perovskite (MHP) materials. 2D perovskite nanosheets (PNSs) have received significant interest due to the advantage of the perovskites and the 2D structural properties. The self-assembly of many metal halide perovskite nanostructures with potential optoelectronic properties has not yet been demonstrated

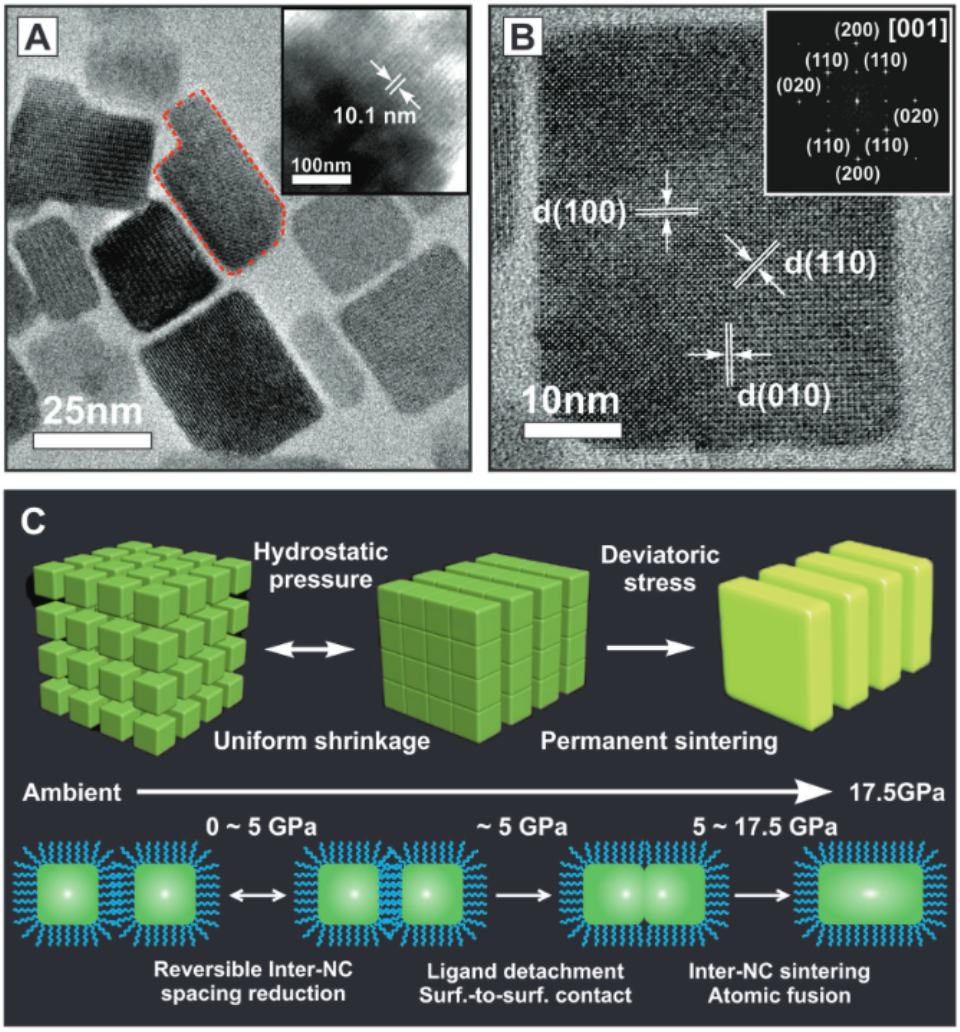

Fig. 5. The pressure-induced formation of $CsPbBr_3$ SLs from $CsPbBr_3$ nanocubes. (a) A TEM image of SLs and inset: the lamellar structure before disassembly. (b) A TEM image and

associated FFTs of compressed $CsPbBr_3$ nanoplates. (c) A schematic representation of the different stages in the formation of $CsPbBr_3$ SLs under pressure. Reprinted with permission from [117].

Significant progress and growth in the pressure response of methylammonium-based lead halide perovskites have been achieved by various groups [118,119]. Recent attempts at the pressure-sintering procedure and band gap modification of $CsPbBr_3$ NCs have highlighted the importance of all inorganic MHP NCs [117,120–127]. Nagoka et al. developed a pressure-induced transformation method for fabricating $CsPbBr_3$ SLs from $CsPbBr_3$ nanocubes (**Fig. 5.**) Up to 5.1 GPa, the nanocubes were shrunk isotropically and reversibly, above this pressure, surface passivating ligands detached from the surface of nanocubes, which were eventually, irreversibly transformed into 2D nanoplatelets by fusing facet-to-facet; this is attributed to the minimization of the surface area in the single cubic phase. In general, $CsPbBr_3$ nanocubes show a d-spacing of approximately 5.8 Å whereas the synthesized SLs show a lattice constant of 12.5 nm (confirming their cubic superstructure) and have better optical properties.

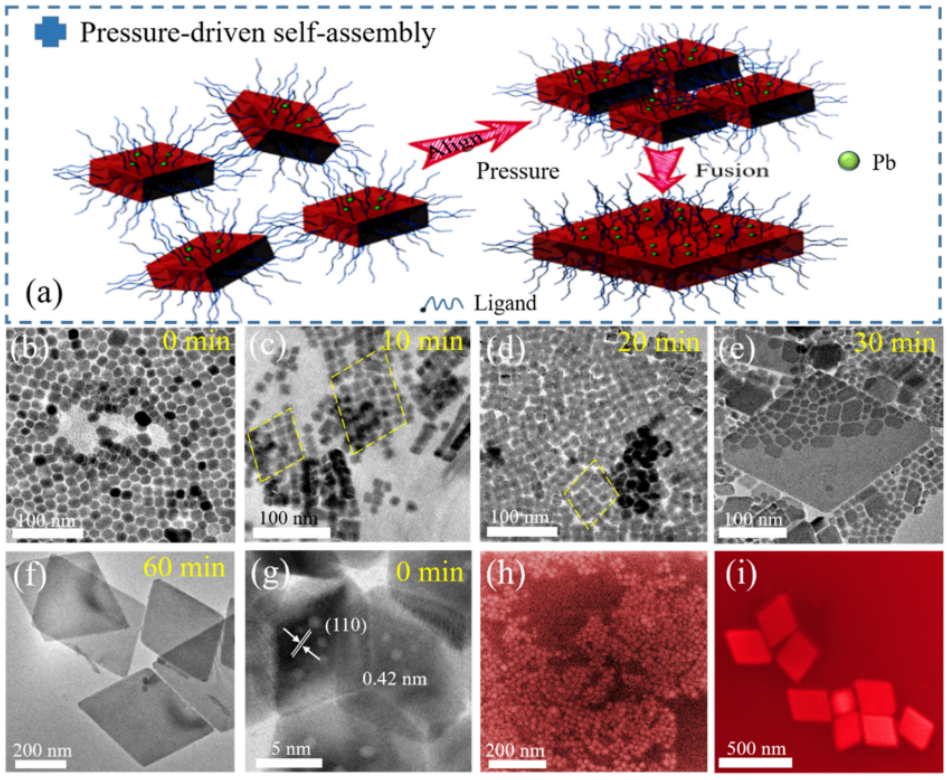

Fig. 6. (a) A schematic of self-assembly of $CsPbBrI_2$ NPs into NPSs under high pressure. (b–i) TEM and SEM images of NPs and PNSs formed under a pressure range of 10 MPa with

variable lengths of time. (b and h) Initial NPs, (c) 2D array (10 min), (d) PNS prototypes (20 min), (e) PNSs (30 min), and (f and i) PNSs (60 min). (g) HRTEM image of initially formed NPs. Reprinted with permission from Ref [128].

Using this method, one can integrate NCs into self-assembled SLs, thereby developing new materials with improved crystallinity, structural stability, and characteristics that can be used in a variety of technologies, including light emitting diodes and solar cells. Ji et al. demonstrated that pressure can produce self-assembled $CsPbBrI_2$ perovskite nanoparticles (NPs) to form 2D PNSs (**Fig. 6**) [128]. Removal of the grain boundaries between single-crystal PNSs and enhanced crystallinity induce the creation of PNSs. In addition, self-assembled PNSs exhibit enhanced PL intensity and excellent chemical stability [128].

5.5. Polymer-assisted self-assembly

Polymeric materials are utilized for fabrication of self-assembled NCs [129]. The assembly of either all-inorganic or hybrid perovskite NCs into superlattices via surface modification is important to understand the intrinsic electronic interaction of these highly ionic NCs. Sardar et al. showed a template-free chemical strategy, in which polymer-passivated $CsPbBr_3$ NCs self-assembled into one-dimensional, individual, and bundled pearl necklaces. They synthesised poly (ethylene glycol) (PEG_6-Y, Y = −COOH, and NH_2)-passivated $CsPbBr_3$ NCs (3 nm diameter). These NCs were transformed into individual pearl necklaces, bundled pearl necklaces (~550 nm in length), close-packed, lamellar, and nanorice assemblies through self-assembly process [130]. Long alkyl chain amines and acids are well-known surfactants for binding with lead and bromide, respectively offering excellent colloidal stability. Interestingly, both amine and acid derivatives of PEG_6 were introduced in synthetic condition and it improved the colloidal stability of perovskite NCs. Three key structural features of these flexible polymers, such as concentration, chain length, and head and tail part, regulate cooperative interactions between individual polymer-capped NCs, allowing for higher-ordered self-assembly. In addition, being a hydrophilic polymer, PEG could better interact NCs in hydrophobic solvents leading intriguing nanostructures via self-assembly process. Post-synthetic ligand treatment was employed to turn individual pearl necklace formations into

lamellar and nanorice structures. This is attributed to dipole-dipole interactions between $CsPbBr_3$ NCs and vdW attraction between surfactants. Generally, long alkyl chain oleyl group forms the most stable inorganic perovskite $CsPbBr_3$ NCs [131]. However, polar solvents are detrimental for their self-assembly as these passivating ligands are highly soluble in a polar solvent due to their ionic nature. In a non-polar solvent, they form clusters due to strong vdW interactions [131]. Therefore, preventing colloidal aggregation from allowing for close-packed monolayer thin films is a difficult task. Garnett et al. developed a method to prevent the colloidal aggregation of $CsPbBr_3$ nanocubes allowing them to form a large-area self-assembly of these NCs. Long-chain alkyl groups (18 carbon chain) attached to the surface of these NCs have been replaced by short-chain thiocyanate (SCN^-)[20]. Short-chain thiocyanate ligands dramatically improve self-assembly by reducing cube-cube interactions. This approach can be used to make ultrasmooth monolayer thin films of perovskite NCs with different morphology. Furthermore, these monolayer films can also be used as a seed layers for fabricating high quality single-crystalline thin films for high-performing optoelectronic devices.

5.6. Temperature-driven self-assembly

Temperature plays a critical role in the self-assembly process of small organic molecules, peptides, and organogels [132]. However, the role of temperature in controlling the perovskite SLs has not been studied extensively. Recently, Arciniegas investigated the transformation of self-assembled $CsPbBr_3$ NPLs into nanobelts into nanoplates, and then nanotiles in bulk solution over a few months at room temperature (**Fig. 7**) [71]. The transformation occurred via a three step mechanism: (1) removal of passivating ligands from the surface of $CsPbBr_3$ NPLs to form nanobelts, (ii) consolidation of nearby nanobelts by oriented attachment for growing more extended nanoplates, (iii) finally, merging of nanobelts and nanoplates, developing mosaic-like broken nanotiles. The aged nanobelts and nanoplates possess less CsBr-rich surface when compared to fresh ones. Oleylammonium ions can replace these Cs^+ ions forming a strong attachment with NCs surface and finally, these large particles self-assembled via oriented attachment. When the temperature is raised, ligand desorption should rise, and when the temperature is lowered, it should decrease. As a result, heating or cooling can be employed to speed up or preserve the qualities of the original NPLs solution. Interestingly, the full transformation from $CsPbBr_3$ NPLs to nanotiles was also observed after heating the solution at 110 °C for 30 min as the desorption occurred at a much faster rate at higher temperature. This

observation indicates that this type of transformation can be expedited by controlling the temperature.

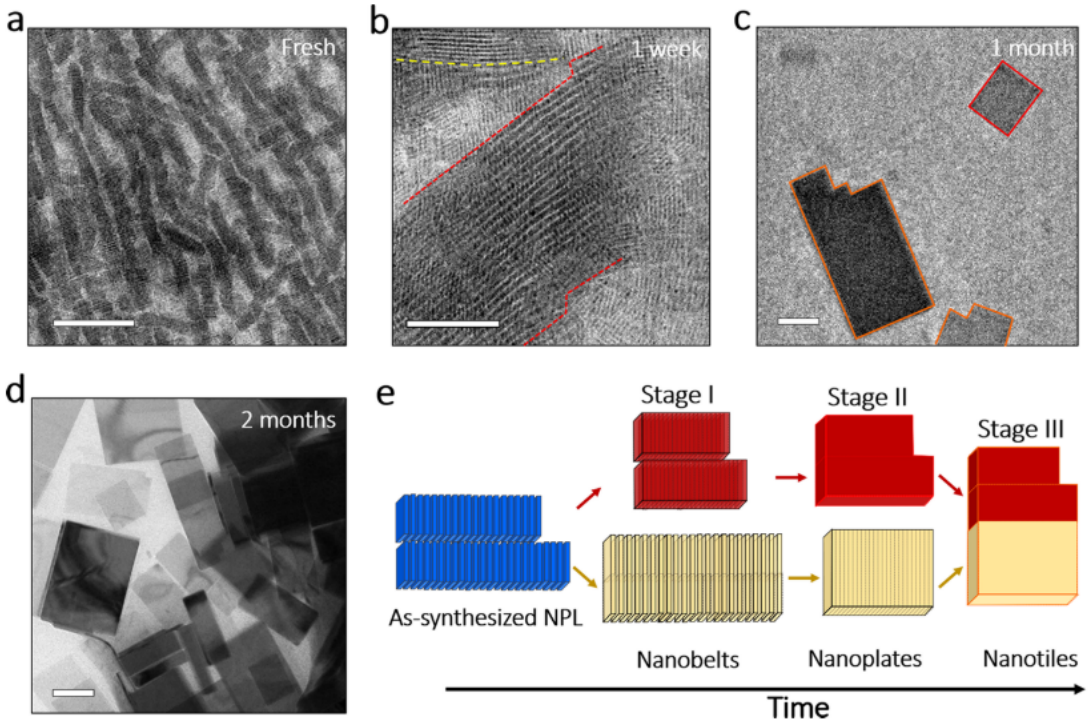

Fig. 7. TEM images revealing the growth of $CsPbBr_3$ NPLs over time. (a) Fresh NPL stacks, (b) nanobelts, (c) different sized nanoplates, and (d) nanotiles. Scale bars: 100 nm. (e) Diagram for the conversion of $CsPbBr_3$ NPL stacks in solution over time. Reprinted with permission from Ref [71].

This process provides critical information for the design and fabrication of perovskite material, in which type and density of defects are essential. It will encourage the development of perovskite NCs with intriguing optoelectronic properties.

5.7. Defect-driven self-assembly

Halide perovskites for photovoltaics have recently attracted attention due to their low cost, solution-processable synthesis, and promising optoelectronic properties [133–137]. Solar power conversion efficiencies of more than 20% have been achieved in recent years for perovskite photovoltaics [138–141]. However, many important issues related to the stability of perovskite halides need to be considered prior to their commercial application despite such promising achievements. Moisture, high temperature, oxygen, and UV irradiation cause faster degradation of perovskite solar cells than polymer and dye-sensitised photovoltaics [142–144].

Solution-processing film fabrication can result in significant structural disorder and crystallographic defects [145,146]. Several studies regarding vacancies and interstitial defects in perovskite photovoltaics have been conducted [147,148]. Defects, especially surface vacancies that can act as surface traps, are often produced during perovskite synthesis. Vacancy defects provide a route for ion movement, which is unfavourable for charge collection with current-voltage hysteresis [149,150]. The surface vacancies play a key role in the stability of perovskite NCs by restricting the ligand binding dynamics on the perovskite NC surfaces [151,152]. Halogen vacancies are the leading source of defects in all-inorganic caesium lead halide perovskite ($CsPbX_3$, where X = Cl, Br or I). Various methods have been adopted to passivate surface traps and reduce defects to enhance device efficiency [153]. Pan et al. reported surface halide-vacancy-rich $CsPbBr_3$ QDs for studying the role of surface vacancies on self-assembly behaviour [154]. These QDs self-assembled into several millimetre-thick NWs in the presence of oleic acid and didodecyldimethylammonium (DDA) sulphide. Sulfur facilitates self-assembly by filling the halide vacancies while DDA passivates the surface of the NWs. Raisa-Ioana et al. suggested that halogen vacancy migration is one of the most important parameters for phase segregation and perovskite material degradation [155]. Halogen defects degrade a device by facilitating rapid ion migration under atmospheric conditions [156,157]. Therefore, it is essential to control halide vacancies to achieve efficient and chemically stable perovskite LEDs. The efficiency and stability of blue MHP LEDs can be significantly improved after suppression or passivation of Cl vacancies in mixed halide (Br/Cl) perovskites (MHPs) by using a non-polar organic pseudohalide (e.g.,(n-dodecyl ammoniumthiocyanate (DAT)] [158].

5.8. Electric field-driven self-assembly

Electrophoretic deposition (EPD) is a promising technique for assembling charged colloidal particles on an electrode's surface by using AC electric field. The advantages of using an external field include simplicity, cost-effectiveness, and a combination of speed, ease of control, and accuracy that is not readily offered through particle-particle colloidal interactions [159–162]. With minor adjustment to electrode design and positioning, deposition can be performed on different surfaces such as flat, cylindrical or any other shape for producing high-quality films with excellent homogeneity. In general, EPD is a two-step process in which the suspended particles are first charged by an electric field, and then attracted to an electrode with the opposite charge, thereby forming the deposited layer through particle coagulation.

Positively and negatively charged colloidal particles preferably deposit on the negative electrode (cathode) and positive electrode (anode), respectively. For high-quality NC films, the

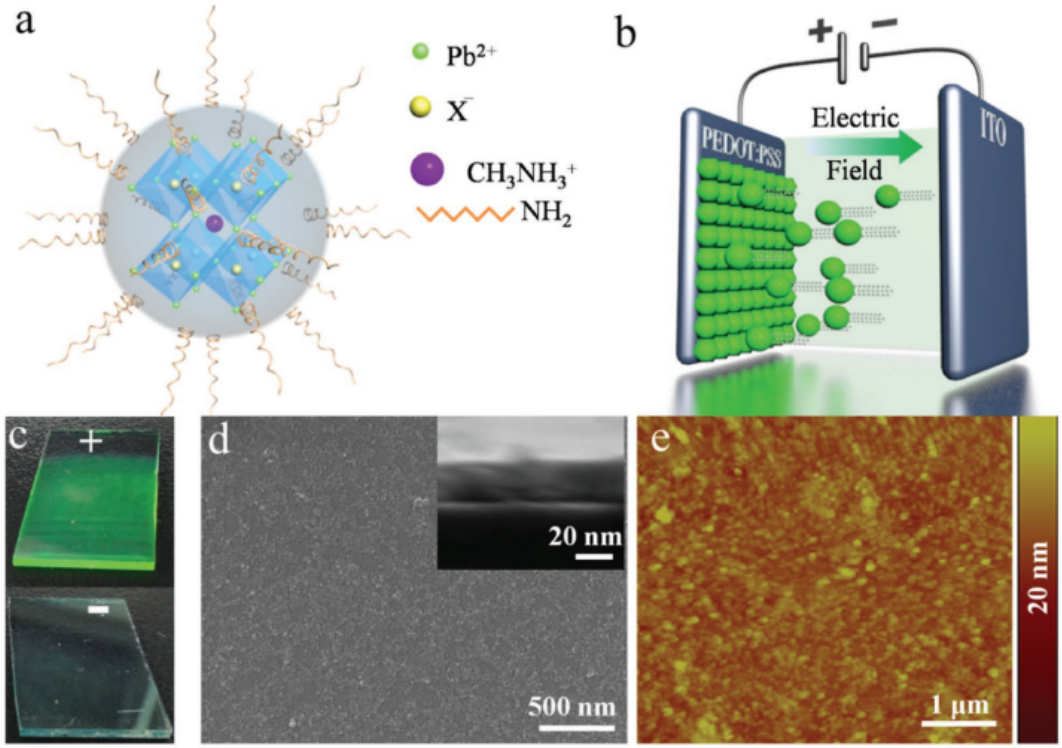

suspension's stability, particle size, ζ-potential, conductivity and viscosity, as well as the solvent's dielectric constant, should be considered and optimized.

Fig. 8. (a) A schematic diagram of the surface of an $MAPbBr_3$ QD. (b) The EPD-mediated self-assembly of QDs on the anode surface (left) covered with PEDOT:PSS. (c) Images of the anode and cathode surfaces after 5 minutes of EPD. (d) An SEM image of a deposited QD thin film. (e) An AFM image of a QD surface with an RMSS of 5.8 nm. Reprinted with permission from [163].

The EPD method is commonly used for depositing graphene [164], Cu, and Au sheets [165], along with producing compact thin films of MHP NCs. The surfaces of MHP NCs are negatively charged due to the presence of halide ions, and thus they can be deposited on the anode surface by applying a certain voltage. In 2018, Zhang et al. fabricated high-quality compact $MAPbBr_3$ QD thin films by using EPD[163] (**Fig. 8)**; the positive electrode comprised indium tin oxide (ITO) coated with poly(ethylenedioxythiophene):polystyrene sulphonate (PEDOT:PSS) while the negative electrode was bare. Both were dipped in toluene containing 0.1 mg/mL QDs and placed at a distance of 0.4 cm apart. As expected, the negatively charged

$MAPbBr_3$ QDs were deposited on the positive electrode under a bias voltage of 20V; they showed a high PL QY of 80-90% and excellent optoelectronic performance with a current efficiency of 12.7 cd A^{-1}, power efficiency of 9.7 lm W^{-1}, and an EQE of 3.2%. The surface of all-inorganic MHP NCs also possesses negative charges as that of organic-inorganic MHP NCs. Kamat et al. exploited the advantage of depositing hierarchical arrays of all-inorganic MHP NCs via EPD to produce self-assembled$PbSO_4$-oleate-capped $CsPbX_3$ (X = Cl/Br/I) peapods on mesoscopic TiO_2 films orderly aligned arrays[166] (**Scheme 10**). $PbSO_4$-oleate-capped $CsPbX_3$ NCs were self-assembled in a linear fashion whereas bundled secondary arrays of nanorods were observed on the positive FTO/TiO_2 electrode in hexane. This was due to the charge neutralization of the nanorods near the electrode surface, which facilitated their aggregation into larger rods.

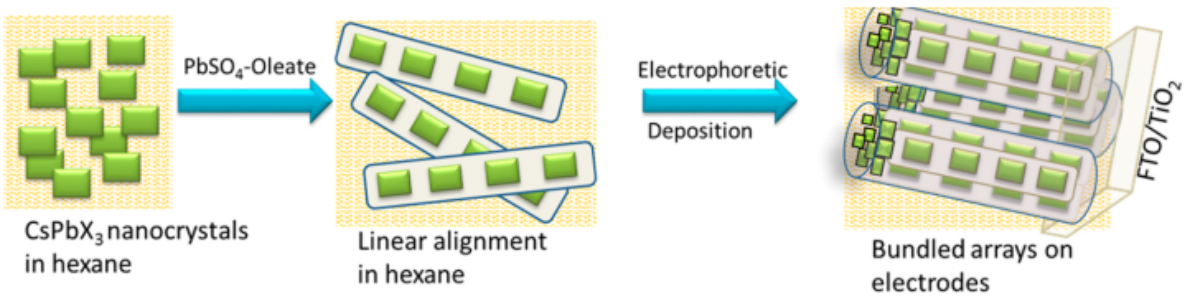

Scheme 10. A schematic diagram of linear alignment of $PbSO_4$-oleate-capped $CsPbX_3$ NCs in hexane and large bundled arrays on the anode surface via EPD. Reprinted with permission from [166].

Recently, our group fabricated a high-quality compact film of polyvinylpyrrolidone capped $CsPbBr_3$ NCs via EPD [167]. The surface of the synthesized NCs were negatively charged with a mean zeta potential of −2.50 mV in toluene, thereby making their deposition on the anode surface advantageous. A disadvantage of EPD is that water cannot be used as the solvent because water-splitting reaction will occur on the electrodes under the applied voltage, thereby deteriorating the quality of the produced films.

6. Synthetic routes for perovskite superlattices through self-assembly

(a) Synthesis of colloidal NCs followed by solvent evaporation

Self-assembled 3D SLs were developed via solvent-drying methods [3,168] (**Fig. 11**). In a typical procedure, monodispersed $CsPbBr_3$ NCs are first synthesized via a hot-injection method, in which a Cs-oleate precursor is inserted promptly into a hot solution of $PbBr_2$ dissolved in a high boiling point solvent such as 1-octadecene along with surfactants (i.e., OA and OAm). A rapid nucleation burst occurs within seconds of injection, accompanied by the formation of small nuclei, and following the rapid depletion of the monomers, the nuclei continue to grow. This process leads to narrow size distribution of the NC population. High-quality NCs can be synthesized by controlling (i) the precursor to surfactant ratio, (ii) the injection temperature, (iii) the reaction time, and (iv) the precursor concentration. After synthesizing the NCs via a hot-injection method, the perovskite NCs are dissolved in toluene and dispersed onto a silicon substrate in a Teflon well. The toluene is gently evaporated by placing a glass slide over the well. Entirely evaporating off the toluene leaves, micrometre-sized 3D SLs of $CsPbBr_3$ NCs form. Kovalenko et al. synthesized 3D $CsPbBr_3$ SLs showing superfluorescence by using this procedure [3].

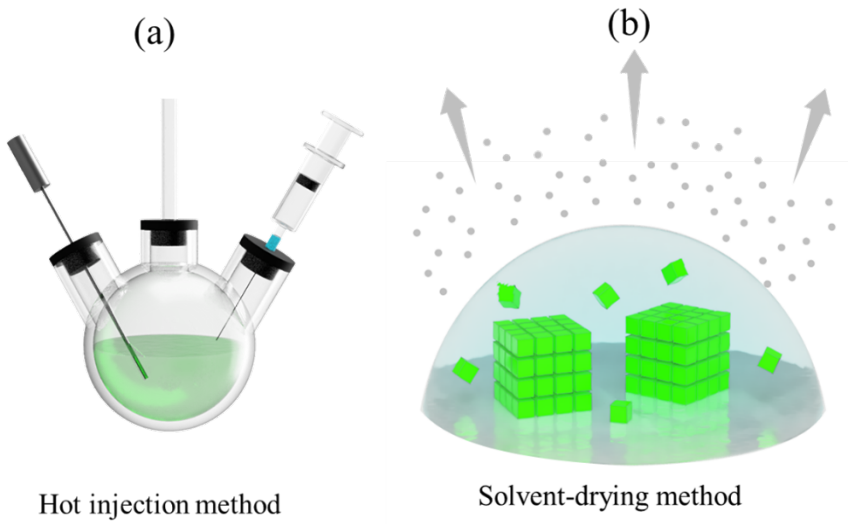

Scheme 11. (a) The hot injection, and (b) solvent-drying methods.

(b) Single-step tip sonication

Perovskite SLs can be synthesized via single-step tip sonication of a highly concentrated solution, a method that is easy to follow and highly cost-effective for synthesizing perovskite SLs. Polavarapu et al. synthesized highly emissive $CsPbBr_3$ SLs by following this method [67] (**Fig. 9**). In a typical synthesis, a large amount of Cs_2CO_3 (1 mmol) and $PbBr_2$ (3 mmol) are added to in 1-octadecene (10 ml), oleic acid (1.5 ml), and oleylamine (1.5 ml) followed by tip sonication. Gradually, the reaction mixture turns yellow, indicating the formation of colloidal perovskite NCs and after that quick precipitation occurs, indicating the formation of perovskite SLs. Interestingly, the formation of NCs and self-assembly occur simultaneously in one pot. A high concentration of colloids in a dispersing medium appears to facilitate the self-assembly of the SCs via the vdW attraction between the hydrophobic ligands and perovskite NC cores. Only the 2D assembly of $CsPbBr_3$ NCs occurs in the case of low concentrations of Cs_2CO_3 (0.1 mmol) and $PbBr_2$ (0.3 mmol) dissolved in 1-octadecene (10 ml), oleic acid (0.5 ml), and oleylamine (0.5 ml).

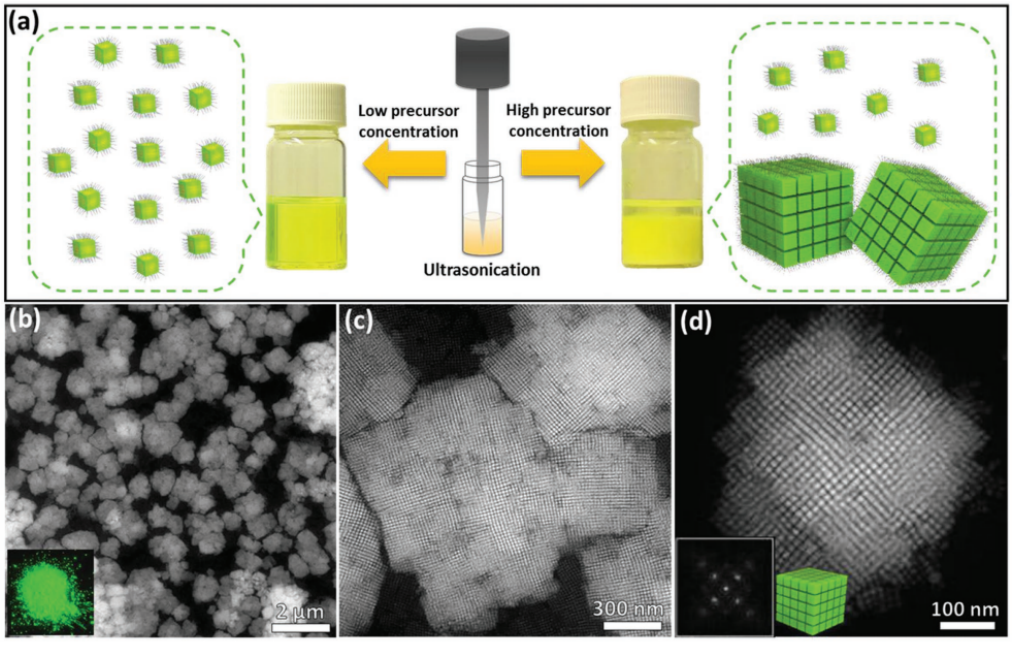

Fig. 9. (a) A schematic diagram of the synthesis of $CsPbBr_3$ NCs and SLs. (b-d) HAADF-STEM images of SLs at different magnifications. (the inset of (b): SLs under UV light, and the inset of (d): FFT of the HAADF-STEM image. Reprinted with permission from [67].

7. Self-assembly of different morphological perovskite nanocrystals

Different methods for synthesising perovskite NCs have been developed to control the composition, size, shape, and connectivity of multiple parts of a multicomponent composition at an extremely high level (**Table 1**). One-, two-, and three-dimensional ordered self-assemblies of particles forming perovskite SLs are of great importance to developing advanced materials for electronic, optoelectronic, thermoelectric, catalytic, and various other applications. In particular, self-assembly mostly relies on the Brownian force, steric force, vdW forces, capillary force, and hydrogen bonding interactions, which are progressively crucial in obtaining diverse structures, such as nanocubes nanoplates, nanorods, nanowires, and polyhedral systems. There has been immense development in perovskite colloidal self-assembly; however, most of the work has been performed at the interface of polar and non-polar solvents with charged colloids [169,170].

7.1. Nanocubes

The use of self-assembly to form complex nanostructures in several optoelectronic devices has been a great challenge. Loredana et al. exploited an inexpensive commercial precursor for synthesising monodisperse self-assembled colloidal nanocubes of fully inorganic $CsPbX_3$ NCs (X = Cl, Br, and I) and mixed halide derivatives [171]. The ionic nature of the chemical bonding in monodispersed $CsPbX_3$ in solution phases provides several benefits. The reaction of Cs-oleate with a Pb(II)-halide in a high boiling octadecene solvent within 140–200 °C results in controlled arrested precipitation of Cs^+, Pb^{2+}, and X^- ions into $CsPbX_3$ nanocubes. They also noticed that the contributions from the surface energy and high temperature would result in the crystallisation of self-assembled $CsPbX_3$ NCs in the cubic phase. At the same time, they found that the size of $CsPbX_3$ nanocubes could be altered via the synthesis temperature (140–200 °C) rather than via the growth time. Furthermore, Bekenstein et al. explored the role of the synthesis temperature in controlling the shape and size of $CsPbBr_3$ NCs [31]. The fast nucleation and growth kinetics of the resultant NCs are attributed to the ionic character of the metathesis reaction. Self-assembled symmetrical nanocubes appeared at 150 °C whereas self-assembled nanoplates appeared at 130 °C. Very thin nanoplates (NPLs) were formed at 90 and 100 °C, accompanied with self-assembled lamellar structures of 200-300 nm length. Organic ligands,

oleates and oleylammonium, act as soft growth templates, which break the inherent cubic symmetry of these NCs, forming the self-assembled two dimensional structure.

The impact of surfactant ligands on the shape, size, and surface properties of perovskite NCs was also investigated by various groups in detail. The surface passivating ligands play an important role during the self-assembly of the perovskite NCs. Pan et al. systematically altered the hydrocarbon chain configuration of carboxylic acids and amines to study their impact on the shape and size of self-assembled perovskite NCs ($CsPbBr_3$ NCs) [172]. They concluded that carboxylate ligands are more efficient in modifying the size of the nanocubes and ammonium ions are more efficient in modifying the growth of platelet structures. They discovered that the shape and size of $CsPbBr_3$ NCs at 170 °C is dependent on the chain length variation of carboxylic acids and amines. The short-chain carboxylic acids ligand results in the larger sized $CsPbBr_3$ nanocubes; however, shorter chain amines result in thinner $CsPbBr_3$ nanoplatelets. Shibin et al. also demonstrated room temperature synthesis of different morphologies of self-assembled $CsPbX_3$ (X = Cl, Br, I, or combinations thereof) perovskites, such as nanocubes, nanorods, quantum dots, and nanoplatelets, can be achieved by different organic acid and amine ligands based reprecipitation process [173]. Dodecylamine with oleic and acetate acid tailor the NCs into nanocubes and nanorods, respectively. Octylamine with hexanoic and oleic acid shapes NCs into spherical QDs and few-unit-cell-thick nanoplatelets, respectively [173,174]. The formation of the various morphologies of $CsPbX_3$ perovskites with different organic acid and amine ligands may be due to the classic micellar transition mechanism, depending on the solvent interaction and electrostatic and hydrophobic interactions with the ions and the ligands. Arkajyoti et al. also synthesised different morphologies (nanorods, nanocubes, and nanoplatelets) of self-assembled $CsPbBr_3$ perovskite NCs using an inexpensive steroidal Cs precursor, caesium cholate [175]. Biplap et al. synthesised surface-modified $CsPbBr_3$ perovskite nanocubes by partially replacing long-chain oleyl groups ligands with a short-chain thiocyanate moiety [20], allowing the self-assembly of close-packed monolayer thin films of nanocubes. It is essential to obtain close-packed monolayer thin films to prevent colloidal aggregation because nanocubes of $CsPbBr_3$ mostly fuse into single crystals [117,176,177]. $CsPbBr_3$ perovskite with a short-chain thiocyanate group provides better self-assembly than a long-chain oleyl group because of the reduced free energy for the cubes. Muhammad et al. developed a new synthesis method to prepare monodispersed and shape pure $CsPbBr_3$ nanocubes using secondary amines [22]. The comparative advantage of this method is that it produces pure nanocubes irrespective of the

alkyl chain lengths and the reaction temperature. The superb phase and shape purity of $CsPbBr_3$ NCs was obtained because of the lack of ability of secondary amines to obtain the appropriate steric conditions at the surface of the NCs, consequently limiting the formation of other nanostructures. Yu et al. reported a one-pot synthesis of $CsPbBr_3$ perovskite SLs in a colloidal dispersion by ultrasonication (**Fig. 10**) [178]. They demonstrated the spontaneous self-assembly of $CsPbBr_3$ NCs into highly emissive perovskite SCs from precursor powders in a highly concentrated solution. Sumanta et al. developed a general methodology to synthesis lead halide-based perovskite nanocubes of $APbX_3$, where A = Cs^+, $CH_3NH_3^+$ (MA), or $CH(NH_2)^{2+}$ (FA) and X = Cl, Br, or I. They used a unique precursor of N-bromosuccinimide as the bromide source in the hot injection method to synthesise $APbX_3$ nanocubes [179]. The nanocubes show uniform size distribution and remarkable stability in ambient conditions, in the presence of water and under UV irradiation. Roberto et al. developed a synthesis method to obtain near unity PL QY of self-assembled $CsPbBr_3$ perovskite nanocubes, with a size-dependent, near unity QY and long-term stable emission. The size control of nanocubes was achieved by varying the synthesis temperature and the appropriate mixture of the perovskite forming elements [180].

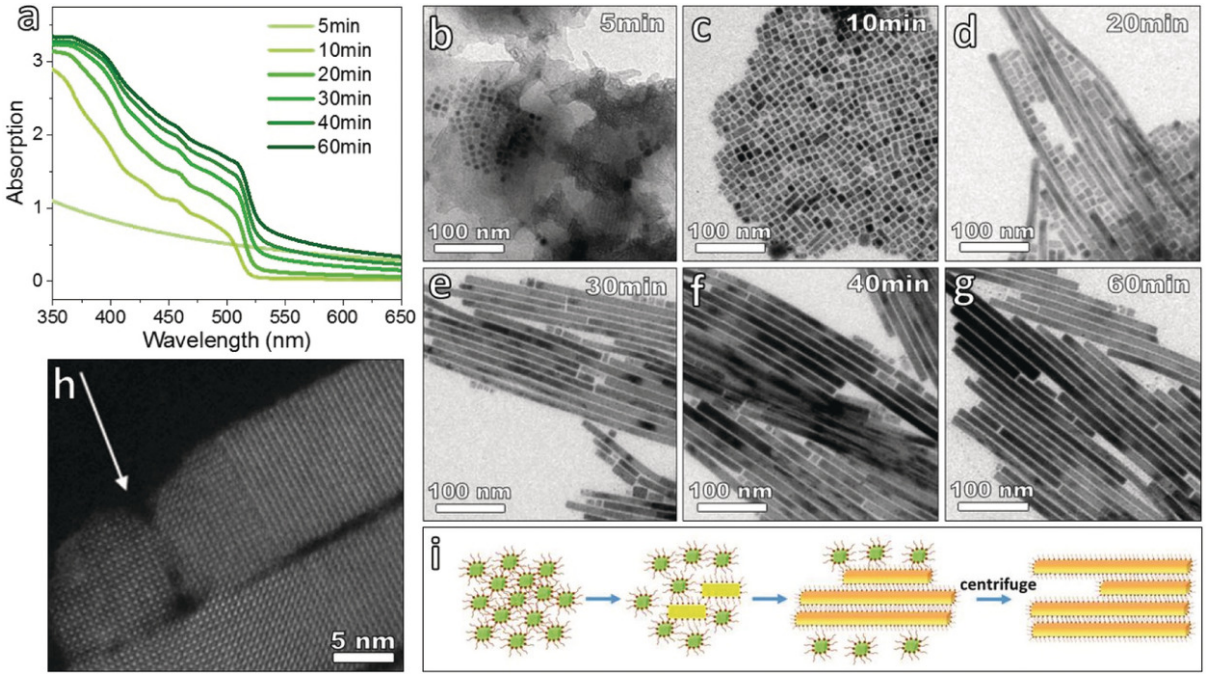

Fig. 10. (a) Absorbance of $CsPbBr_3$ NCs over time and (b–g) the respective TEM images. (h) HAAD-STEM image of NCs (20 min). The arrow indicates the oriented attachment of nanocubes that transformed into NWs. Reprinted with permission from Ref [178].

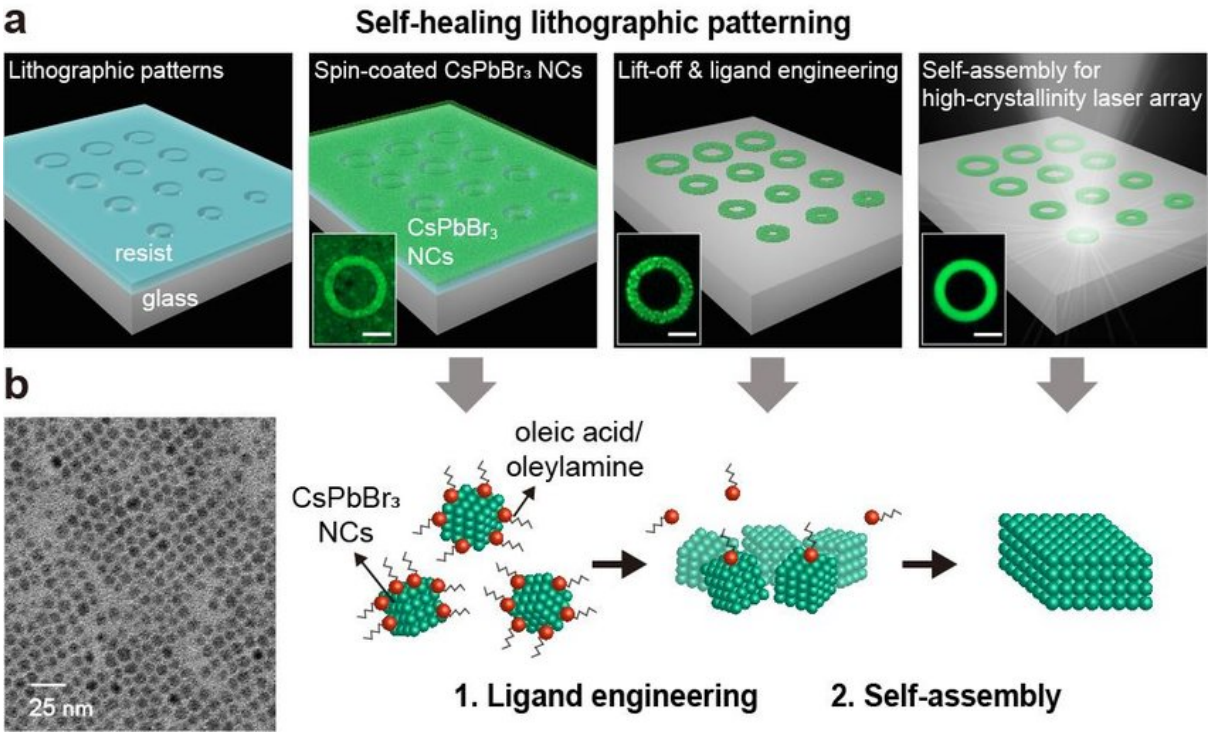

Fig. 11. (a) Lithographic patterning using $CsPbBr_3$ NCs. Insets: μ-PL images of the $CsPbBr_3$ micro-ring patterns. Scale bars: 2 μm. (b) TEM image of the $CsPbBr_3$ NCs (left) and illustration of ligand engineering and self-assembly process for self-healing process. Reprinted with permission from Ref [181].

Xing et al. suggested a breakthrough self-healing lithographic patterning approach to fabricate large-area laser arrays of $CsPbBr_3$ NCs (**Fig. 11**) [181]. This self-healing lithographic patterning technology, incorporating ligand engineering and perovskite NC self-assembly, is compatible with traditional top-down lithography processes. It allows the construction of high-quality, crystallinity-controlled optical cavities.

Table 1: Various building units and surfactants for self-assembly of perovskite NCs

Perovskite NCs	Building unit	Surface-passivating ligand	Self-assembled structures	Reference
$CsPbBr_3$	nanocube	oleic acid, oleylamine	nanocubes	[182]
	nanoplatelet	oleic acid, oleylamine	nanobelts	[114]
	nanocube	oleic acid, hexanoic acid oleylamine, tetrabutylammonium hydrogen sulfate	1D assembly of nanocubes	[116]
	nanodisk	oleic acid, oleylamine, octylamine, dodecylamine, octanoic acid	nanoribbons	[52]
	nanocube	oleic acid, oleylamine	1D SL chain	[99]
	nanosheet	oleic acid, oleylamine	nanocubes, 1D SL chain	[53]
	nanoplate, nanocube	oleic acid, octylamine, cetylamine	nanoplates	[44]
	nanocube	oleic acid, oleylamine, octylphosphonic acid	nanocubes	[85]
	nanocube	oleic acid, oleylamine	nanowire	[178]
	quantum dot	phenylalanine+HBr, 3-(decyldimethylammonio) propane-1-sulfonate	core-shell structured quantum dots	[183]
	nanocube	oleic acid, oleylamine	cubes	[67]
	nanocube	tetrabutylammonium bromide, oleic acid, oleylamine	cubes	[184]
	nanocube	oleic acid, oleylamine	cuboidal supraparticles	[185]
	nanocube	oleic acid, oleylamine, tertiary butyl hydrogen sulfate	hierarchical arrays of nanorods	[166]
	nanocube	oleic acid, oleylamine, dihexylamine, dioctylamine,	cubes	[22]

$CsPbBr_3$		didecylamine, dioctdecylamine, didodecylamine, benzoyl bromide		
	nanoplate	oleic acid, octanoic acid, oleylamine, octylamine	cuboids	[186]
	nanocube	tetraethyl orthosilicate, (3-aminopropyl)-triethoxysilane, trimethoxy(octadecyl)silane, oleic acid, oleylamine	serpentine nanowires	[42]
	nanosheet	octanoic acid, oleic acid, oleylamine, octylamine	2D-layered Ruddlesden−Popper phase	[187]
	nanoplatelet	oleic acid, oleylamine, octanoic acid	layered nanoplatelets	[102]
	rhombic dodecahedron	phenacyl bromide, oleic acid, oleylamine ;	hexagonal close packing, square close packing	[188]
	rhombicuboctahedron	phenacyl bromide, oleic acid, oleylamine	square pattern assembly	[188]
	nanoplatelet	oleic acid, oleylamine	nanobelts, nanoplates, nanotiles	[71]
	nanocube	cholic acid, oleic acid, oleylamine	nanorods	[175]
	nanocube	oleic acid, oleylamine	nanowires	[112]
	nanorod	oleic acid, oleylamine	2D arrays of nanorods	[189]
	quasi-spherical nanocrystals	poly(ethylene glycols) amine, poly(ethylene glycols) acid	pearl necklaces, lamellar, and nanorice assemblies	[64]
	hexapod	oleic acid, oleylamine-HBr	hexapods	[190]

	quantum dot	oleic acid, oleylamine, didodecyldimethylammonium bromide	nanowires	[154]
	nanoplatelet, nanocube	oleic acid, oleylamine	polyhedron shaped NCs	[18]
	quantum dot	10-undecynoic acid, 5-hexynoic acid, oleic acid, oleylamine	cuboids, spindles	[191]
	nanocube	oleic acid, oleylamine, octadecene, ammonium thiocyanate	monolayer thin films of nanocubes	[20]
	nanocube	oleic acid, oleylamine	2D photonic supercrystals	[192]
$CsPbCl_3$	hexapod	oleic acid, oleylamine-HBr	hexapods	[190]
	nanocube	oleic acid, oleylamine, tertiary butyl hydrogen sulfate	hierarchical arrays of nanorods	[166]
	nanocube	oleic acid, oleylamine, dihexylamine, dioctylamine, didecylamine, dioctdecylamine, didodecylamine, benzoyl bromide	nanocube arrays	[22]
$CsPbI_3$	nanocube	oleic acid, oleylamine, tertiary butyl hydrogen sulfate	hierarchical arrays of nanorods	[166]
	nanocube	oleic acid, oleylamine, dihexylamine, dioctylamine, didecylamine, dioctdecylamine, benzoyl iodide	nanocubes	[22]
$MAPbBr_3$	quasi-spherical nanocrystals	L-cysteine, L-alanine	cubic supercrystals	[193]

	spherical nanocrystal	oleic acid, oleylamine, tetrafluoroborate salts ($NaBF_4$, NH_4BF_4)	strip-shaped nanoplates	[194]
	nanocube	PbBr(OH)	rods	[195]
$FAPbBr_3$	nanocube	oleic acid, oleylammonium bromide,	nanocubes	[196]
	nanoplate	oleic acid, oleylamine	nanoplates	[197]
	nanoplate	oleic acid, oleylamine	nanoplates	[48]
	quasi-spherical shaped nanocrystals	phenacyl bromide, oleic acid, oleylamine	nanocubes, nanoplatelets, nanosheets	[198]

7.2. Nanoplates

Yehonadav et al. synthesised $CsPbBr_3$ perovskite nanoplates (NPLs) and demonstrated their stacked columnar and crystallographic oriented thin-sheet structures obtained through self-assembly process [31]. The self-assembly occurs in a concentrated NPL solution, in which strong interaction between ligands results into stacked columnar phases. Lateral crystallographic oriented attachment of single plates results in crystallographic oriented large thin-sheet structures. Quinten et al. developed a colloidal synthesis method to fabricate $CsPbBr_3$ nanoplatelets (NPLs) with precise thickness tunability at room temperature [199]. They developed a method in which acetone was injected to stimulate the fusion and growth of platelets in a mixture of chemical precursors that would otherwise remain inactive until acetone was introduced. The shape and plate thickness up to 3 to 5 monolayers can be controlled by this synthetic method. Javad et al. synthesised single crystal $CsPbBr_3$ PNSs with a thickness of less than 5 nm and lateral sizes control of up to a few micrometres [35]. The control of lateral size of $CsPbBr_3$ PNSs was achieved by changing the ratio of short (octanoic acid and octylamine) to long (oleic acid and oleylamine) ligands in the synthesis; however, the thickness remained primarily constant, unaffected by this parameter. Bernhard et al. obtained thickness-controlled $CsPbBr_3$ nanoplatelets monolayer and high PL QY [200]. The $CsPbBr_3$ nanoplatelets synthesis using the reprecipitation method and controlled over thickness were achieved by varying the molar ratio of the precursors (Cs/Pb). Yasutaka et al. developed a new pressure processing of $CsPbBr_3$ perovskite nanocube SLs into lateral 2D nanoplatelets [117].

They studied in detail the behaviour of self-assembled $CsPbBr_3$ perovskite under high pressure; they noticed that periodically ordered NCs converted lateral 2D nanoplatelets with uniform thicknesses, high crystallinity, and improved optical properties. Xuexi et al. developed a general strategy to synthesise all inorganic $CsPbX_3$ perovskite nanoplates by introducing additional metal halides, MX'_2 or MX'_3 (M = Cu, Zn, Al or Pb; X' = Cl, Br, or I). The thickness and size of the $CsPbX_3$ perovskite nanoplates can be modified by the metal halides and ligands ratio, temperature, and reaction time [29]. Uddin et al. transformed $CsPbCl_3$ nanocubes into $CsPbX_3$ (X= Cl, Br, and I) nanoplates from ligand-mediated anion exchange reaction by adding a mixture of dodecanethiol (DDT) and AlX_3 to a solution of $CsPbX_3$ NCs (**Fig. 12**). They observed that the self-assembly followed by perovskite NCs fusion plays a significant role in converting the parent nanocubes into nanoplates [23]. The XRD pattern of synthesized $CsPbCl_3$ nanocubes showed high intensity peaks corresponding to the (100), (200), and (100) planes. However, the intensity of (100) plane get reduce after DDT-AlX_3 treatment. This is due to the exfoliation of these NCs along the (001) plane and fusing along the (010) and (100) planes during anion exchange processes.

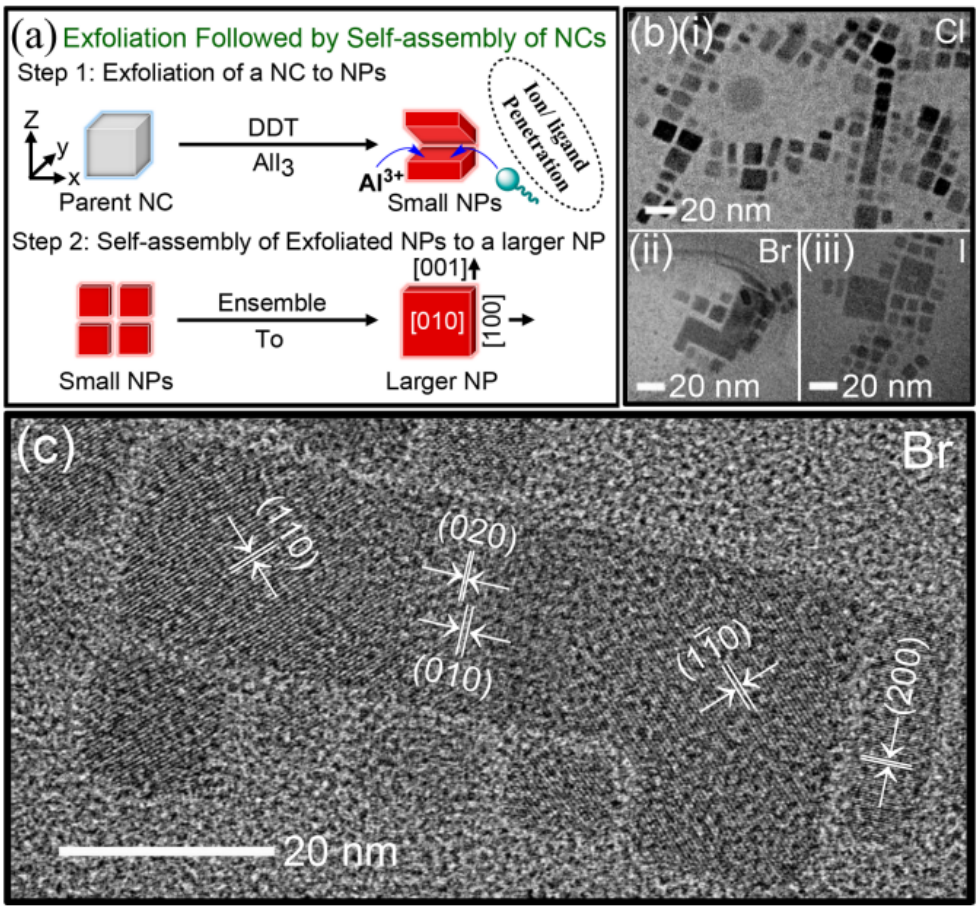

Fig. 12. Schematic diagram of self-assembly and fusion of $CsPbX_3$ (X = Cl, Br, I) nanocubes. (b) TEM images of self-assembled larger nanoplates after treatment of nanocubes with DDT-AlX_3. (c) HRTEM images of larger fused $CsPbBr_3$ nanoplates showing lattice fringes. Reprinted with permission from Ref. [23].

Li et al. described a two-step procedure for fabricating 2D $CsPbX_3$ (X = Cl, Br, I) NCs with thicknesses ranging from 3-6 nm and lateral dimensions ranging from 100 nm to 1 μm without the use of anion exchange **(Fig. 13)** [201]. First, they synthesized 1D $CsPbX_3$ (X = Cl, Br, I) nanorods by reacting Cs-oleate with PbX_2 (X = Cl, Br, I) at 80-120 °C in a mixture of long-chain (OA and OAm), shorter-chain (octanoic acid and octylamine) ligands, and octadecene as solvent. Subsequently, they fabricated 2D $CsPbX_3$ NPLs and NSs via self-assembling the corresponding NRs at 160 °C for 15 hours under solvothermal condition.

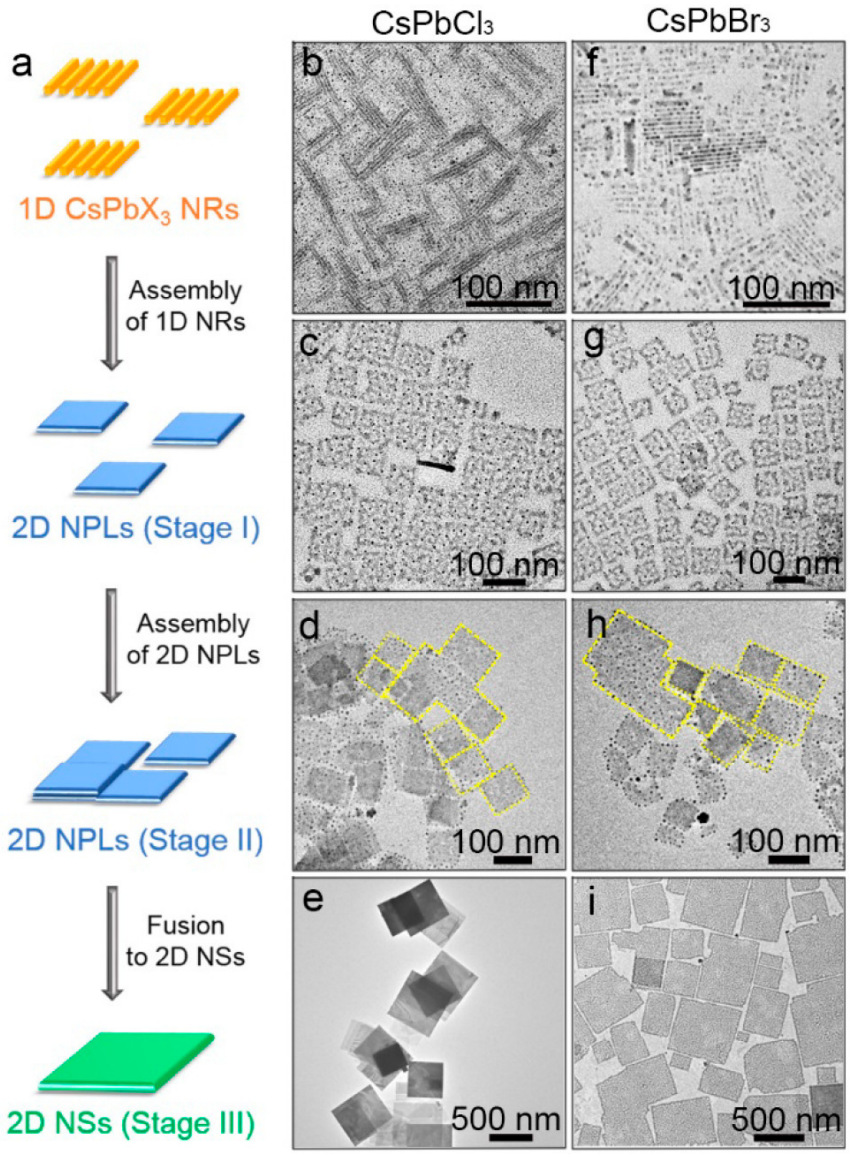

Fig. 13. (a) Illustration of the growth of 2D $CsPbX_3$ NPLs and NSs through oriented attachment of NRs. TEM images of (b) $CsPbCl_3$ and (f) $CsPbBr_3$ NRs. TEM image of 2D $CsPbCl_3$ NCs synthesized at 160 °C for (c) 2.0 h (NPLs), (d) 2.5 h (large NPLs), and (e) 3.0 h (NSs). TEM images of $CsPbBr_3$ NCs synthesized at 160 °C for (g) 3.0 h (NPLs), (h) 4.0 h (large NPLs), and (i) 5.0 h (NSs). Reprinted with permission from Ref [201].

7.3. Nanorods

Perovskite nanorods (NRs) have many useful properties, including fast charge transfer, reduced lasing threshold, and linearly polarised light emission, which makes them stand out in various applications, such as photocatalysis, liquid crystal displays, lasers, and solar cells. Organic surfactants are important in controlling the anisotropic growth of perovskite NRs; OAm and OA are currently highly utilised surfactants in NRs fabrication. Wenna et al. synthesised $CsPbBr_3$ perovskite NCs with tuneable morphologies within a few minutes using microwave technique [202]. The size of nanoparticles was tuned by controlling the microwave powers and irradiation times; the molar ratio of OA to OAm play a key role in changing the dimensionality of the products from 0D nanocubes to 1D NRs and then to 2D nanoplates. Furthermore, other amines, such as octylamine and hexadecylamine, were also used to facilitate the growth of perovskite NRs [38,173]. Yanxiu et al. developed a colloidal synthesis method using tip sonication to fabricate $CsPbBr_3$ NRs with a width of approximately 5 nm and average lengths of 10.8 and 23.2 nm, respectively, in two samples, which show a high PL QY of 60–76% [38]. From $CsPbBr_3$ NRs they also drive the synthesis of $CsPbCl_3$ and $CsPbI_3$ NRs with similar shape and size by using anion exchange reaction. They synthesised NRs in moderately polar solvents, a class of solvents that are generally not considered to be useful solvents in conventional perovskite nanoparticle synthesis, expanding their processing possibilities when assembling optoelectronic devices. Bapi et al. synthesised size tuneable uniform colloidal $Cs_3Sb_2Cl_9$ perovskite NWs and NRs of several microns length [36]. Jaya et al. reported the colloidal synthesis method for tuning the morphology of $Cs_3Sb_2Cl_9$ NCs into nanoplates and NRs by varying reaction temperature while adopting octanoic acid and OLA as surfactants. These $Cs_3Sb_2I_9$ NCs show sharp band-edge emissions in the red-yellow region [203]. Sigalit et al. used a facile, low temperature synthesis of $(C_8H_{17}NH_3)_2(CH_3NH_3)_2Pb_3(I_xBr_{1-x})_{10}$ $(0 > x > 1)$ perovskite NRs [39]. These NRs show tuneable optical properties and high PL with very good size distribution. Modifying the halide composition enables tunability of the optical properties

of NRs. They provided the formation mechanism of these novel perovskite NRs by changing the ratio of octylammonium iodide (OAI) and oleic acid (OAc). The surface of the NRs was stabilised using OAI as a strong ligand; however, OAc was accountable for balancing the binding capacity of OAI in the growth of NRs. Therefore, there should be sufficient OAI to stabilise the NRs perovskite surface; however, there is sufficient OAc to balance the growth into NRs morphology. Shen et al. developed an intermediate monomer reservoir synthetic method to achieve the controllable growth of uniform, highly emissive, stable, and low defect $CsPbBr_3$ perovskite NRs using ris(diethylamino)phosphine (TDP) as the surfactant. Jer et al. synthesised a lead-free caesium tin halide perovskite quantum rods ($CsSnX_3$, where X = Cl, Br, and I) by a simple solvothermal method for solar cell applications [204].

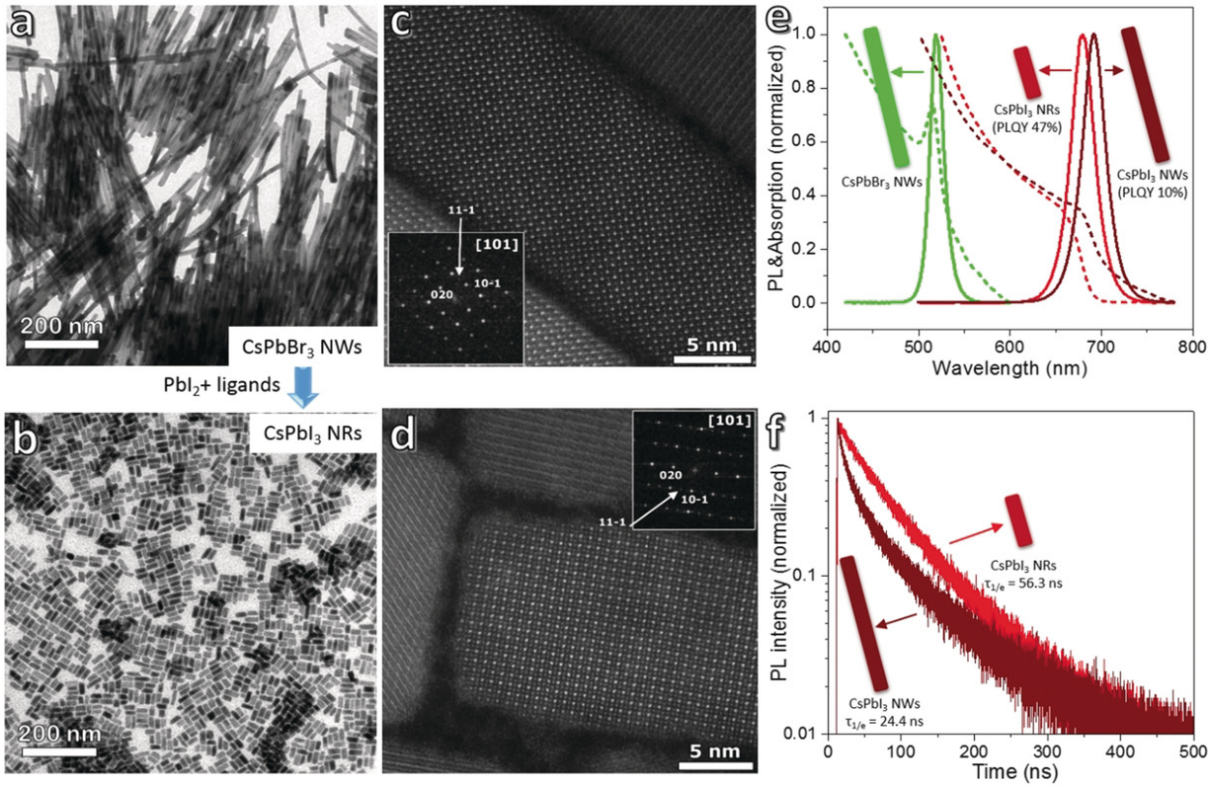

Fig. 14. (a, b) Bright-field TEM and (c, d) HAADF-STEM images of parent $CsPbBr_3$ NWs and the $CsPbI_3$ NRs. Inset: The diffractograms of orthorhombic (a) $CsPbBr_3$ NWs (b) $CsPbI_3$ NRs. (e) Absorbance and corresponding PL spectra of $CsPbBr_3$ NWs, $CsPbI_3$ NWs, and $CsPbI_3$ NRs. f) Time-resolved PL decay curves of $CsPbI_3$ NWs and NRs. Reprinted with permission from Ref [205].

Tong et al. reported a ligand-induced fragmentation of $CsPbBr_3$ NWs into low aspect-ratio $CsPbX_3$ (X=Cl, Br, and I) self-assembled NRs during halide ion exchange reaction with PbX_2 (X = Cl or I) ligands solution (**Fig. 14**). Interestingly, the orthorhombic crystal structure of single NCs is retained during shape transformation into $CsPbI_3$ NRs, as shown by high-angle annular dark-field scanning TEM (HAADF-STEM) and related diffractograms. This fragmentation of perovskites NWs to NRs resulted in an improved PL QY due to a decrease in nonradiative decay rates. They used oleylamine and oleic acid ligands to dissolve the PbX_2 precursors in organic solvent and concluded that the excess ligands in the precursor solution drive the process of perovskites NWs fragmentation [205].

7.4. Nanowires

NWs have emerged as a promising candidate in various types of applications, such as sensing, photovoltaics, optoelectronics, and thermoelectricity. Zhang et al. developed the solution-phase synthesis of $CsPbX_3$ nanowires for optoelectronic applications (**Fig. 15)** [206]. The formation of $CsPbBr_3$ NWs was achieved through the hot injection method using OA and OAm in octadecene at 150°C most. The NWs were formed through a surfactant guided dimensional growth mode. These NWs were grown along the (100) plane in orthorhombic phase.

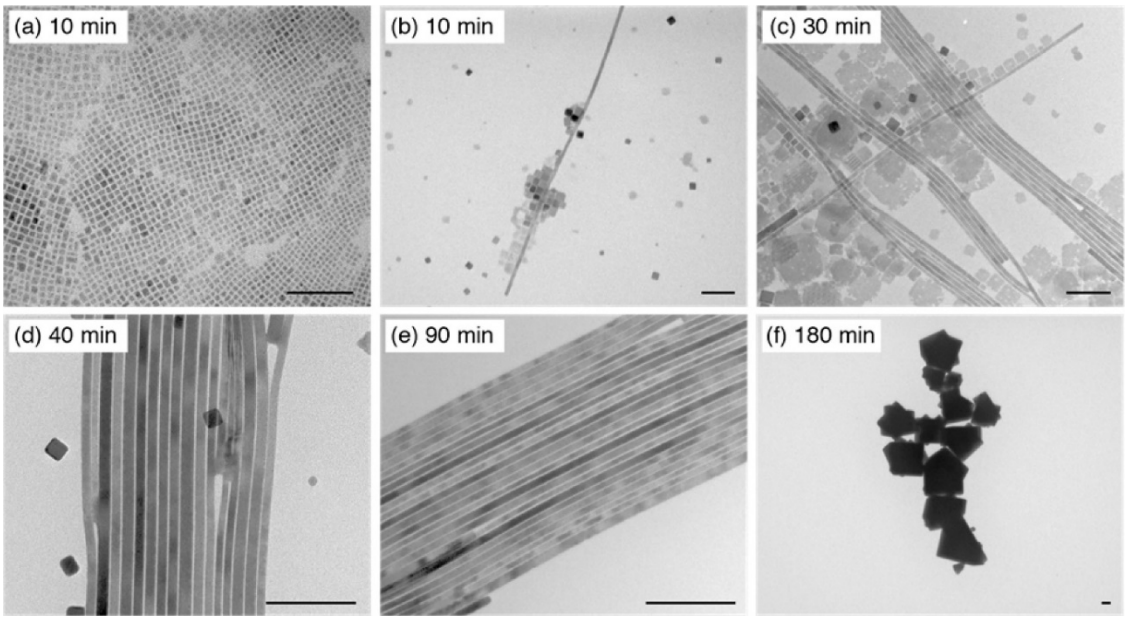

Fig. 15. Change in morphology of $CsPbBr_3$ NCs at different reaction times (Scale bar: 100 nm). The NWs disappeared at longer time (180 min), leaving only the large crystals. Reprinted with permission from Ref [206].

Zhang et al. also successfully synthesized brightly emitting compositional integrated $CsPbX_3$ (X = Cl, Br, I) NWs perovskite with uniform diameters and tuneable compositions [207]. The NWs showed bright photoluminescence tuned over the entire visible spectrum, with PL QY ranging from 20% to 80%. They used monodisperse $CsPbBr_3$ NWs as templates; the NWs' composition can be independently controlled through anion-exchange reactions by reacting it with other halide precursors. Meghan et al. reported self-assembled $MAPbBr_3$ (MA = CH_3NH_3) quantum wires by controlling their surface ligand chemistry to achieve different superstructures [208]. The formation of quantum wire proceeded through dipolar interactions, resulting in a pearl-like assembly of spherical $MAPbBr_3$. The vdW interactions of surface passivating ligands drive the mesoscale growth and assembly into $MAPbBr_3$ quantum wires. Imran et al. reported a hot injection technique to synthesise $CsPbBr_3$ nanowires with a tuneable width down to the quantum confinement regime (a few unit cells thick) using a short alkyl carboxylic acid as a growth medium and a mixture of alkylamines [209] (**Fig. 16**).

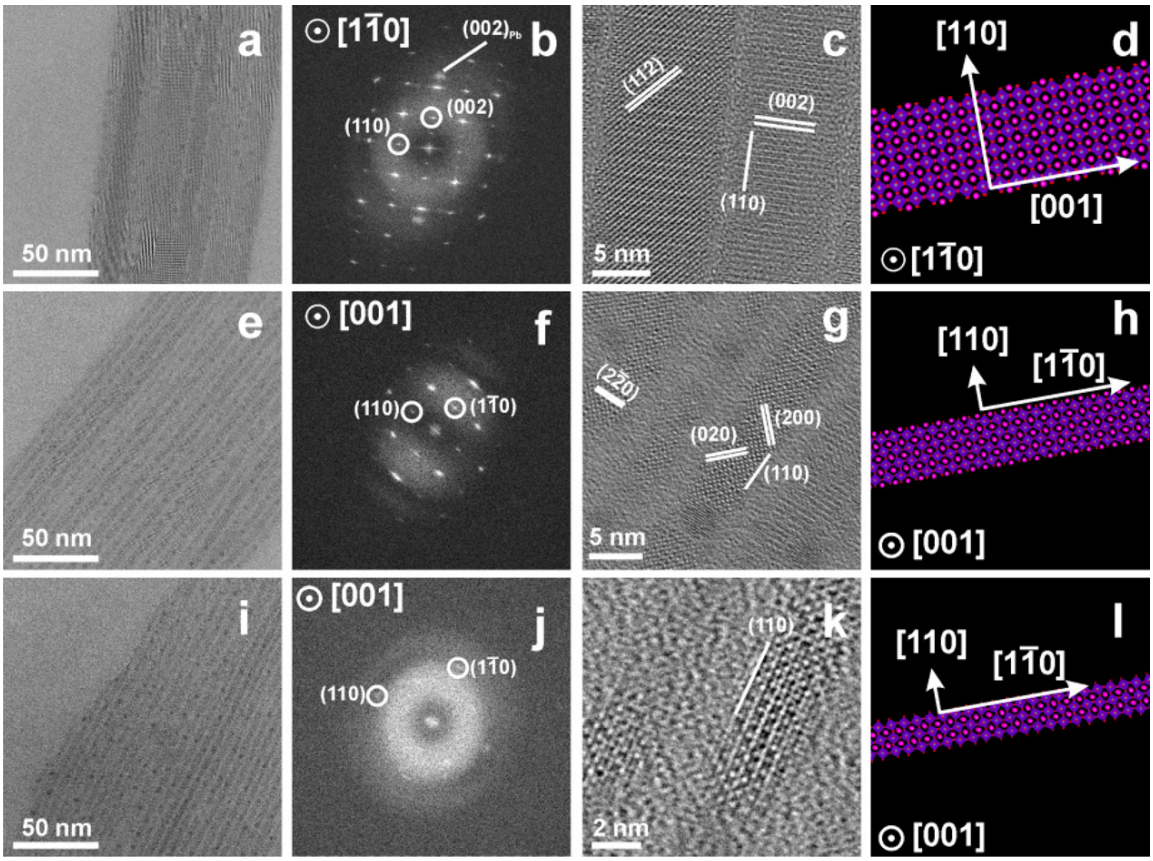

Fig. 16. Change in aspect-ratio of $CsPbBr_3$ NWs. (a–d) 10 nm, (e–h) 5.1 nm and (i–l) 3.4 nm-wide NWs. (a, e, i) wide field of view HRTEM images of NWs and their corresponding (b, f,

g) fast Fourier transform FFTs, (c, g, k) enlarged view, (d, h, l) schematic crystallographic models of the NWs. Reprinted with permission from Ref [209].

The width of the $CsPbBr_3$ nanowires was tuned from the nonconfined regime (10 ± 1) to the strong quantum confinement regime (3.4 ± 0.5 nm) by increasing the ratios of short aliphatic carboxylic acids (octanoic acid or hexanoic acid) to the amine ligands (octylamine and OAm). All of the NWs were limited along the (110) direction by facets (110), (1-10), and (001). The thinner NWs (5.11 and 3.4 nm) were oriented in the (001) direction and extended along the (1-10) axis, while NWs 10 nm thick were oriented in the (1-10) axis and extended in the (001) axis. This is attributed to the preferable binding of short chain acids along the (001) direction. Thus, the self-assembled NWs favour to grow along (1-10) axis confining along (001) direction. The temperature and reaction time are also essential parameters for controlling the width of the NWs. Daniel et al. reported ($CsPbBr_3$) NWs having quantum-confined dimensions of up to five unit cells exhibiting a significant quantum size effect in the absorption and emission spectra [210]. The length, composition, and optical properties of NW can be tuned by adding hydrohalic acids (HX, X = Cl, Br, I). They found that HX modifies the NWs in two aspects: (1) increasing the concentration of acid results in shortening of nanowires and (2) halide exchange reactions in nonidentical ions of the acid and crystal-induced alteration of compositional structure and optical properties. Structural analysis also suggests that the wire arrays follow the symmetry of mica substrate through incommensurate epitaxy, providing a possible mechanism for epitaxially growing mixed halide perovskite wires.

8. Facet chemistry for developing superlattices of various-shaped perovskite nanocrystals

Controlling the single building block unit of perovskite SLs is crucial for developing SLs with the desired morphology and optoelectronic properties. Facets of perovskite NCs play an important role in determining the morphology of NCs. A cube resembles an isotropic nanocrystal with identical facets and a centre of symmetry with regard to all facets or vertices. For tuning the shape architecture and directional expansion, different facets with varying energies are essential and thereby NCs with varied atom configurations on their facets would provide a new platform for facet-dependent ligand binding and anisotropic growth. The hexahedron cubic or platelet shape was found to be the most common shape for $CsPbX_3$ (X = Cl, Br, I) NCs. Therefore, it is urgently required to develop a method for synthesizing different

multifaceted NCs shape perovskite NCs in a controlled way. Cube-shaped $CsPbX_3$ NCs have six equivalent {100} facets in the cubic phase whereas orthorhombic $CsPbBr_3$ NCs possess four side $\{100\}_o$ facets, two bottom $\{001\}_o$ facets, 12 edge facets (four $\{100\}_o$ and eight $\{112\}_o$ facets. Different anisotropic structures of perovskite NCs can be synthesized by stabilizing the facets of these NCs e.g., Manna et al. synthesized truncated octahedron $CsPbBr_3$ NCs in the orthorhombic phase by stabilizing the new facets {110} and {111} by alkylphosphonates [211]. In the orthorhombic phase of $CsPbBr_3$ NCs, $\{001\}_o$ and $\{110\}_o$ facets are terminated with a CsBr surface, which can be replaced with surfactants for fabricating multifaceted NCs. Multifaceted NCs have several advantages, including the ability to generate anisotropic growth, self-assembly, oriented attachment, and the potential to create more efficient catalytic adsorption sites. Alkyl amines and acids are the most common ligands for cubes. There is also a report of a truncated cuboctahedron [211] stabilized by alkyl phosphonic acids. These findings further suggest that surface-passivating ligands can tune the stability of facets and control the growth of the NCs. In a typical synthesis of cubic $CsPbBr_3$ NCs, CsBr gradually changes into cube-shaped $CsPbBr_3$ through indirect production of nanocubes from seed CsBr NCs. Manna et al. showed that the Cs(I) atoms in the sublattice may have remained unaltered during the transformation [212]. This result that $CsPbBr_3$ may form cubes also suggests that the material is susceptible to cube formation despite the synthetic process used. This further complicates the question of whether ligands control facet stabilization or if it is a dominating perovskite feature at the nanoscale. More research and examination in this area is required to establish the underlying notion of perovskite NCs production. $CsPbBr_3$ has various facets (**Scheme 12**), which can be stabilised by various functional groups creating different units for the self-assembly process [21]. Cations and anions are commonly present in all six facets of conventional cubes of orthorhombic $CsPbBr_3$ NCs. Facets, such as {200} and {112} alternately organise halide anions and metal cations. Therefore, stabilizing these facets can necessitate the use of polar solvents other than 1-octadecene or the use of polar chemicals that would limit the growth of these directions. At the surface of NCs, ligands stabilising numerous halides or replacing them with suitable functional groups may aid in the stabilization of these new facets while retaining high emission. Ligands that terminate in di- or trihalides, e.g., would immediately coordinate with surface Pb (II). These ligands may be considered better for stabilizing {200} facets rather than {110} facets due to their strong affinity because they have different halide ions at the binding sites. Appropriate ligands with correct functional locations

to coordinate distinct halide ions on different facets, on the other hand, would aid in saturating the halide ions of $[PbX_6]^{4-}$ octahedra.

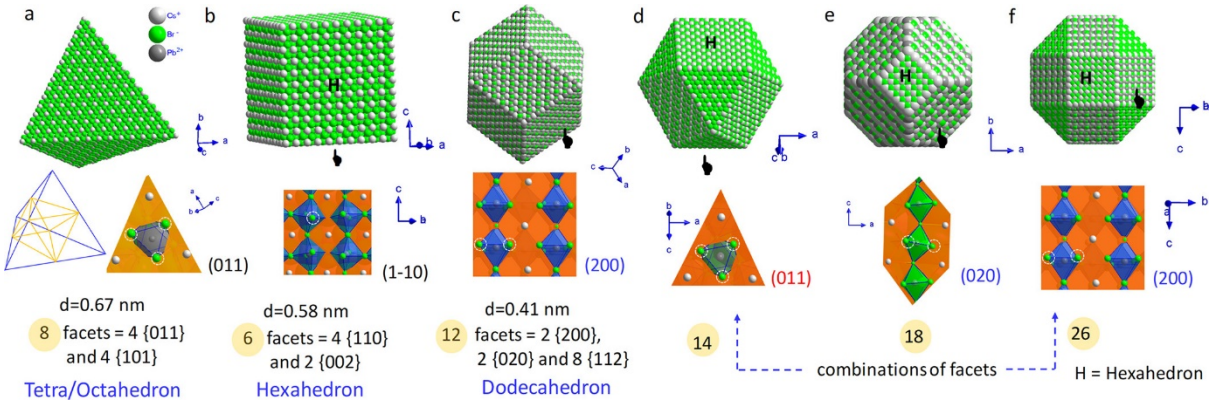

Scheme 12. Representation of polyhedrons with various facets: (a) tetrahedron (4-facet) (b) hexahedron (6-facet), (c) rhombic dodecahedron (12-facet), (d) cuboctahedron (14-facet) (e) polyhedron (18-facet) and (f) rhombicuboctahedron (26-facet). Bottom panels represent planes passing through terminated sites. Reprinted with permission from Ref [21].

Perovskite NCs and supercrystals have already been shown to self-assemble into cubes. However, NCs with different shapes that are believed to have an anisotropic structure can cause wide-area self-assembly and orientated attachments, resulting in new nanostructures. Using a halide precursor of α-bromo ketone, Pradhan et al. produced various shaped NCs without affecting PL QY [188]. The resulting NCs are stabilized by 12 facets ({200}, {020}, {112}) and result in 12 faceted rhombic dodecahedrons. In most of the reactions, these 12 faceted NCs self-assembled over a large region. Primary ammonium ions produced six faceted NCs, while tertiary ammonium ions stabilized a separate group of facets.

9. Properties and application of perovskite superlattices

A variety of optoelectronic devices have been constructed using perovskite NCs and their SLs, and their cooperative effects have proven invaluable in adjusting optoelectronic properties in ways that chemical engineering efforts at individual quantum dots can't. When emitters interact coherently via a common light field, they can behave significantly differently than their separate constituents. Collective coupling can result in a many-body quantum phenomenon that results in short, intense bursts of light known as superfluorescence—after such an ensemble is excited e.g., Rainò et al developed self-assembled 3D $CsPbX_3$ (X = Cl, Br) NCs SLs which exhibited signatures of superfluorescence [3]. Miniaturized photonic sources made of semiconducting two-dimensional (2D) materials hold promise for technological improvements beyond current III-V platforms. The transition dipole moment (TDM) of bright excitons in quantum-confined two-dimensional (2D) materials is orientated parallel to the surface plane, which is required for high-efficiency quantum optics and electroluminescent devices. Decoupled multi-quantum well (MQW) superlattices can be made by putting atomically thin quantum barriers (QBs) between individual 2D material layers. Following the path of III–V semiconductors, one of the key motivations for developing 2D material-based MQW SLs is to achieve high spontaneous emission without activating multiexciton quenching mechanisms like the Auger process, which diminish the PL QY significantly. Jagielski et al. demonstrated the lead halide perovskites SLs as ultrathin 2D material-based excellent quantum emitters [213].

The capacity of redox species to adsorb on the surface of perovskite NCs determines their rate of catalytic activity. While perovskite NCs have already demonstrated a high level of light absorption, fine-tuning their facets may aid to improve their adsorption capacity and hence catalytic effectiveness. Furthermore, creating polar surfaces could improve their solubility in polar solvents, affecting catalysis rate. It has previously been shown that non-cubic perovskite NCs are more catalytically active than nanocubes in the reduction of CO_2 [214]. Different facets possess different atomic terminations, which play an important role in the anisotropic growth and self-assembly process [215]. Anisotropic NC assemblies typically have strong plasmonic, electronic and excitonic interactions which makes them suitable for sensing, catalysis, energy harvesting, and other technological applications.

10. Outlook and challenges

10.1. New design strategies

$CsPbBr_3$ nanocubes have a proclivity for fusing together to form single crystals, making them ideal for self-assembling thin films and luminous nanopatterned devices. However, they quickly dissolve in a polar solvent due to their ionic nature; they cluster due to high vdW interactions between the lengthy capping ligands in a non-polar solvent. Hence, preventing colloidal aggregation from achieving close-packed monolayer thin films is still a work in progress. Improved radiative characteristics and superfluorescence result from QDs self-assembling into SL structures. The large organic ligands that passivate the surface of these QDs, on the other hand, generate significant spatial confinement, resulting in high Auger recombination rates. When temporally long excitation pulses are used, the long-chain organic ligands also inhibit heat dissipation, causing significant thermal loads with acute impacts. Furthermore, the lengthy ligands result in reduced packing factors (volume of QDs per unit volume), lowering the laser active layer's total refractive index. As a result, modal confinement is reduced, and the threshold lasing fluence is increased even further. The packing factor can be increased and Auger recombination can be reduced by substituting inorganic compounds for long-chain organic ligands.

10.2. Self-assembled structure of chiral perovskites

Chiral perovskites have gained significant scientific attention owing to their novel optoelectronic characteristics. Theoretically, chiral organic-inorganic hybrid perovskites with considerable optical activity were anticipated and fabricated with chirality due to the included chiral organic molecules. The creation of optically chiral perovskite NCs relies primarily on symmetry breaking through chiral defects or chiral assembly structures of the inorganic perovskite NCs, unlike electronic interactions with chiral molecules. The high-temperature cubic phase and the low-temperature tetragonal and orthorhombic phases of $CsPbBr_3$ are achiral. All-inorganic perovskite NCs with intrinsic chiral characteristics are rarely documented because it is challenging to have exact control over the enantiomeric synthesis of chiral NCs. Furthermore, questions about effective characterisation methods, incisive simulations, and theoretical support remain unresolved.

10.3. Multicomponent perovskite nanocrystals self-assembly

The emergence of collective phenomena, such as enhanced optical properties, coherent long-range energy transport, and their potential use as light sources and in photovoltaics have piqued interest in atomically defined assemblies of dye molecules. The organisation of colloidal $CsPbBr_3$-LaF_3 has already been reported (**Scheme 13**) [97,98,216]. These kinds of metamaterials will be beneficial to achieve better collective phenomena.

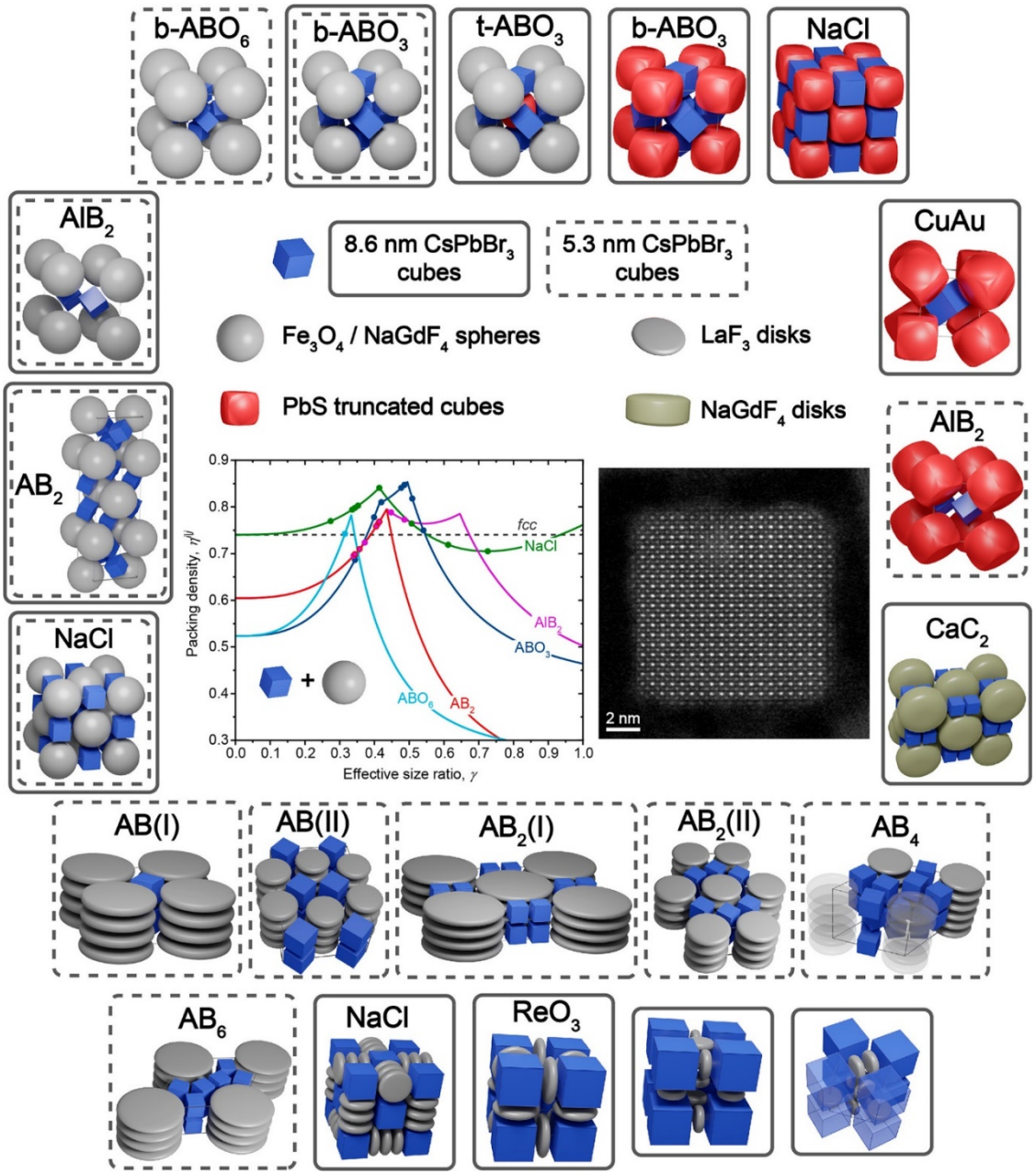

Scheme 13. (a) Schematic diagram of self-assembly of binary and ternary SLs. Self-assembly of $CsPbBr_3$ nanocubes (5.3 and 8.6 nm) with spherical Fe_3O_4 (11.2–25.1 nm), spherical

$NaGdF_4$ NCs (10.7–11.7 nm), truncated cuboid PbS NCs (10.7–11.7 nm), $NaGdF_4$ disks (31.5 nm in diameter and 18.5 nm thick), and disk-shaped LaF_3 NCs (6.5–28.4 nm). Reprinted with permission from Ref [217].

semiconductor NCs into long-range-ordered SLs is another method to construct adaptable and controlled aggregates that show collective phenomena. Due to the strong oscillator power of brilliant triplet excitons, gradual dephasing (coherence periods of up to 80 picoseconds), and minimum inhomogeneous broadening of emission lines, caesium lead halide perovskite NCs are attractive building blocks for such SLs. The self-assembly of two or three different NCs of separate materials into their corresponding binary or ternary SL can produce a wide range of metamaterials with controlled chemical compositions and well-packed components [218]. To form these self-assembled SLs, the NC packing density must be maximized. Various multicomponent hetero SLs, such as $CsPbBr_3$-Fe_3O_4, $CsPbBr_3$-PbS, $CsPbBr_3$-$NaGdF_4$, and

10.4. Self-assembly of perovskite heterostructure

Colloidal synthesis techniques produce colloidal NCs with progressively large numbers of elements and nanoheterostructures with increasingly sophisticated sizes, shapes, and compositions (**Scheme 14)**. This shift toward more complex NCs is in response to an increasing desire for chemical compositions that are both earth-friendly and non-toxic, as well as optimal optoelectronic properties. Dou et al. used two 2D halide perovskites based on bulky and rigid thiophene-based conjugated organic cations to create atomically flat vertical heterostructures [219,220]. In comparison to short aliphatic chains, these ligands were found to be substantially more effective stabilizers and inhibitors of halide interdiffusion. These findings offer fresh insights into molecular engineering options for inhibiting intrinsic interdiffusion in halide perovskites and reducing the instability of perovskite devices. Yuan et al. reported self-assembled core−shell structured perovskite quantum dots with PL QY of 85%, which is highly beneficial for perovskite LEDs [183]. However, there is no report on self-assembly of core-shell perovskite nanorods to date. These kinds of materials would show better charge transfer properties with excellent stability under humid conditions.

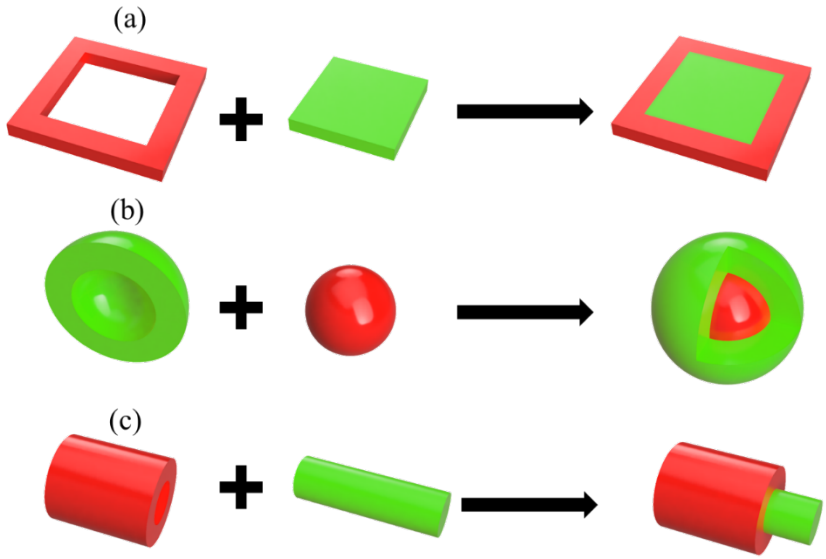

Scheme 14. Self-assembly of different types of core-shell nanoparticles. (a) 2D halide perovskite lateral heterostructures, (b) core-shell structured quantum dots, and (c) core-shell nanorods.

10.5. Liquid-cell TEM technique

Ex-situ characterisation of perovskite SLs has traditionally been done on dry materials stored in a vacuum chamber of a TEM apparatus. The arrangement of perovskites SLs after evaporation can be determined using this method; however, it does not reveal the self-assembly mechanism. Liquid-cell TEM techniques have been developed in recent years, allowing wet materials to be delivered into the vacuum chamber of an instrument [221,222]. This method visualises NCs in solution by encapsulating small amounts of NCs solution between silicon nitride or graphene layers. Liquid-cell TEM has recently revealed vital information on interparticle interactions and crystallite atomic structure NCs in solution. The development of NCs SLs may also be observed in situ. With the advancement of imaging tools [223], it will promising to compare the dynamics of the ordering transition to those known for micrometre-sized colloidal perovskite SLs, where direct imaging is already well-established.

10.6. Solving the stability issue for superlattices

Self-assembled $CsPbBr_3$ NCs aged in vacuum or air produce optical fingerprints that resemble cooperative emission at cryogenic temperatures: narrow, low-energy PL peaks with rapid, oscillating emission decays. The bulk-like $CsPbBr_3$ NCs developed in the SLs are responsible for these optical characteristics. The labile caesium oleate ligands appear insufficient to construct long-lasting assemblies despite the size uniformity and shape purity of the initial $CsPbBr_3$ NCs. Surface-enhanced $CsPbX_3$ NCs capped with ZnX_2, phosphonate, or zwitterions and improved ligand exchanges with quaternary ammonium halides, thiocyanates, and other Lewis bases are likely to enable the manufacture of ageing and air-resistant assemblies in the future. A shape-pure $CsPbX_3$ NCs SLs with a near-unity PL QY and stability against coalescence and reactivity in the air is a viable contender for future collective phenomena study and applications.

Full Title: Self-assembly of perovskite nanocrystals

Short title (limit 20 words): Self-assembly of perovskite

Declaration of Competing Interest

The authors declare that they have no known competing financial interests or personal relationships that could have appeared to influence the work reported in this paper.

Acknowledgments

This work was supported by the National Research Foundation (NRF) of Korea (grant nos. 2021R1A2B5B01001796, 2021R1F1A1062672, 2021R1F1A1062528, and 2021R1A4A5031805), and the Technology Innovation Program (grant no. 20013597) funded by the Ministry of Trade, Industry & Energy.

References

[1] Lee YS. Self-Assembly and Nanotechnology: A Force Balance Approach. John Wiley & Sons, Inc.; 2017. https://doi.org/10.1002/9780470292525.

[2] Goddard WA, Brenner DW, Lyshevski SE, Iafrate GJ. Handbook of Nanoscience, Engineering, and Technology. CRC Press (3rd Ed); 2012. https://doi.org/10.1201/9781315217178.

[3] Rainò G, Becker MA, Bodnarchuk MI, Mahrt RF, Kovalenko MV, Stöferle T. Superfluorescence from lead halide perovskite quantum dot superlattices. Nature 2018;563:671–5. https://doi.org/10.1038/s41586-018-0683-0.

[4] Zhou C, Zhong Y, Dong H, Zheng W, Tan J, Jie Q, et al. Cooperative excitonic quantum ensemble in perovskite-assembly superlattice microcavities. Nat Commun 2020;11:329. https://doi.org/10.1038/s41467-019-14078-1.

[5] Jana A, Cho S, Patil SA, Meena A, Jo Y, Sree VG, et al. Perovskite: Scintillators, direct detectors, and X-ray imagers. Mater Today 2022;xxx. https://doi.org/10.1016/j.mattod.2022.04.009.

[6] Chen Y, Liu S, Zhou N, Li N, Zhou H, Sun L-D, et al. An overview of rare earth coupled lead halide perovskite and its application in photovoltaics and light emitting devices. Prog Mater Sci 2021;120:100737. https://doi.org/10.1016/j.pmatsci.2020.100737.

[7] Jena AK, Kulkarni A, Miyasaka T. Halide Perovskite Photovoltaics: Background, Status, and Future Prospects. Chem Rev 2019;119:3036–103. https://doi.org/10.1021/acs.chemrev.8b00539.

[8] Chen J, Dong C, Idriss H, Mohammed OF, Bakr OM. Metal Halide Perovskites for Solar-to-Chemical Fuel Conversion. Adv Energy Mater 2020;10:1902433. https://doi.org/10.1002/aenm.201902433.

[9] Liu X-K, Xu W, Bai S, Jin Y, Wang J, Friend RH, et al. Metal halide perovskites for light-emitting diodes. Nat Mater 2021;20:10–21. https://doi.org/10.1038/s41563-020-0784-7.

[10] Ahmadi M, Wu T, Hu B. A Review on Organic–Inorganic Halide Perovskite Photodetectors: Device Engineering and Fundamental Physics. Adv Mater 2017;29:1605242. https://doi.org/10.1002/adma.201605242.

[11] Protesescu L, Yakunin S, Bodnarchuk MI, Krieg F, Caputo R, Hendon CH, et al. Nanocrystals of Cesium Lead Halide Perovskites ($CsPbX_3$, X = Cl, Br, and I): Novel Optoelectronic Materials Showing Bright Emission with Wide Color Gamut. Nano Lett 2015;15:3692–6. https://doi.org/10.1021/nl5048779.

[12] Huang H, Polavarapu L, Sichert JA, Susha AS, Urban AS, Rogach AL. Colloidal lead halide perovskite nanocrystals: synthesis, optical properties and applications. NPG Asia Mater 2016;8:e328. https://doi.org/10.1038/am.2016.167.

[13] Pourdavoud N, Wang S, Mayer A, Hu T, Chen Y, Marianovich A, et al. Photonic Nanostructures Patterned by Thermal Nanoimprint Directly into Organo-Metal Halide Perovskites. Adv Mater 2017;29:1605003. https://doi.org/10.1002/adma.201605003.

[14] Jana A, Park S, Cho S, Kim H, Im H. Monodispersed perovskite quantum wells for efficient LEDs. Matter 2022;5:384–6. https://doi.org/10.1016/j.matt.2022.01.007.

[15] Jana A, Park S, Cho S, Kim H, Im H. Bounce back with triplet excitons for efficient X-ray scintillation. Matter 2022;5:20–2. https://doi.org/10.1016/j.matt.2021.12.004.

[16] Akkerman QA, Rainò G, Kovalenko M V., Manna L. Genesis, challenges and opportunities for colloidal lead halide perovskite nanocrystals. Nat Mater 2018;17:394–405. https://doi.org/10.1038/s41563-018-0018-4.

[17] Hintermayr VA, Richter AF, Ehrat F, Döblinger M, Vanderlinden W, Sichert JA, et al. Tuning the Optical Properties of Perovskite Nanoplatelets through Composition and Thickness by Ligand-Assisted Exfoliation. Adv Mater 2016;28:9478–85. https://doi.org/10.1002/adma.201602897.
[18] Hudait B, Dutta SK, Pradhan N. Isotropic $CsPbBr_3$ Perovskite Nanocrystals beyond Nanocubes: Growth and Optical Properties. ACS Energy Lett 2020;5:650–6. https://doi.org/10.1021/acsenergylett.9b02729.
[19] Wang K-H, Yang J-N, Ni Q-K, Yao H-B, Yu S-H. Metal Halide Perovskite Supercrystals: Gold–Bromide Complex Triggered Assembly of $CsPbBr_3$ Nanocubes. Langmuir 2018;34:595–602. https://doi.org/10.1021/acs.langmuir.7b03432.
[20] Patra BK, Agrawal H, Zheng J-Y, Zha X, Travesset A, Garnett EC. Close-Packed Ultrasmooth Self-assembled Monolayer of $CsPbBr_3$ Perovskite Nanocubes. ACS Appl Mater Interfaces 2020;12:31764–9. https://doi.org/10.1021/acsami.0c05945.
[21] Pradhan N. Why Do Perovskite Nanocrystals Form Nanocubes and How Can Their Facets Be Tuned? A Perspective from Synthetic Prospects. ACS Energy Lett 2021;6:92–9. https://doi.org/10.1021/acsenergylett.0c02099.
[22] Imran M, Ijaz P, Baranov D, Goldoni L, Petralanda U, Akkerman Q, et al. Shape-Pure, Nearly Monodispersed $CsPbBr_3$ Nanocubes Prepared Using Secondary Aliphatic Amines. Nano Lett 2018;18:7822–31. https://doi.org/10.1021/acs.nanolett.8b03598.
[23] Uddin MA, Glover JD, Park SM, Pham JT, Graham KR. Growth of Highly Stable and Luminescent $CsPbX_3$ (X = Cl, Br, and I) Nanoplates via Ligand Mediated Anion Exchange of $CsPbCl_3$ Nanocubes with AlX_3. Chem Mater 2020;32:5217–25. https://doi.org/10.1021/acs.chemmater.0c01325.
[24] Cho S, Kim S, Kim J, Jo Y, Ryu I, Hong S, et al. Hybridisation of perovskite nanocrystals with organic molecules for highly efficient liquid scintillators. Light Sci Appl 2020;9:156. https://doi.org/10.1038/s41377-020-00391-8.
[25] Zhou C, M. Pina J, Zhu T, H. Parmar D, Chang H, Yu J, et al. Quantum Dot Self-Assembly Enables Low-Threshold Lasing. Adv Sci 2021;2101125:2101125. https://doi.org/10.1002/advs.202101125.
[26] Lamba RS, Basera P, Bhattacharya S, Sapra S. Band Gap Engineering in Cs 2 (Na x Ag 1– x)BiCl 6 Double Perovskite Nanocrystals. J Phys Chem Lett 2019;10:5173–81. https://doi.org/10.1021/acs.jpclett.9b02168.
[27] Lamba RS, Basera P, Singh S, Bhattacharya S, Sapra S. Lead-Free Alloyed Double-Perovskite Nanocrystals of Cs 2 (Na x Ag 1– x)BiBr 6 with Tunable Band Gap. J Phys Chem C 2021;125:1954–62. https://doi.org/10.1021/acs.jpcc.0c09554.
[28] Yang D, Li X, Zhou W, Zhang S, Meng C, Wu Y, et al. CsPbBr 3 Quantum Dots 2.0: Benzenesulfonic Acid Equivalent Ligand Awakens Complete Purification. Adv Mater 2019;31:1900767. https://doi.org/10.1002/adma.201900767.
[29] Sheng X, Chen G, Wang C, Wang W, Hui J, Zhang Q, et al. Polarized Optoelectronics of $CsPbX_3$ (X = Cl, Br, I) Perovskite Nanoplates with Tunable Size and Thickness. Adv Funct Mater 2018;28:1800283. https://doi.org/10.1002/adfm.201800283.
[30] Xiao X, Li Y, Xie R-J. Blue-emitting and self-assembled thinner perovskite $CsPbBr_3$ nanoplates: synthesis and formation mechanism. Nanoscale 2020;12:9231–9. https://doi.org/10.1039/c9nr10885h.
[31] Bekenstein Y, Koscher BA, Eaton SW, Yang P, Alivisatos AP. Highly Luminescent Colloidal Nanoplates of Perovskite Cesium Lead Halide and Their Oriented Assemblies. J Am Chem Soc 2015;137:16008–11. https://doi.org/10.1021/jacs.5b11199.
[32] Yin T, Fang Y, Chong WK, Ming KT, Jiang S, Li X, et al. High-Pressure-Induced

Comminution and Recrystallization of $CH_3NH_3PbBr_3$ Nanocrystals as Large Thin Nanoplates. Adv Mater 2018;30:1705017. https://doi.org/10.1002/adma.201705017.
[33] Jana A, Mittal M, Singla A, Sapra S. Solvent-free, mechanochemical syntheses of bulk trihalide perovskites and their nanoparticles. Chem Commun 2017;53:3046–9. https://doi.org/10.1039/c7cc00666g.
[34] Ji C, Wang S, Wang Y, Chen H, Li L, Sun Z, et al. 2D Hybrid Perovskite Ferroelectric Enables Highly Sensitive X-Ray Detection with Low Driving Voltage. Adv Funct Mater 2020;30:1905529. https://doi.org/10.1002/adfm.201905529.
[35] Shamsi J, Dang Z, Bianchini P, Canale C, Di Stasio F, Brescia R, et al. Colloidal Synthesis of Quantum Confined Single Crystal $CsPbBr_3$ Nanosheets with Lateral Size Control up to the Micrometer Range. J Am Chem Soc 2016;138:7240–3. https://doi.org/10.1021/jacs.6b03166.
[36] Pradhan B, Kumar GS, Sain S, Dalui A, Ghorai UK, Pradhan SK, et al. Size Tunable Cesium Antimony Chloride Perovskite Nanowires and Nanorods. Chem Mater 2018;30:2135–42. https://doi.org/10.1021/acs.chemmater.8b00427.
[37] Ciszek JW, Huang L, Tsonchev S, Wang Y, Shull KR, Ratner MA, et al. Assembly of Nanorods into Designer Superstructures: The Role of Templating, Capillary Forces, Adhesion, and Polymer Hydration. ACS Nano 2010;4:259–66. https://doi.org/10.1021/nn901383d.
[38] Li Y, Huang H, Xiong Y, Richter AF, Kershaw SV, Feldmann J, et al. Using Polar Alcohols for the Direct Synthesis of Cesium Lead Halide Perovskite Nanorods with Anisotropic Emission. ACS Nano 2019;13:8237–45. https://doi.org/10.1021/acsnano.9b03508.
[39] Aharon S, Etgar L. Two Dimensional Organometal Halide Perovskite Nanorods with Tunable Optical Properties. Nano Lett 2016;16:3230–5. https://doi.org/10.1021/acs.nanolett.6b00665.
[40] Jana A, Kim KS. Water-Stable, Fluorescent Organic−Inorganic Hybrid and Fully Inorganic Perovskites. ACS Energy Lett 2018;3:2120–6. https://doi.org/10.1021/acsenergylett.8b01394.
[41] Jana A, Ba Q, Kim KS. Compositional and Dimensional Control of 2D and Quasi-2D Lead Halide Perovskites in Water. Adv Funct Mater 2019;29:1900966. https://doi.org/10.1002/adfm.201900966.
[42] Pan A, Jurow MJ, Wu Y, Jia M, Zheng F, Zhang Y, et al. Highly Stable Luminous "Snakes" from CsPbX3 Perovskite Nanocrystals Anchored on Amine-Coated Silica Nanowires. ACS Appl Nano Mater 2019;2:258–66. https://doi.org/10.1021/acsanm.8b01889.
[43] Dong Y, Wang Y-K, Yuan F, Johnston A, Liu Y, Ma D, et al. Bipolar-shell resurfacing for blue LEDs based on strongly confined perovskite quantum dots. Nat Nanotechnol 2020;15:668–74. https://doi.org/10.1038/s41565-020-0714-5.
[44] Yuan Y, Liu Z, Liu Z, Peng L, Li Y, Tang A. Photoluminescence and self-assembly of cesium lead halide perovskite nanocrystals: Effects of chain length of organic amines and reaction temperature. Appl Surf Sci 2017;405:280–8. https://doi.org/10.1016/j.apsusc.2017.02.024.
[45] Pan A, He B, Fan X, Liu Z, Urban JJ, Alivisatos AP, et al. Insight into the Ligand-Mediated Synthesis of Colloidal $CsPbBr_3$ Perovskite Nanocrystals: The Role of Organic Acid, Base, and Cesium Precursors. ACS Nano 2016;10:7943–54. https://doi.org/10.1021/acsnano.6b03863.
[46] Jana A, Bathula C, Park Y, Kadam A, Sree VG, Ansar S, et al. Facile synthesis and optical study of organic-inorganic lead bromide perovskite-clay (kaolinite,

montmorillonite, and halloysite) composites. Surfaces and Interfaces 2022;29:101785. https://doi.org/10.1016/j.surfin.2022.101785.
[47] Bera S, Pradhan N. Perovskite Nanocrystal Heterostructures: Synthesis, Optical Properties, and Applications. ACS Energy Lett 2020;5:2858–72. https://doi.org/10.1021/acsenergylett.0c01449.
[48] Zu Y, Xi J, Li L, Dai J, Wang S, Yun F, et al. High-Brightness and Color-Tunable $FAPbBr_3$ Perovskite Nanocrystals 2.0 Enable Ultrapure Green Luminescence for Achieving Recommendation 2020 Displays. ACS Appl Mater Interfaces 2020;12:2835–41. https://doi.org/10.1021/acsami.9b18140.
[49] Boles MA, Engel M, Talapin DV. Self-Assembly of Colloidal Nanocrystals: From Intricate Structures to Functional Materials. Chem Rev 2016;116:11220–89. https://doi.org/10.1021/acs.chemrev.6b00196.
[50] Shevchenko EV, Talapin DV. Self-assembly of semiconductor nanocrystals into ordered superstructures. Semicond. Nanocrystal Quantum Dots. In: Rogach, Springer Vienna; 2008, p. 119–69. https://doi.org/10.1007/978-3-211-75237-1_5.
[51] Lash MH, Fedorchak M V., McCarthy JJ, Little SR. Scaling up self-assembly: bottom-up approaches to macroscopic particle organization. Soft Matter 2015;11:5597–609. https://doi.org/10.1039/C5SM00764J.
[52] Xu Y, Zhang Q, Lv L, Han W, Wu G, Yang D, et al. Synthesis of ultrasmall $CsPbBr_3$ nanoclusters and their transformation to highly deep-blue-emitting nanoribbons at room temperature. Nanoscale 2017;9:17248–53. https://doi.org/10.1039/c7nr06959f.
[53] Ji Y, Wang M, Yang Z, Ji S, Qiu H. Nanowire-assisted self-assembly of one-dimensional nanocrystal superlattice chains. J Mater Chem C 2019;7:8471–6. https://doi.org/10.1039/C9TC02118C.
[54] Yadav S, Sharma AK, Kumar P. Nanoscale Self-Assembly for Therapeutic Delivery. Front Bioeng Biotechnol 2020;8:1–24. https://doi.org/10.3389/fbioe.2020.00127.
[55] Hamaker HC. The London—van der Waals attraction between spherical particles. Physica 1937;4:1058–72. https://doi.org/10.1016/S0031-8914(37)80203-7.
[56] Margenau H. Van der waals forces. Rev Mod Phys 1939;11:1–35. https://doi.org/10.1103/RevModPhys.11.1.
[57] Li Q, Jonas U, Zhao XS, Kappl M. The forces at work in colloidal self-assembly: a review on fundamental interactions between colloidal particles. Asia-Pac J Chem Eng 2008;3:255–68. https://doi.org/10.1002/apj.144.
[58] Hotze EM, Phenrat T, Lowry GV. Nanoparticle Aggregation: Challenges to Understanding Transport and Reactivity in the Environment. J Environ Qual 2010;39:1909–24. https://doi.org/10.2134/jeq2009.0462.
[59] Inoue M. Structural integrity of metal–polymer adhesive interfaces in microelectronics. Adv. Adhes. Electron., Elsevier; 2011, p. 157–98. https://doi.org/10.1533/9780857092892.2.157.
[60] Wu Z, Li Y, Liu J, Lu Z, Zhang H, Yang B. Colloidal Self-Assembly of Catalytic Copper Nanoclusters into Ultrathin Ribbons. Angew Chem Int Ed 2014;53:12196–200. https://doi.org/10.1002/anie.201407390.
[61] Talapin DV, Shevchenko EV, Murray CB, Titov AV, Král P. Dipole−Dipole Interactions in Nanoparticle Superlattices. Nano Lett 2007;7:1213–9. https://doi.org/10.1021/nl070058c.
[62] Musˇevicˇ I, Sˇkarabot M, Tkalec U, Ravnik M, Zˇumer S. Two-Dimensional Nematic Colloidal Crystals Self-Assembled by Topological Defects. Science 2006;313:954–8. https://doi.org/10.1126/science.1129660.
[63] Wu Z, Liu J, Li Y, Cheng Z, Li T, Zhang H, et al. Self-Assembly of Nanoclusters into

Mono-, Few-, and Multilayered Sheets via Dipole-Induced Asymmetric van der Waals Attraction. ACS Nano 2015;9:6315–23. https://doi.org/10.1021/acsnano.5b01823.
[64] Yang Y, Lee JT, Liyanage T, Sardar R. Flexible Polymer-Assisted Mesoscale Self-Assembly of Colloidal $CsPbBr_3$ Perovskite Nanocrystals into Higher Order Superstructures with Strong Inter-Nanocrystal Electronic Coupling. J Am Chem Soc 2019;141:1526–36. https://doi.org/10.1021/jacs.8b10083.
[65] Ohara PC, Leff DV, Heath JR, Gelbart WM. Crystallization of Opals from Polydisperse Nanoparticles. Phys Rev Lett 1995;75:3466–70. https://doi.org/https://doi.org/10.1103/PhysRevLett.75.3466.
[66] Soetan N, Erwin WR, Tonigan AM, Walker DG, Bardhan R. Solvent-Assisted Self-Assembly of $CsPbBr_3$ Perovskite Nanocrystals into One-Dimensional Superlattice. J Phys Chem C 2017;121:18186–94. https://doi.org/10.1021/acs.jpcc.7b03939.
[67] Tong Y, Yao E-P, Manzi A, Bladt E, Wang K, Döblinger M, et al. Spontaneous Self-Assembly of Perovskite Nanocrystals into Electronically Coupled Supercrystals: Toward Filling the Green Gap. Adv Mater 2018;30:1801117. https://doi.org/10.1002/adma.201801117.
[68] Lin S, He X, Li Y, Lin J, Nose T. Brownian Molecular Dynamics Simulation on Self-Assembly Behavior of Diblock Copolymers: Influence of Chain Conformation. J Phys Chem B 2009;113:13926–34. https://doi.org/10.1021/jp904707a.
[69] Hunter RJ. Foundations of Colloid Science. (2nd Ed). Oxford Univ Press; 2009.
[70] Murray CA, Grier DG. Video Microscopy of Monodisperse Colloidal Systems. Annu Rev Phys Chem 1996;47:421–62. https://doi.org/10.1146/annurev.physchem.47.1.421.
[71] Dang Z, Dhanabalan B, Castelli A, Dhall R, Bustillo KC, Marchelli D, et al. Temperature-Driven Transformation of $CsPbBr_3$ Nanoplatelets into Mosaic Nanotiles in Solution through Self-Assembly. Nano Lett 2020;20:1808–18. https://doi.org/10.1021/acs.nanolett.9b05036.
[72] Bishop KJM, Wilmer CE, Soh S, Grzybowski BA. Nanoscale Forces and Their Uses in Self-Assembly. Small 2009;5:1600–30. https://doi.org/10.1002/smll.200900358.
[73] Min Y, Akbulut M, Kristiansen K, Golan Y, Israelachvili J. The role of interparticle and external forces in nanoparticle assembly. Nat Mater 2008;7:527–38. https://doi.org/https://doi.org/10.1038/nmat2206.
[74] Miszta K, de Graaf J, Bertoni G, Dorfs D, Brescia R, Marras S, et al. Hierarchical self-assembly of suspended branched colloidal nanocrystals into superlattice structures. Nat Mater 2011;10:872–6. https://doi.org/10.1038/nmat3121.
[75] Grzelczak M, Sánchez-Iglesias A, Mezerji HH, Bals S, Pérez-Juste J, Liz-Marzán LM. Steric Hindrance Induces crosslike Self-Assembly of Gold Nanodumbbells. Nano Lett 2012;12:4380–4. https://doi.org/10.1021/nl3021957.
[76] Fan Y, Cheng L, Liu C, Xie Y, Liu W, Li Y, et al. Steric effect on the self-assembly behaviours of amino acid derivatives. RSC Adv 2014;4:52245–9. https://doi.org/10.1039/C4RA06582D.
[77] Mimura K, Kato K. Fabrication and piezoresponse properties of {100} BaTiO3 films containing highly ordered nanocube assemblies on various substrates. J Nanoparticle Res 2013;15:1995. https://doi.org/10.1007/s11051-013-1995-5.
[78] Wang QJ, Chung Y-W. Encyclopedia of Tribology. Springer, Boston; 2013. https://doi.org/10.1007/978-0-387-92897-5.
[79] Neukirch S, Roman B, de Gaudemaris B, Bico J. Piercing a liquid surface with an elastic rod: Buckling under capillary forces. J Mech Phys Solids 2007;55:1212–35. https://doi.org/10.1016/j.jmps.2006.11.009.
[80] Gracias DH, Kavthekar V, Love JC, Paul KE, Whitesides GM. Fabrication of

Micrometer-Scale, Patterned Polyhedra by Self-Assembly. Adv Mater 2002;14:235–8. https://doi.org/10.1002/1521-4095(20020205)14:3<235::AID-ADMA235>3.0.CO;2-B.
[81] Zhou Y, Zhou X, Park DJ, Torabi K, Brown KA, Jones MR, et al. Shape-Selective Deposition and Assembly of Anisotropic Nanoparticles. Nano Lett 2014;14:2157–61. https://doi.org/10.1021/nl500471g.
[82] Steiner T. The Hydrogen Bond in the Solid State. Angew Chem Int Ed 2002;41:48–76. https://doi.org/10.1002/1521-3773(20020104)41:1<48::AID-ANIE48>3.0.CO;2-U.
[83] Jones MR, Seeman NC, Mirkin CA. Programmable materials and the nature of the DNA bond. Science 2015;347:1260901. https://doi.org/10.1126/science.1260901.
[84] Rogers WB, Shih WM, Manoharan VN. Using DNA to program the self-assembly of colloidal nanoparticles and microparticles. Nat Rev Mater 2016;1:16008. https://doi.org/10.1038/natrevmats.2016.8.
[85] Brown AAM, Hooper TJN, Veldhuis SA, Chin XY, Bruno A, Vashishtha P, et al. Self-assembly of a robust hydrogen-bonded octylphosphonate network on cesium lead bromide perovskite nanocrystals for light-emitting diodes. Nanoscale 2019;11:12370–80. https://doi.org/10.1039/C9NR02566A.
[86] Meng X, Lin J, Liu X, He X, Wang Y, Noda T, et al. Highly Stable and Efficient $FASnI_3$ -Based Perovskite Solar Cells by Introducing Hydrogen Bonding. Adv Mater 2019;31:1903721. https://doi.org/10.1002/adma.201903721.
[87] Li X, Ibrahim Dar M, Yi C, Luo J, Tschumi M, Zakeeruddin SM, et al. Improved performance and stability of perovskite solar cells by crystal crosslinking with alkylphosphonic acid ω-ammonium chlorides. Nat Chem 2015;7:703–11. https://doi.org/10.1038/nchem.2324.
[88] Li N, Tao S, Chen Y, Niu X, Onwudinanti CK, Hu C, et al. Cation and anion immobilization through chemical bonding enhancement with fluorides for stable halide perovskite solar cells. Nat Energy 2019;4:408–15. https://doi.org/10.1038/s41560-019-0382-6.
[89] Wang S, Popović J, Burazer S, Portniagin A, Liu F, Low K, et al. Strongly Luminescent Dion–Jacobson Tin Bromide Perovskite Microcrystals Induced by Molecular Proton Donors Chloroform and Dichloromethane. Adv Funct Mater 2021;31:2102182. https://doi.org/10.1002/adfm.202102182.
[90] Park MS, Kim JK. Breath Figure Patterns Prepared by Spin Coating in a Dry Environment. Langmuir 2004;20:5347–52. https://doi.org/10.1021/la035915g.
[91] Ou Y, Wang L-Y, Zhu L-W, Wan L-S, Xu Z-K. In-Situ Immobilization of Silver Nanoparticles on Self-Assembled Honeycomb-Patterned Films Enables Surface-Enhanced Raman Scattering (SERS) Substrates. J Phys Chem C 2014;118:11478–84. https://doi.org/10.1021/jp503166g.
[92] S. de León A, de la Mata M, Sanchez-Alarcon IR, Abargues R, Molina SI. Self-Assembly of CsPbBr 3 Perovskites in Micropatterned Polymeric Surfaces: Toward Luminescent Materials with Self-Cleaning Properties. ACS Appl Mater Interfaces 2022;14:20023–31. https://doi.org/10.1021/acsami.2c01567.
[93] Penzo E, Loiudice A, Barnard ES, Borys NJ, Jurow MJ, Lorenzon M, et al. Long-Range Exciton Diffusion in Two-Dimensional Assemblies of Cesium Lead Bromide Perovskite Nanocrystals. ACS Nano 2020;14:6999–7007. https://doi.org/10.1021/acsnano.0c01536.
[94] Karnaushenko D, Kang T, Schmidt OG. Shapeable Material Technologies for 3D Self-Assembly of Mesoscale Electronics. Adv Mater Technol 2019;4:1800692. https://doi.org/10.1002/admt.201800692.

[95] Ikkala O, ten Brinke G. Hierarchical self-assembly in polymeric complexes: Towards functional materials. Chem Commun 2004:2131. https://doi.org/10.1039/b403983a.
[96] Zhou Y, Yan D. Supramolecular self-assembly of amphiphilic hyperbranched polymers at all scales and dimensions: progress, characteristics and perspectives. Chem Commun 2009:1172. https://doi.org/10.1039/b814560c.
[97] Cherniukh I, Rainò G, Stöferle T, Burian M, Travesset A, Naumenko D, et al. Perovskite-type superlattices from lead halide perovskite nanocubes. Nature 2021;593:535–42. https://doi.org/10.1038/s41586-021-03492-5.
[98] Cherniukh I, Rainò G, Sekh T V., Zhu C, Shynkarenko Y, John RA, et al. Shape-Directed Co-Assembly of Lead Halide Perovskite Nanocubes with Dielectric Nanodisks into Binary Nanocrystal Superlattices. ACS Nano 2021:acsnano.1c06047. https://doi.org/10.1021/acsnano.1c06047.
[99] Soetan N, Erwin WR, Tonigan AM, Walker DG, Bardhan R. Solvent-Assisted Self-Assembly of $CsPbBr_3$ Perovskite Nanocrystals into One-Dimensional Superlattice. J Phys Chem C 2017;121:18186–94. https://doi.org/10.1021/acs.jpcc.7b03939.
[100] Quan Z, Xu H, Wang C, Wen X, Wang Y, Zhu J, et al. Solvent-Mediated Self-Assembly of Nanocube Superlattices. J Am Chem Soc 2014;136:1352–9. https://doi.org/10.1021/ja408250q.
[101] Choi JJ, Bian K, Baumgardner WJ, Smilgies D-M, Hanrath T. Interface-Induced Nucleation, Orientational Alignment and Symmetry Transformations in Nanocube Superlattices. Nano Lett 2012;12:4791–8. https://doi.org/10.1021/nl3026289.
[102] Mehetor SK, Ghosh H, Pradhan N. Acid-Amine Equilibria for Formation and Long-Range Self-Organization of Ultrathin $CsPbBr_3$ Perovskite Platelets. J Phys Chem Lett 2019;10:1300–5. https://doi.org/10.1021/acs.jpclett.9b00333.
[103] Wang L, Liu B, Zhao X, Demir HV, Gu H, Sun H. Solvent-Assisted Surface Engineering for High-Performance All-Inorganic Perovskite Nanocrystal Light-Emitting Diodes. ACS Appl Mater Interfaces 2018;10:19828–35. https://doi.org/10.1021/acsami.8b06105.
[104] Babu R, Singh SP. Solvent-Assisted Tuning of the Size and Shape of $CsPbBr_3$ Nanocrystals via Redispersion Process at Ambient Condition. Langmuir 2018;34:15507–16. https://doi.org/10.1021/acs.langmuir.8b02477.
[105] Yamada M, Shen Z, Miyake M. Self-assembly of discotic liquid crystalline molecule-modified gold nanoparticles: control of 1D and hexagonal ordering induced by solvent polarity. Chem Commun 2006:2569–71. https://doi.org/10.1039/b604001b.
[106] Nie Z, Fava D, Kumacheva E, Zou S, Walker GC, Rubinstein M. Self-assembly of metal–polymer analogues of amphiphilic triblock copolymers. Nat Mater 2007;6:609–14. https://doi.org/10.1038/nmat1954.
[107] Zhao N, Liu K, Greener J, Nie Z, Kumacheva E. Close-Packed Superlattices of Side-by-Side Assembled Au-CdSe Nanorods. Nano Lett 2009;9:3077–81. https://doi.org/10.1021/nl901567a.
[108] Quintana M, Prato M. Supramolecular aggregation of functionalized carbon nanotubes. Chem Commun 2009:6005–7. https://doi.org/10.1039/b915126e.
[109] García I, Sánchez-Iglesias A, Henriksen-Lacey M, Grzelczak M, Penadés S, Liz-Marzán LM. Glycans as Biofunctional Ligands for Gold Nanorods: Stability and Targeting in Protein-Rich Media. J Am Chem Soc 2015;137:3686–92. https://doi.org/10.1021/jacs.5b01001.
[110] Luo J, Im J-H, Mayer MT, Schreier M, Nazeeruddin MK, Park N-G, et al. Water photolysis at 12.3% efficiency via perovskite photovoltaics and Earth-abundant catalysts. Science 2014;345:1593–6. https://doi.org/10.1126/science.1258307.

[111] Lee S-W, Kim S, Bae S, Cho K, Chung T, Mundt LE, et al. UV Degradation and Recovery of Perovskite Solar Cells. Sci Rep 2016;6:38150. https://doi.org/10.1038/srep38150.
[112] Liu J, Song K, Shin Y, Liu X, Chen J, Yao KX, et al. Light-Induced Self-Assembly of Cubic $CsPbBr_3$ Perovskite Nanocrystals into Nanowires. Chem Mater 2019;31:6642–9. https://doi.org/10.1021/acs.chemmater.9b00680.
[113] Wang Y, Li X, Sreejith S, Cao F, Wang Z, Stuparu MC, et al. Photon Driven Transformation of Cesium Lead Halide Perovskites from Few-Monolayer Nanoplatelets to Bulk Phase. Adv Mater 2016;28:10637–43. https://doi.org/10.1002/adma.201604110.
[114] Shamsi J, Rastogi P, Caligiuri V, Abdelhady AL, Spirito D, Manna L, et al. Bright-Emitting Perovskite Films by Large-Scale Synthesis and Photoinduced Solid-State Transformation of $CsPbBr_3$ Nanoplatelets. ACS Nano 2017;11:10206–13. https://doi.org/10.1021/acsnano.7b04761.
[115] Vila-Liarte D, Feil MW, Manzi A, Garcia-Pomar JL, Huang H, Döblinger M, et al. Templated-Assembly of $CsPbBr_3$ Perovskite Nanocrystals into 2D Photonic Supercrystals with Amplified Spontaneous Emission. Angew Chem Int Ed 2020;59:17750–6. https://doi.org/10.1002/anie.202006152.
[116] Pan A, Jurow M, Zhao Y, Qiu F, Liu Y, Yang J, et al. Templated self-assembly of one-dimensional $CsPbX_3$ perovskite nanocrystal superlattices. Nanoscale 2017;9:17688–93. https://doi.org/10.1039/C7NR06579E.
[117] Nagaoka Y, Hills-Kimball K, Tan R, Li R, Wang Z, Chen O. Nanocube Superlattices of Cesium Lead Bromide Perovskites and Pressure-Induced Phase Transformations at Atomic and Mesoscale Levels. Adv Mater 2017;29:1606666. https://doi.org/10.1002/adma.201606666.
[118] Wang Y, Lü X, Yang W, Wen T, Yang L, Ren X, et al. Pressure-Induced Phase Transformation, Reversible Amorphization, and Anomalous Visible Light Response in Organolead Bromide Perovskite. J Am Chem Soc 2015;137:11144–9. https://doi.org/10.1021/jacs.5b06346.
[119] Szafrański M, Katrusiak A. Mechanism of Pressure-Induced Phase Transitions, Amorphization, and Absorption-Edge Shift in Photovoltaic Methylammonium Lead Iodide. J Phys Chem Lett 2016;7:3458–66. https://doi.org/10.1021/acs.jpclett.6b01648.
[120] Ma Z, Liu Z, Lu S, Wang L, Feng X, Yang D, et al. Pressure-induced emission of cesium lead halide perovskite nanocrystals. Nat Commun 2018;9:4506. https://doi.org/10.1038/s41467-018-06840-8.
[121] Wang X, Zhao D, Qiu Y, Huang Y, Wu Y, Li G, et al. PIN Diodes Array Made of Perovskite Single Crystal for X-Ray Imaging. Phys Status Solidi RRL 2018;12:1800380. https://doi.org/10.1002/pssr.201800380.
[122] Zhang L, Zeng Q, Wang K. Pressure-Induced Structural and Optical Properties of Inorganic Halide Perovskite $CsPbBr_3$. J Phys Chem Lett 2017;8:3752–8. https://doi.org/10.1021/acs.jpclett.7b01577.
[123] Xiao G, Cao Y, Qi G, Wang L, Liu C, Ma Z, et al. Pressure Effects on Structure and Optical Properties in Cesium Lead Bromide Perovskite Nanocrystals. J Am Chem Soc 2017;139:10087–94. https://doi.org/10.1021/jacs.7b05260.
[124] Li B, Wen X, Li R, Wang Z, Clem PG, Fan H. Stress-induced phase transformation and optical coupling of silver nanoparticle superlattices into mechanically stable nanowires. Nat Commun 2014;5:4179. https://doi.org/10.1038/ncomms5179.
[125] Xiao G, Yang X, Zhang X, Wang K, Huang X, Ding Z, et al. A Protocol to Fabricate Nanostructured New Phase: B31-Ype MnS Synthesized Under High Pressure. J Am

Chem Soc 2015;137:10297–303. https://doi.org/10.1021/jacs.5b05629.
[126] Wang Y, Bai L, Wen T, Yang L, Gou H, Xiao Y, et al. Giant Pressure-Driven Lattice Collapse Coupled with Intermetallic Bonding and Spin-State Transition in Manganese Chalcogenides. Angew Chem 2016;128:10506–9. https://doi.org/10.1002/ange.201605410.
[127] Wu H, Bai F, Sun Z, Haddad RE, Boye DM, Wang Z, et al. Pressure-Driven Assembly of Spherical Nanoparticles and Formation of 1D-Nanostructure Arrays. Angew Chem 2010;122:8609–12. https://doi.org/10.1002/ange.201001581.
[128] Ji Y, Wang M, Yang Z, Qiu H, Kou S, Padhiar MA, et al. Pressure-Driven Transformation of CsPbBrI2 Nanoparticles into Stable Nanosheets in Solution through Self-Assembly. J Phys Chem Lett 2020;11:9862–8. https://doi.org/10.1021/acs.jpclett.0c02747.
[129] Korth BD, Keng P, Shim I, Bowles SE, Tang C, Kowalewski T, et al. Polymer-Coated Ferromagnetic Colloids from Well-Defined Macromolecular Surfactants and Assembly into Nanoparticle Chains. J Am Chem Soc 2006;128:6562–3. https://doi.org/10.1021/ja0609147.
[130] Yang Y, Lee JT, Liyanage T, Sardar R. Flexible Polymer-Assisted Mesoscale Self-Assembly of Colloidal $CsPbBr_3$ Perovskite Nanocrystals into Higher Order Superstructures with Strong Inter-Nanocrystal Electronic Coupling. J Am Chem Soc 2019;141:1526–36. https://doi.org/10.1021/jacs.8b10083.
[131] He X, Qiu Y, Yang S. Fully-Inorganic Trihalide Perovskite Nanocrystals: A New Research Frontier of Optoelectronic Materials. Adv Mater 2017;29:1700775. https://doi.org/10.1002/adma.201700775.
[132] Huang R, Wang Y, Qi W, Su R, He Z. Temperature-induced reversible self-assembly of diphenylalanine peptide and the structural transition from organogel to crystalline nanowires. Nanoscale Res Lett 2014;9:653. https://doi.org/10.1186/1556-276X-9-653.
[133] Chin XY, Cortecchia D, Yin J, Bruno A, Soci C. Lead iodide perovskite light-emitting field-effect transistor. Nat Commun 2015;6:7383. https://doi.org/10.1038/ncomms8383.
[134] Xing G, Mathews N, Lim SS, Yantara N, Liu X, Sabba D, et al. Low-temperature solution-processed wavelength-tunable perovskites for lasing. Nat Mater 2014;13:476–80. https://doi.org/10.1038/nmat3911.
[135] Hoye RLZ, Chua MR, Musselman KP, Li G, Lai ML, Tan ZK, et al. Enhanced performance in fluorene-free organometal halide perovskite light-emitting diodes using tunable, low electron affinity oxide electron injectors. Adv Mater 2015;27:1414–9. https://doi.org/10.1002/adma.201405044.
[136] Lin Q, Armin A, Nagiri RCR, Burn PL, Meredith P. Electro-optics of perovskite solar cells. Nat Photonics 2015;9:106–112. https://doi.org/10.1038/nphoton.2014.284.
[137] Tan Z-K, Moghaddam RS, Lai ML, Docampo P, Higler R, Deschler F, et al. Bright light-emitting diodes based on organometal halide perovskite. Nat Nanotechnol 2014;9:687–92. https://doi.org/10.1038/nnano.2014.149.
[138] Eperon GE, Leijtens T, Bush KA, Prasanna R, Green T, Wang JTW, et al. Perovskite-perovskite tandem photovoltaics with optimized band gaps. Science 2016;354:861–5. https://doi.org/10.1126/science.aaf9717.
[139] McMeekin DP, Sadoughi G, Rehman W, Eperon GE, Saliba M, Hörantner MT, et al. A mixed-cation lead mixed-halide perovskite absorber for tandem solar cells. Science 2016;351:151–5. https://doi.org/10.1126/science.aad5845.
[140] Yang WS, Noh JH, Jeon NJ, Kim YC, Ryu S, Seo J, et al. High-performance photovoltaic perovskite layers fabricated through intramolecular exchange. Science

2015;348:1234–7. https://doi.org/10.1126/science.aaa9272.
[141] Chen W, Wu Y, Yue Y, Liu J, Zhang W, Yang X, et al. Efficient and stable large-area perovskite solar cells with inorganic charge extraction layers. Science 2015;350:944–8. https://doi.org/10.1126/science.aad1015.
[142] Tiep NH, Ku Z, Fan HJ. Recent Advances in Improving the Stability of Perovskite Solar Cells. Adv Energy Mater 2016;6:1501420. https://doi.org/10.1002/aenm.201501420.
[143] Yang J, Siempelkamp BD, Liu D, Kelly TL. Investigation of $CH_3NH_3PbI_3$ degradation rates and mechanisms in controlled humidity environments using in situ techniques. ACS Nano 2015;9:1955–63. https://doi.org/10.1021/nn506864k.
[144] Berhe TA, Su WN, Chen CH, Pan CJ, Cheng JH, Chen HM, et al. Organometal halide perovskite solar cells: Degradation and stability. Energy Environ Sci 2016;9:323–56. https://doi.org/10.1039/c5ee02733k.
[145] Manser JS, Saidaminov MI, Christians JA, Bakr OM, Kamat P V. Making and Breaking of Lead Halide Perovskites. Acc Chem Res 2016;49:330–8. https://doi.org/10.1021/acs.accounts.5b00455.
[146] Choi JJ, Yang X, Norman ZM, Billinge SJL, Owen JS. Structure of methylammonium lead iodide within mesoporous titanium dioxide: Active material in high-performance perovskite solar cells. Nano Lett 2014;14:127–33. https://doi.org/10.1021/nl403514x.
[147] Kim J, Lee SH, Lee JH, Hong KH. The role of intrinsic defects in methylammonium lead iodide perovskite. J Phys Chem Lett 2014;5:1312–7. https://doi.org/10.1021/jz500370k.
[148] Yin WJ, Shi T, Yan Y. Unusual defect physics in CH3NH3PbI3 perovskite solar cell absorber. Appl Phys Lett 2014;104:063903. https://doi.org/10.1063/1.4864778.
[149] Azpiroz JM, Mosconi E, Bisquert J, De Angelis F. Defect migration in methylammonium lead iodide and its role in perovskite solar cell operation. Energy Environ Sci 2015;8:2118–27. https://doi.org/10.1039/c5ee01265a.
[150] Eames C, Frost JM, Barnes PRF, O'Regan BC, Walsh A, Islam MS. Ionic transport in hybrid lead iodide perovskite solar cells. Nat Commun 2015;6:7497. https://doi.org/10.1038/ncomms8497.
[151] Smock SR, Williams TJ, Brutchey RL. Quantifying the Thermodynamics of Ligand Binding to CsPbBr3 Quantum Dots. Angew Chem- Int Ed 2018;57:11711–5. https://doi.org/10.1002/anie.201806916.
[152] De Roo J, Ibáñez M, Geiregat P, Nedelcu G, Walravens W, Maes J, et al. Highly Dynamic Ligand Binding and Light Absorption Coefficient of Cesium Lead Bromide Perovskite Nanocrystals. ACS Nano 2016;10:2071–81. https://doi.org/10.1021/acsnano.5b06295.
[153] Pan J, Sarmah SP, Murali B, Dursun I, Peng W, Parida MR, et al. Air-Stable Surface-Passivated Perovskite Quantum Dots for Ultra-Robust, Single- and Two-Photon-Induced Amplified Spontaneous Emission. J Phys Chem Lett 2015;6:5027–33. https://doi.org/10.1021/acs.jpclett.5b02460.
[154] Pan J, Li X, Gong X, Yin J, Zhou D, Sinatra L, et al. Halogen Vacancies Enable Ligand-Assisted Self-Assembly of Perovskite Quantum Dots into Nanowires. Angew Chem 2019;131:16223–7. https://doi.org/10.1002/ange.201909109.
[155] Biega R-I, Leppert L. Halogen Vacancy Migration at Surfaces of CsPbBr$_3$ Perovskites: Insights from Density Functional Theory. JPhys Energy 2021;3:034017. https://doi.org/10.1088/2515-7655/ac10fe.
[156] Gualdrón-Reyes AF, Yoon SJ, Barea EM, Agouram S, Muñoz-Sanjosé V, Meléndez ÁM, et al. Controlling the Phase Segregation in Mixed Halide Perovskites through

Nanocrystal Size. ACS Energy Lett 2019;4:54–62. https://doi.org/10.1021/acsenergylett.8b02207.
[157] Seth S, Ahmed T, De A, Samanta A. Tackling the Defects, Stability, and Photoluminescence of $CsPbX_3$ Perovskite Nanocrystals. ACS Energy Lett 2019;4:1610–8. https://doi.org/10.1021/acsenergylett.9b00849.
[158] Zheng X, Yuan S, Liu J, Yin J, Yuan F, Shen W-S, et al. Chlorine Vacancy Passivation in Mixed Halide Perovskite Quantum Dots by Organic Pseudohalides Enables Efficient Rec. 2020 Blue Light-Emitting Diodes. ACS Energy Lett 2020;5:793–8. https://doi.org/10.1021/acsenergylett.0c00057.
[159] Zhang KQ, Liu XY. In situ observation of colloidal monolayer nucleation driven by an alternating electric field. Nature 2004;429:739–43. https://doi.org/10.1038/nature02630.
[160] Leunissen ME, Vutukuri HR, Van Blaaderen A. Directing colloidal self-assembly with biaxial electric fields. Adv Mater 2009;21:3116–20. https://doi.org/10.1002/adma.200900640.
[161] Bhatt KH, Velev OD. Control and Modeling of the Dielectrophoretic Assembly of On-Chip Nanoparticle Wires. Langmuir 2004;20:467–76. https://doi.org/10.1021/la0349976.
[162] Hermanson KD, Lumsdon SO, Williams JP, Kaler EW, Velev OD. Dielectrophoretic assembly of electrically functional microwires from nanoparticle suspensions. Science 2001;294:1082–6. https://doi.org/10.1126/science.1063821.
[163] Jin X, Zhang X, Fang H, Deng W, Xu X, Jie J, et al. Facile Assembly of High-Quality Organic-Inorganic Hybrid Perovskite Quantum Dot Thin Films for Bright Light-Emitting Diodes. Adv Funct Mater 2018;28:1705189. https://doi.org/10.1002/adfm.201705189.
[164] Sheng K, Bai H, Sun Y, Li C, Shi G. Layer-by-layer assembly of graphene/polyaniline multilayer films and their application for electrochromic devices. Polymer (Guildf) 2011;52:5567–72. https://doi.org/10.1016/j.polymer.2011.10.001.
[165] Liu J, Wu Z, Li T, Zhou D, Zhang K, Sheng Y, et al. Electrophoretic deposition of fluorescent Cu and Au sheets for light-emitting diodes. Nanoscale 2016;8:395–402. https://doi.org/10.1039/C5NR06599B.
[166] Ravi VK, Scheidt RA, DuBose J, Kamat PV. Hierarchical Arrays of Cesium Lead Halide Perovskite Nanocrystals through Electrophoretic Deposition. J Am Chem Soc 2018;140:8887–94. https://doi.org/10.1021/jacs.8b04803.
[167] Fulari A V., Thanh Duong N, Anh Nguyen D, Jo Y, Cho S, Young Kim D, et al. Achieving direct electrophoretically deposited highly stable polymer induced CsPbBr3 colloidal nanocrystal films for high-performance optoelectronics. Chem Eng J 2022;433:133809. https://doi.org/10.1016/j.cej.2021.133809.
[168] Krieg F, Sercel PC, Burian M, Andrusiv H, Bodnarchuk MI, Stöferle T, et al. Monodisperse Long-Chain Sulfobetaine-Capped CsPbBr 3 Nanocrystals and Their Superfluorescent Assemblies. ACS Cent Sci 2021;7:135–44. https://doi.org/10.1021/acscentsci.0c01153.
[169] Vogel N, Retsch M, Fustin C-A, del Campo A, Jonas U. Advances in Colloidal Assembly: The Design of Structure and Hierarchy in Two and Three Dimensions. Chem Rev 2015;115:6265–311. https://doi.org/10.1021/cr400081d.
[170] Dong A, Jiao Y, Milliron DJ. Electronically Coupled Nanocrystal Superlattice Films by in Situ Ligand Exchange at the Liquid–Air Interface. ACS Nano 2013;7:10978–84. https://doi.org/10.1021/nn404566b.
[171] Protesescu L, Yakunin S, Bodnarchuk MI, Krieg F, Caputo R, Hendon CH, et al.

Nanocrystals of Cesium Lead Halide Perovskites ($CsPbX_3$, X = Cl, Br, and I): Novel Optoelectronic Materials Showing Bright Emission with Wide Color Gamut. Nano Lett 2015;15:3692–6. https://doi.org/10.1021/nl5048779.
[172] Pan A, He B, Fan X, Liu Z, Urban JJ, Alivisatos AP, et al. Insight into the Ligand-Mediated Synthesis of Colloidal $CsPbBr_3$ Perovskite Nanocrystals: The Role of Organic Acid, Base, and Cesium Precursors. ACS Nano 2016;10:7943–54. https://doi.org/10.1021/acsnano.6b03863.
[173] Sun S, Yuan D, Xu Y, Wang A, Deng Z. Ligand-Mediated Synthesis of Shape-Controlled Cesium Lead Halide Perovskite Nanocrystals via Reprecipitation Process at Room Temperature. ACS Nano 2016;10:3648–57. https://doi.org/10.1021/acsnano.5b08193.
[174] Tanford C. Theory of micelle formation in aqueous solutions. J Phys Chem 1974;78:2469–79. https://doi.org/10.1021/j100617a012.
[175] Chakrabarty A, Satija S, Gangwar U, Sapra S. Precursor-Mediated Synthesis of Shape-Controlled Colloidal $CsPbBr_3$ Perovskite Nanocrystals and Their Nanofiber-Directed Self-Assembly. Chem Mater 2020;32:721–33. https://doi.org/10.1021/acs.chemmater.9b03700.
[176] Gomez L, Lin J, de Weerd C, Poirier L, Boehme SC, von Hauff E, et al. Extraordinary Interfacial Stitching between Single All-Inorganic Perovskite Nanocrystals. ACS Appl Mater Interfaces 2018;10:5984–91. https://doi.org/10.1021/acsami.7b17432.
[177] Hudait B, Dutta SK, Patra A, Nasipuri D, Pradhan N. Facets Directed Connecting Perovskite Nanocrystals. J Am Chem Soc 2020;142:7207–17. https://doi.org/10.1021/jacs.0c02168.
[178] Tong Y, Bohn BJ, Bladt E, Wang K, Müller-Buschbaum P, Bals S, et al. From Precursor Powders to CsPbX3 Perovskite Nanowires: One-Pot Synthesis, Growth Mechanism, and Oriented Self-Assembly. Angew Chem Int Ed 2017;56:13887–92. https://doi.org/10.1002/anie.201707224.
[179] Paul S, Samanta A. N -Bromosuccinimide as Bromide Precursor for Direct Synthesis of Stable and Highly Luminescent Green-Emitting Perovskite Nanocrystals. ACS Energy Lett 2020;5:64–9. https://doi.org/10.1021/acsenergylett.9b02363.
[180] Grisorio R, Conelli D, Fanizza E, Striccoli M, Altamura D, Giannini C, et al. Size-tunable and stable cesium lead-bromide perovskite nanocubes with near-unity photoluminescence quantum yield. Nanoscale Adv 2021;3:3918–28. https://doi.org/10.1039/D1NA00142F.
[181] Xing D, Lin CC, Ho YL, Kamal ASA, Wang IT, Chen CC, et al. Self-Healing Lithographic Patterning of Perovskite Nanocrystals for Large-Area Single-Mode Laser Array. Adv Funct Mater 2021;31:1–9. https://doi.org/10.1002/adfm.202006283.
[182] Protesescu L, Yakunin S, Bodnarchuk MI, Krieg F, Caputo R, Hendon CH, et al. Nanocrystals of Cesium Lead Halide Perovskites ($CsPbX_3$, X = Cl, Br, and I): Novel Optoelectronic Materials Showing Bright Emission with Wide Color Gamut. Nano Lett 2015;15:3692–6. https://doi.org/10.1021/nl5048779.
[183] Yuan S, Wang Z-K, Zhuo M-P, Tian Q-S, Jin Y, Liao L-S. Self-Assembled High Quality $CsPbBr_3$ Quantum Dot Films toward Highly Efficient Light-Emitting Diodes. ACS Nano 2018;12:9541–8. https://doi.org/10.1021/acsnano.8b05185.
[184] Fu X, Zhang C, Peng Z, Xia Y, Zhang J, Luo W, et al. Self-assembly and photoactivation of blue luminescent $CsPbBr_3$ mesocrystals synthesized at ambient temperature. J Mater Chem C 2018;6:1701–8. https://doi.org/10.1039/C7TC05505F.
[185] van der Burgt JS, Geuchies JJ, van der Meer B, Vanrompay H, Zanaga D, Zhang Y, et al. Cuboidal Supraparticles Self-Assembled from Cubic $CsPbBr_3$ Perovskite

Nanocrystals. J Phys Chem C 2018;122:15706–12. https://doi.org/10.1021/acs.jpcc.8b02699.
[186] Bi C, Wang S, Kershaw SV, Zheng K, Pullerits T, Gaponenko S, et al. Spontaneous Self-Assembly of Cesium Lead Halide Perovskite Nanoplatelets into Cuboid Crystals with High Intensity Blue Emission. Adv Sci 2019;6:1900462. https://doi.org/10.1002/advs.201900462.
[187] Liu Y, Siron M, Lu D, Yang J, dos Reis R, Cui F, et al. Self-Assembly of Two-Dimensional Perovskite Nanosheet Building Blocks into Ordered Ruddlesden–Popper Perovskite Phase. J Am Chem Soc 2019;141:13028–32. https://doi.org/10.1021/jacs.9b06889.
[188] Bera S, Behera RK, Pradhan N. α-Halo Ketone for Polyhedral Perovskite Nanocrystals: Evolutions, Shape Conversions, Ligand Chemistry, and Self-Assembly. J Am Chem Soc 2020;142:20865–74. https://doi.org/10.1021/jacs.0c10688.
[189] Mehetor SK, Ghosh H, Pradhan N. Blue-Emitting $CsPbBr_3$ Perovskite Quantum Rods and Their Wide-Area 2D Self-Assembly. ACS Energy Lett 2019;4:1437–42. https://doi.org/10.1021/acsenergylett.9b01028.
[190] Peng L, Dutta SK, Mondal D, Hudait B, Shyamal S, Xie R, et al. Arm Growth and Facet Modulation in Perovskite Nanocrystals. J Am Chem Soc 2019;141:16160–8. https://doi.org/10.1021/jacs.9b09157.
[191] Li H, Liu X, Ying Q, Wang C, Jia W, Xing X, et al. Self-Assembly of Perovskite $CsPbBr_3$ Quantum Dots Driven by a Photo-Induced Alkynyl Homocoupling Reaction. Angew Chem 2020;132:17360–6. https://doi.org/10.1002/ange.202004947.
[192] Vila-Liarte D, Feil MW, Manzi A, Garcia-Pomar JL, Huang H, Döblinger M, et al. Templated-Assembly of $CsPbBr_3$ Perovskite Nanocrystals into 2D Photonic Supercrystals with Amplified Spontaneous Emission. Angew Chem Int Ed 2020;59:17750–6. https://doi.org/10.1002/anie.202006152.
[193] Wang S, Zhou L, Huang F, Xin Y, Jin P, Ma Q, et al. Hybrid Organic-inorganic Lead Bromide Perovskite Supercrystals Self-Assembled with L-cysteine and Their Highly Luminescent Properties. J Mater Chem C 2018;6:10994–1001. https://doi.org/10.1039/C8TC03668C.
[194] Yang X, Li F, Wang X, Xu Y, Wei H, Wang L. In situ tetrafluoroborate-modified $MAPbBr_3$ nanocrystals showing high photoluminescence, stability and self-assembly behavior. J Mater Chem C 2020;8:1989–97. https://doi.org/10.1039/C9TC04978A.
[195] Liu K-K, Liu Q, Yang D-W, Liang Y-C, Sui L-Z, Wei J-Y, et al. Water-induced $MAPbBr_3$@PbBr(OH) with enhanced luminescence and stability. Light Sci Appl 2020;9:44. https://doi.org/10.1038/s41377-020-0283-2.
[196] Protesescu L, Yakunin S, Bodnarchuk MI, Bertolotti F, Masciocchi N, Guagliardi A, et al. Monodisperse Formamidinium Lead Bromide Nanocrystals with Bright and Stable Green Photoluminescence. J Am Chem Soc 2016;138:14202–5. https://doi.org/10.1021/jacs.6b08900.
[197] Li F, Yang L, Cai Z, Wei K, Lin F, You J, et al. Enhancing exciton binding energy and photoluminescence of formamidinium lead bromide by reducing its dimensions to 2D nanoplates for producing efficient light emitting diodes. Nanoscale 2018;10:20611–7. https://doi.org/10.1039/C8NR04986F.
[198] Patra A, Bera S, Nasipuri D, Dutta SK, Pradhan N. Tuning Facets and Controlling Monodispersity in Organic–Inorganic Hybrid Perovskite $FAPbBr_3$ Nanocrystals. ACS Energy Lett 2021;6:2682–9. https://doi.org/10.1021/acsenergylett.1c01108.
[199] Akkerman QA, Motti SG, Srimath Kandada AR, Mosconi E, D'Innocenzo V, Bertoni G, et al. Solution Synthesis Approach to Colloidal Cesium Lead Halide Perovskite

Nanoplatelets with Monolayer-Level Thickness Control. J Am Chem Soc 2016;138:1010–6. https://doi.org/10.1021/jacs.5b12124.
[200] Bohn BJ, Tong Y, Gramlich M, Lai ML, Döblinger M, Wang K, et al. Boosting Tunable Blue Luminescence of Halide Perovskite Nanoplatelets through Postsynthetic Surface Trap Repair. Nano Lett 2018;18:5231–8. https://doi.org/10.1021/acs.nanolett.8b02190.
[201] Li Z-J, Hofman E, Davis AH, Maye MM, Zheng W. General Strategy for the Growth of $CsPbX_3$ (X = Cl, Br, I) Perovskite Nanosheets from the Assembly of Nanorods. Chem Mater 2018;30:3854–60. https://doi.org/10.1021/acs.chemmater.8b01283.
[202] Liu W, Zheng J, Cao S, Wang L, Gao F, Chou K-C, et al. General Strategy for Rapid Production of Low-Dimensional All-Inorganic $CsPbBr_3$ Perovskite Nanocrystals with Controlled Dimensionalities and Sizes. Inorg Chem 2018;57:1598–603. https://doi.org/10.1021/acs.inorgchem.7b02941.
[203] Pal J, Manna S, Mondal A, Das S, Adarsh K V., Nag A. Colloidal Synthesis and Photophysics of $M_3Sb_2I_9$ (M=Cs and Rb) Nanocrystals: Lead-Free Perovskites. Angew Chem Int Ed 2017;56:14187–91. https://doi.org/10.1002/anie.201709040.
[204] Chen L-J, Lee C-R, Chuang Y-J, Wu Z-H, Chen C. Synthesis and Optical Properties of Lead-Free Cesium Tin Halide Perovskite Quantum Rods with High-Performance Solar Cell Application. J Phys Chem Lett 2016;7:5028–35. https://doi.org/10.1021/acs.jpclett.6b02344.
[205] Tong Y, Fu M, Bladt E, Huang H, Richter AF, Wang K, et al. Chemical Cutting of Perovskite Nanowires into Single-Photon Emissive Low-Aspect-Ratio $CsPbX_3$ (X=Cl, Br, I) Nanorods. Angew Chem Int Ed 2018;57:16094–8. https://doi.org/10.1002/anie.201810110.
[206] Zhang D, Eaton SW, Yu Y, Dou L, Yang P. Solution-Phase Synthesis of Cesium Lead Halide Perovskite Nanowires. J Am Chem Soc 2015;137:9230–3. https://doi.org/10.1021/jacs.5b05404.
[207] Zhang D, Yang Y, Bekenstein Y, Yu Y, Gibson NA, Wong AB, et al. Synthesis of Composition Tunable and Highly Luminescent Cesium Lead Halide Nanowires through Anion-Exchange Reactions. J Am Chem Soc 2016;138:7236–9. https://doi.org/10.1021/jacs.6b03134.
[208] Teunis MB, Jana A, Dutta P, Johnson MA, Mandal M, Muhoberac BB, et al. Mesoscale Growth and Assembly of Bright Luminescent Organolead Halide Perovskite Quantum Wires. Chem Mater 2016;28:5043–54. https://doi.org/10.1021/acs.chemmater.6b01793.
[209] Imran M, Di Stasio F, Dang Z, Canale C, Khan AH, Shamsi J, et al. Colloidal Synthesis of Strongly Fluorescent $CsPbBr_3$ Nanowires with Width Tunable down to the Quantum Confinement Regime. Chem Mater 2016;28:6450–4. https://doi.org/10.1021/acs.chemmater.6b03081.
[210] Amgar D, Stern A, Rotem D, Porath D, Etgar L. Tunable Length and Optical Properties of $CsPbX_3$ (X = Cl, Br, I) Nanowires with a Few Unit Cells. Nano Lett 2017;17:1007–13. https://doi.org/10.1021/acs.nanolett.6b04381.
[211] Zhang B, Goldoni L, Zito J, Dang Z, Almeida G, Zaccaria F, et al. Alkyl Phosphonic Acids Deliver $CsPbBr_3$ Nanocrystals with High Photoluminescence Quantum Yield and Truncated Octahedron Shape. Chem Mater 2019;31:9140–7. https://doi.org/10.1021/acs.chemmater.9b03529.
[212] Toso S, Baranov D, Manna L. Hidden in Plain Sight: The Overlooked Influence of the Cs^+ Substructure on Transformations in Cesium Lead Halide Nanocrystals. ACS Energy Lett 2020;5:3409–14. https://doi.org/10.1021/acsenergylett.0c02029.

[213] Jagielski J, Solari SF, Jordan L, Scullion D, Blülle B, Li Y-T, et al. Scalable photonic sources using two-dimensional lead halide perovskite superlattices. Nat Commun 2020;11:387. https://doi.org/10.1038/s41467-019-14084-3.
[214] Shyamal S, Dutta SK, Das T, Sen S, Chakraborty S, Pradhan N. Facets and Defects in Perovskite Nanocrystals for Photocatalytic CO_2 Reduction. J Phys Chem Lett 2020;11:3608–14. https://doi.org/10.1021/acs.jpclett.0c01088.
[215] Liu J, Zheng X, Mohammed OF, Bakr OM. Self-Assembly and Regrowth of Metal Halide Perovskite Nanocrystals for Optoelectronic Applications. Acc Chem Res 2022;55:262–74. https://doi.org/10.1021/acs.accounts.1c00651.
[216] Jana A, Jo Y, Im H. Multicomponent perovskite superlattices. Matter 2021;4:2607–9. https://doi.org/10.1016/j.matt.2021.06.020.
[217] Cherniukh I, Sekh T V., Rainò G, Ashton OJ, Burian M, Travesset A, et al. Structural Diversity in Multicomponent Nanocrystal Superlattices Comprising Lead Halide Perovskite Nanocubes. ACS Nano 2022. https://doi.org/10.1021/acsnano.1c10702.
[218] Shevchenko E V., Talapin D V., Kotov NA, O'Brien S, Murray CB. Structural diversity in binary nanoparticle superlattices. Nature 2006;439:55–9. https://doi.org/10.1038/nature04414.
[219] Shi E, Yuan B, Shiring SB, Gao Y, Akriti, Guo Y, et al. Two-dimensional halide perovskite lateral epitaxial heterostructures. Nature 2020;580:614–20. https://doi.org/10.1038/s41586-020-2219-7.
[220] Mandal TN, Jana A. Lateral Epitaxial Heterostructures of Halide Perovskites for Diode Application. Matter 2020;3:617–9. https://doi.org/10.1016/j.matt.2020.06.027.
[221] Pu S, Gong C, Robertson AW. Liquid cell transmission electron microscopy and its applications. R Soc Open Sci 2020;7:191204. https://doi.org/10.1098/rsos.191204.
[222] Li X, Mitsuishi K, Takeguchi M. Fabrication of a liquid cell for in situ transmission electron microscopy. Microscopy 2021;70:327–32. https://doi.org/10.1093/jmicro/dfaa076.
[223] Qin F, Wang Z, Wang ZL. Anomalous Growth and Coalescence Dynamics of Hybrid Perovskite Nanoparticles Observed by Liquid-Cell Transmission Electron Microscopy. ACS Nano 2016;10:9787–93. https://doi.org/10.1021/acsnano.6b04234.